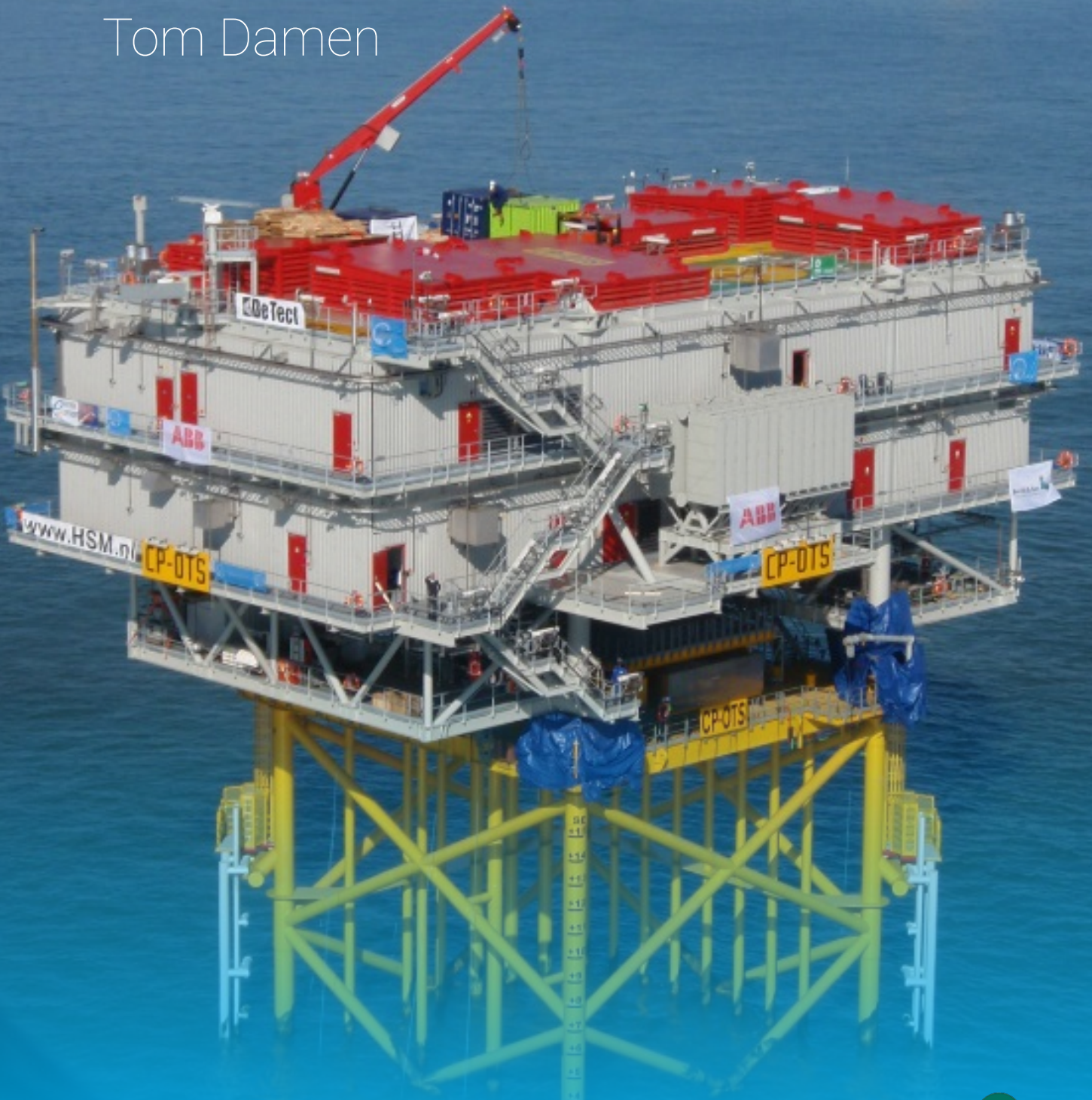


Stressed Skin Design in Offshore Modules

A comparative study

Tom Damen



Technische Universiteit Delft

Stressed Skin Design in Offshore Modules

A comparative study

by

Tom Damen

to obtain the degree of Master of Science

at the Delft University of Technology,

to be defended publicly on December 14, 2016, at 16:00 hours.

Student number: 4011198
Project duration: October 5, 2015 – December 14, 2016
Thesis committee: Prof. ir. F. S. K. Bijlaard, TU Delft, chairman
Ir. R. Abspoel, TU Delft, Structural and Building Engineering
Dr. ir. P. C. J. Hoogenboom, TU Delft, Structural Mechanics
Ir. E. Boender, Iv-Oil & Gas
Ir. R. Teuling, Iv-Oil & Gas

An electronic version of this thesis is available at <http://repository.tudelft.nl/>.



Preface

This master's thesis deals with the different ways to design offshore module structures. The study has been carried out between October 2015 and December 2016 at the office of Iv-Oil & Gas in order to obtain the degree of Master of Science at the Delft University of Technology.

Without the help of others, I would never have been able to complete the work. Therefore, I would like to express my gratitude to Prof. Ir. E.S.K. Bijlaard, Ir. R. Abspoel, and Dr. Ir. P.C.J. Hoogenboom for supervising and guiding me through the process of this master's thesis.

I would also like to thank my co-workers at the office of Iv-Oil & Gas for their support. In particular, I would like to thank Ir. E. Boender and Ir. R. Teuling for their constructive input.

Lastly, I would like to thank my family and friends for their support.

Tom Damen
Papendrecht, November 2016

Abstract

Offshore wind power provides an alternative to fossil fuels while negating the effect of visual and auditive distortion of onshore wind turbines. Located several kilometres offshore, the transmission cable resistance becomes substantial. To limit the losses, the voltage in the cables is increased in a substation. As this structure is often the largest in a wind farm, profits can be expected when optimizing this topside structure.

Topside structures for the oil & gas industry generally require to be ventilated in order to prevent gas stacking. The equipment in the substation module, however, is vulnerable for the corrosive sea environment. Therefore, the structure needs to be sheltered. Hereby, the question rises if a weight reduction can be obtained by incorporating the shelter in the structural design.

The thesis is carried out at Iv-Oil & Gas, who provided the basis of a comparative case study. For the research to be generally applicable, the case study design is simplified. Then a frame form the simplified model is chosen as a basis for the comparison. For a single governing load combination, two designs are constructed: a beam-column design complying to the conventional oil & gas design practice and a stressed skin design that incorporates the sheltering wall as a structural element.

Both of the designs are then compared on steel mass and weld labour. The stressed skin design is found to be considerably lighter than the beam-column design. However, in terms of welds, the stressed skin design consists of a higher weld volume and a higher weld pass length. These aspects contribute to the total manufacturing costs of the design.

Concluding, both of the designs have their advantages and disadvantages. It is made clear that applying the dividing wall as a structural element in the format of a stressed skin design provides a competitive design in terms of structural mass and weld labour. The final conclusions based on the comparison may vary dependent on the resources available at the manufacturer.

Contents

List of Figures	ix
List of Tables	xi
List of Abbreviations	xiii
1 Introduction	1
1.1 Company and thesis background	1
1.2 Objective	1
1.3 Substation design	2
1.4 Thesis outline & boundary conditions	8
2 Literature review	9
2.1 Books & theses	9
2.2 Papers & codes	9
3 Numerical modelling	11
3.1 Numerical modelling in SACS	11
3.2 Numerical modelling in Ansys	12
4 Design requirements	23
4.1 Codes	23
4.2 Materials	23
4.3 Loading conditions	24
4.4 Loads	24
4.5 Load combinations	27
4.6 Support conditions	28
4.7 Failure criteria	28
4.8 Fatigue	29
5 Simplified Beam-Column Design	31
5.1 Geometry and loading	31
5.2 Member results	32
5.3 Frame loading	36
6 Variant study	37
6.1 Input for all models	37
6.2 Beam-column design in SACS	39
6.3 Beam-column design in Ansys	42
6.4 Stressed skin design	46
7 Comparison	49
7.1 Software comparison	49
7.2 Comparison of designs	52
8 Conclusions and Recommendations	57
8.1 Conclusions	57
8.2 Recommendations	59

Appendices

A Literature review	61
A.1 Books	61
A.2 Previously conducted theses	62
A.3 Papers	65
A.4 Codes	75
A.5 Plate buckling	77
B Ansys APDL test script	89
C SACS output	91
C.1 Simplified beam-column design	91
C.2 Beam-column design	106
D Ansys output	111
D.1 Beam-column design	111
D.2 Stressed skin design	115
E Hand calculations	119
E.1 Hand calculations to verify the SACS model	119
F Number of weld passes	125
Bibliography	129

List of Figures

1.1	Offshore wind generating capacity in Europe installed per year and in total	2
1.2	Maximum wind turbine size by year	3
1.3	Equipment housed in separate encasements	3
1.4	All equipment in one encasement	4
1.5	The HelWin beta HVDC topside during transport	4
1.6	Stressed skin methodology applied in the roof of a building	5
1.7	Location of the Thornton Bank Wind Farm	6
1.8	Thornton Bank substation as built	7
1.9	Model as designed by Iv-AGA	7
3.1	Member length L_1 that is taken into account in the analyses	12
3.2	Integration scheme of the Shell181 and the Shell281 elements	13
3.3	First buckling mode shape of a rectangular plate	14
3.4	Eigenvalue buckling load plotted against number of nodes and element type	15
3.5	Applied loading plotted against lateral deflection	16
3.6	Applied loading plotted against lateral deflection of the non-linear analysis	17
3.7	Plate with one longitudinal stringer for analysis	19
3.8	Detail of the node at a support	20
3.9	Stress distribution in the plate under different stress levels	21
4.1	Stress-strain relationship considered in the Ansys analyses	24
4.2	Equipment loading locations	26
4.3	Occurring beam deflections	29
5.1	Geometry of the beam-column design	32
5.2	Visualisation of the member results of the simplified beam-column design	34
5.3	Internal forces in the frame	35
5.4	Loading locations and values on the frame	36
6.1	Node numbers considered in the analysis	38
6.2	Frame analysed in SACS for the comparison with Ansys	39
6.3	Internal forces under equivalent loading	40
6.4	Horizontal deflection of the beam-column model in SACS under SLS loading	41
6.5	Frame analysed in Ansys for the comparison with SACS	42
6.6	Joint details including the diamond plate and the widened flanges and stiffeners	43
6.7	Strain of the beam-column model in Ansys under failure loading	44
6.8	Horizontal deflection of the beam-column model in Ansys under SLS loading	44
6.9	Geometry of the stressed skin design	46
6.10	Cross section I-I of the geometry of stringers in the stressed skin design	46
6.11	Deformations in the stressed skin model under SLS loading	48
7.1	Displacement of the beam-column designs	50
7.2	Comparison of the deformed shape in SACS and Ansys	51
7.3	Load-deflection diagram at distinct nodes for the different designs	53
7.4	Standardized geometry of the welds	54
A.1	Effective width regarding plate buckling of a uniformly loaded stiffened plate	63
A.2	Influence of shear stress on in-plane stress distribution	64
A.3	Flowchart of analysis as performed by Aberkrom	64
A.4	Minimum required plate thickness	66

A.5	Design idealisations	67
A.6	Plate buckling and post-buckling deflection	70
A.7	Stress distributions on simply supported plates	71
A.8	Corrugation types considered in this paper	73
A.9	Loading on the shear wall and transverse stiffener location	73
A.10	Basis of effective width method	75
A.11	Plate geometry and loadings on the plates as considered in the derivations	77
A.12	Values for k_c depending on aspect ratio and number of half wave lengths	79
A.13	Values for $k_{c,b}$ depending on aspect ratio and number of half wave lengths	82
A.14	Shear loading on the plate	82
A.15	Values for k_s depending on aspect ratio	85
A.16	Assumed deflection field for and infinitely long shear plate	85
D.1	Deformation of the frame in y-direction under SLS loading	111
D.2	Deformation of the frame in y-direction under ULS loading	112
D.3	Deformation of the frame in y-direction under failure loading	112
D.4	Deformation of the frame in x-direction under SLS loading	113
D.5	Von Mises-stresses in the frame under ULS loading	113
D.6	Von Mises-stresses in the frame under failure loading	114
D.7	Deformations in the stressed skin design in x-direction under SLS loading	115
D.8	Deformations in the stressed skin design in x-direction under ULS loading	116
D.9	Deformations in the stressed skin design in x-direction under failure loading	116
D.10	Von Mises-stresses in the stressed skin design under ULS loading	117
D.11	Von Mises-stresses in the stressed skin design under failure loading	117
E.1	Considered cross sections in the hand verification	120
E.1	Minimum weld passes required to complete a butt weld	126
E.2	Minimum weld passes required to complete a fillet weld	127

List of Tables

3.1	Comparison of results from Ansys APDL and Workbench	15
3.2	Comparison of full stringer modelling vs. stringer modelling using beam elements	19
4.1	Equipment loading on the structure	25
4.2	Distributed equipment loads	25
4.3	Load indications in finite element packages	27
4.4	Load combinations for the in-place condition	27
4.5	Load combinations lifting condition	28
4.6	Resulting inertial load in transport condition	28
4.7	Load combination in the transport condition	28
4.8	Requirements for deflection in the SLS	29
5.1	Unity checks above 0.7 in the line model	33
7.1	Structural masses of the models	52
7.2	Decomposition of the welds in the beam-column design	55
7.3	Decomposition of the welds in the stressed skin design	55
A.1	Buckling factors for plates simply supported on four edges under single loading	76
A.2	Buckling factors for plates simply supported on three edges under single loading	76
E.1	Member results used for the analysis	119
E.2	Member properties of the members considered	120
E.3	Governing member design loads in member 56-6	121
E.4	Governing member design loads in member 10B-10	121
E.5	Governing member design loads in member 9B-9A	122
E.6	Governing member design loads in member 3A-56	123

List of Abbreviations

ABS	American Bureau of Shipping
API	American Petroleum Institute
ASD	Allowable stress design
CGCH	Change in centre of gravity during the lifting condition
CHS	Circular hollow section
DEAD	Dead load including modelled steel
DNV	Det Norske Veritas
EQPT	Equipment loading
FEM	Finite Element Method
HVAC	High Voltage Alternating Current
HVDC	High Voltage Direct Current
kV	Kilovolt
LIF1	Load combination during the lifting condition (general members)
LIF2	Load combination during the lifting condition (members framing onto the lifting points)
LIVE	Live loading
LRFD	Load and Resistance Factor Design
MISC	Miscellaneous loading
mT	Metric tonnes
MW	Megawatt
RHS	Rectangular hollow section
RIG	Rigging load
SHS	Square hollow section
SLS	Serviceability Limit State

TRNS	Load combination during the transport condition
ULS	Ultimate Limit State
WIND	Wind loading in specified direction



Introduction

1.1. Company and thesis background

Iv-Groep is a consulting and engineering company focused on cutting edge technology in several fields of engineering. By making innovative and sustainable designs, Iv-Groep has been granted with the design of a number of outstanding projects, such as the new Panama Canal lock doors and the London Eye. Iv-Oil & Gas is a branch of Iv-Groep that specializes in offshore structures and is primarily focused on the oil and gas market. Together with Iv-AGA (which is another branch of Iv-Groep) they perform the structural calculations on the offshore structures.

As natural resources deplete and there is an increasing demand in renewable energy sources, Iv-Oil & Gas more often gets asked to develop structures used in this field. Most predominantly amongst these are the offshore substations. These platform structures house the equipment needed to transfer the energy generated by offshore wind turbines to the shore without too much power losses on the way. Corrosive sea environment is maleficent for the equipment, and therefore, the whole structure must be provided with a protective shelter.

The need for offshore substations to be sheltered from the environment leads to the question if it is possible for this shelter to be integrated in the structural design of the substation. For an answer to this question, a solution in the form of stressed skin design is researched. The stressed skin design is a design methodology in which structural integrity is provided by plated steel elements, that are doubling as shelter structure in this particular application.

This thesis will analyse the feasibility of using load bearing steel plated elements in offshore structures, with an application to offshore substation modules (see section 1.3). Based on a comparative analysis in a case study, the most effective design is determined. From that, conclusions can be drawn to this particular case, which will be extended into a general qualitative conclusion about offshore substation design.

1.2. Objective

In the thesis, the goal is to investigate the application of the stressed skin method to offshore module structures. The feasibility of such a structure will be assessed in comparison to a design using a beam and column type of support structure. The overall question answered in the thesis is:

Will a design of an offshore module using steel plated elements be competitive in comparison to a design using beams and columns in terms of mass and weld labour?

1.3. Substation design

In search to reduce carbon emissions and fossil fuel consumption, alternative energy sources are being investigated. One of the promising concepts is that of wind energy. Traditional, on-shore wind turbines, however, can be aesthetically undesirable. A solution for that can be found in offshore wind generation. Additionally, due to the relative smooth surface at sea, winds are often stronger and more consistent.

Increased technical abilities reduce the cost of each Watt of harvested energy. This is reflected in the amount of installed capacity of offshore wind turbines. Figure 1.1 shows the capacity of installed wind turbines annually and cumulatively. It can be seen that since the 2000's, the operating capacity of the installed generators has grown rapidly, with the expectation that this trend will continue.

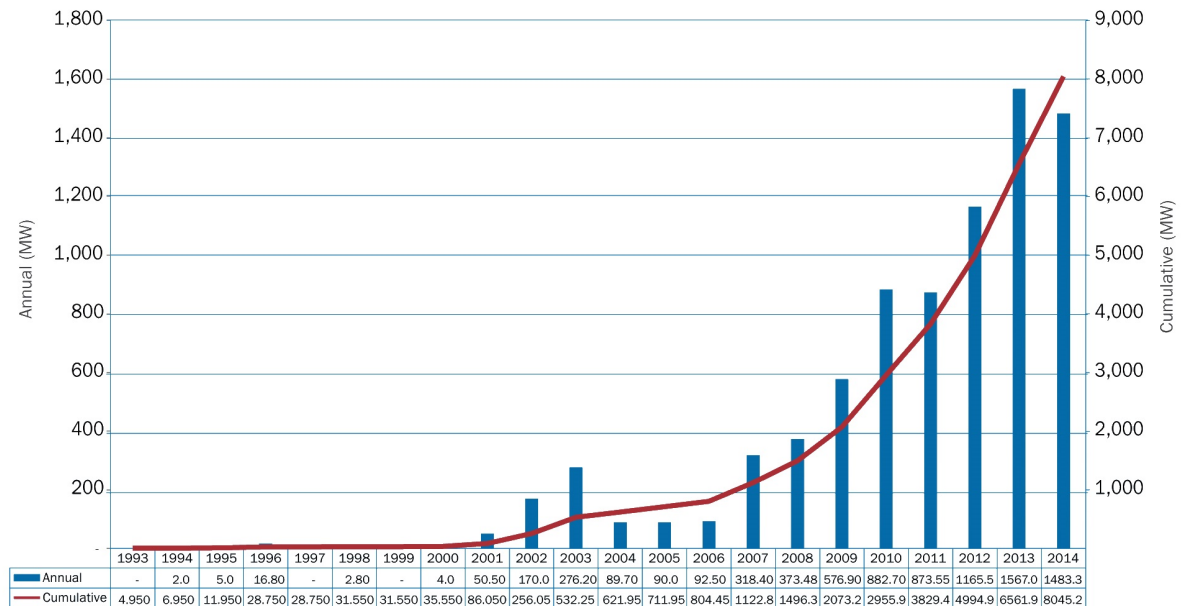


Figure 1.1: Offshore wind generating capacity in Europe installed per year and in total (image from: <http://www.offshorewindindustry.com/>)

Alongside the increase of total installed wind generating capacity, the capacity of individual wind turbine generators also increases. As is seen in figure 1.2, both the size and energy output of these generators tend to increase rapidly. On the one hand, this is an advantage, because less structures are needed to produce the same energy capacity. On the other hand, the bigger the turbines become, the farther they need to be placed offshore in order to not be visible from land.

Placing the wind farm farther offshore means that power loss in the cable can become substantial. In the early offshore wind farms, this was less of an issue, since the distances covered and the power that was harvested were relatively small. However, with the increase of distance to shore and power output in the generators, measures have to be taken to reduce the loss of power. This is done by implementing a transformer substation in the wind farm which collects the energy and steps up the voltage to a value in which these losses are acceptable.

1.3.1. By function

The transformer substation comes in two forms, the High Voltage Alternating Current (HVAC) and the High Voltage Direct Current (HVDC) substation types. In section 1.3.1 and 1.3.1, the pros and cons of both of these types is given.

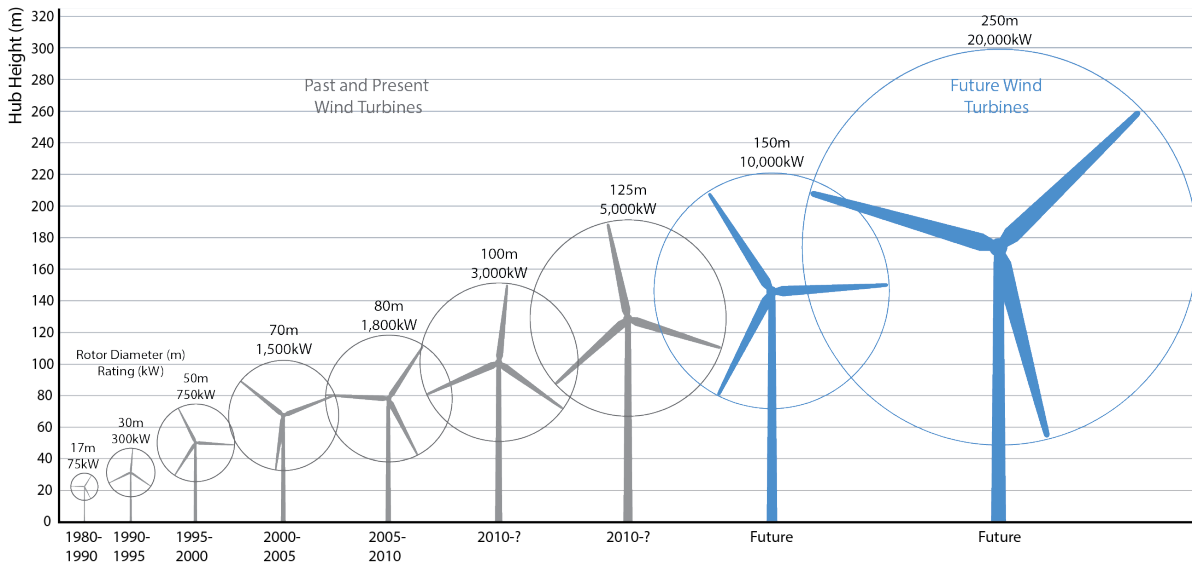


Figure 1.2: Maximum wind turbine size by year (image from: <http://www.myfloridahomeenergy.com/>)

High Voltage Alternating Current

In the case when the distance to the shore is not too big, a High Voltage Alternating Current (HVAC) substation can be implemented in the design of the wind farm. In this type of substation, the power from the wind turbines is stepped up to reduce the transportation losses. Generally, the power output from wind turbine generators is around 33 Kilovolt (kV), which is consequently stepped up to around 150 kV. Stepping up the voltage reduces the current, which is a factor in determining the resistance of a length of cable.

HVAC substations generally measure around $L \times B \times H = 40 \times 30 \times 20m^3$ and weigh in the range of 1000mT to 3000mT.

In these substations, the equipment for stepping up the voltage is housed. This electrical equipment is vulnerable to the conductive sea water, requiring this equipment to be sheltered from the environment. The sheltering can be made in different ways: the equipment can be housed in separate encasements (as is seen in figure 1.3) or the entire structure can be encased (as is seen in figure 1.4). Both of these structures are constructed using the conventional beam-column design methodology (see section 1.3.2).



Figure 1.3: Equipment housed in separate encasements (image courtesy of Overdick: <http://www.overdick.com/>)



Figure 1.4: All equipment in one encasement

High Voltage Direct Current

If distances to shore are of such magnitude that even stepping up to HVAC does not reduce the transportation losses to an acceptable level, additional measures have to be taken. One way of doing this is incorporating a High Voltage Direct Current (HVDC) substation into the wind farm. By the use of direct current, the capacity of the cable is used more effectively. Because the power has to be converted from alternating current to direct current, more equipment is needed. Therefore, the structure may become much larger than a HVAC substation. Generally, the dimensions of this type of substation lay in the order of $L \times B \times H = 75 \times 50 \times 30m^3$ and can weigh in excess of $10000mT$.

Typically, HVDC substations are implemented in the very large wind farms. Herein, power losses from the wind turbine generator to the HVDC substation may become substantial. It can therefore be decided to apply one or more collector HVAC substations in the project. In figure 1.5, the $10200mT$ topside of the HelWin beta HVDC substation is shown. In this topside, the stressed skin design methodology is used (see section 1.3.2).



Figure 1.5: The HelWin beta HVDC topside during transport (image courtesy of Heerema: <http://www.hfg.heerema.com/>)

1.3.2. Design methodology

The structural design of the topside can consist of one of several design methodologies. In this thesis, the conventional beam-column design is compared to the stressed skin design methodology. These are elaborated below.

Beam-column design

The more traditional approach for offshore structures, the beam and column design methodology is used extensively in the offshore oil & gas industry. The general absence of enclosed spaces prevents gas stacking up and provides a natural ventilation. As most of the offshore structures are used in the oil & gas industry, the beam and column design methodology is the most predominant.

The beam-column design methodology uses linear elements, e.g. (hot rolled) Circular hollow sections (CHS) and hot rolled wide flange sections. These elements are connected by welding, ultimately creating a space frame in which all of the equipment is housed. The use of the heaviest catalogue profiles is common. As these elements cannot be individually optimised, some parts of the structure might be overdimensioned. The beam-column design methodology is shown in figure 1.3 and 1.4.

Stressed skin

Commonly used in offshore living quarters, the stressed skin design methodology is not a new concept in the oil & gas industry. However, the application of the methodology on a topside as a whole is not done as frequently.

In the stressed skin design methodology, the function of the braces that provide the stability in a beam-column type of structure is replaced by plating present in e.g. the roof structure. The loading perpendicular to the structure is taken by the plating as shear load. In figure 1.6, the concept is visualised in the roof of a building. In contrast, the vertical portion of the structure is braced in the way as would be done when using a beam-column design methodology.

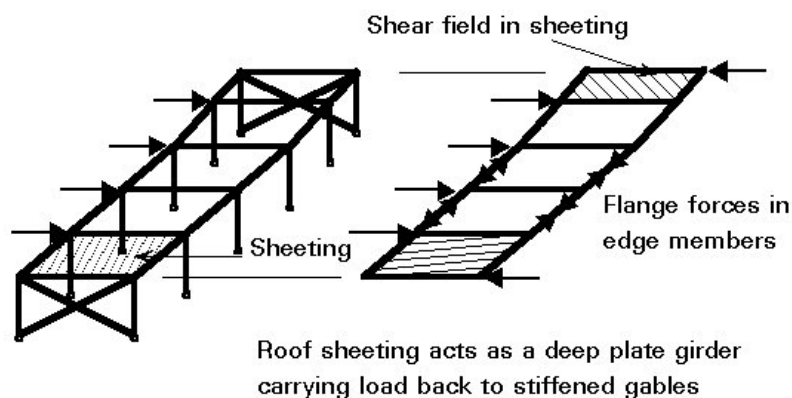


Figure 1.6: Stressed skin methodology applied in the roof of a building (image from ESDEP lecture 9.5)

The sheeting that is used for the stressed skin design methodology is generally unable to resist compressive stresses. Therefore, an edge strengthening is to be applied. Generally, this is done using a hot rolled section or a custom composed profile. The stressed skin panel can be regarded as the web of a deep plate girder, taking on the shear in. The edge strengthening can then be regarded as the flange of this member, taking on the compression and tension, analogue to the compression and tension in the flanges of a hot rolled member. The stressed skin design methodology is shown in figure 1.5.

1.3.3. Case study

The comparison of the different design methodologies described in section 1.3.2 is based on a case study. A suitable project for the analyses is found in the Thornton Bank wind farm substation. The structural design of this substation has been carried out by Iv-AGA [1].

The Thornton Bank wind farm is an offshore wind farm off the coast of Belgium. To hide it from view from land, it is situated about 30 km from the coast. The location of the wind farm is indicated in figure 1.7. Commissioned in 2013, the wind farm consists of 54 turbines delivering a combined power of maximum 325 Megawatt (MW). In order to reduce transmission losses in the export cables to the shore, the voltage has to be stepped up in an offshore substation.



Figure 1.7: Location of the Thornton Bank Wind Farm (image from <http://www.maps.google.com/>)

The substation structure consists of a four-legged jacket structure and a topside containing the electronic equipment. The water depth at this site is about 27 meters. On top of the jacket, a 2000mT topside has been placed. Figure 1.8 shows the Thornton Bank substation as it has been realized. In the thesis, only the topside is considered. A render of the reference design is given in figure 1.9.



Figure 1.8: Thornton Bank substation as built

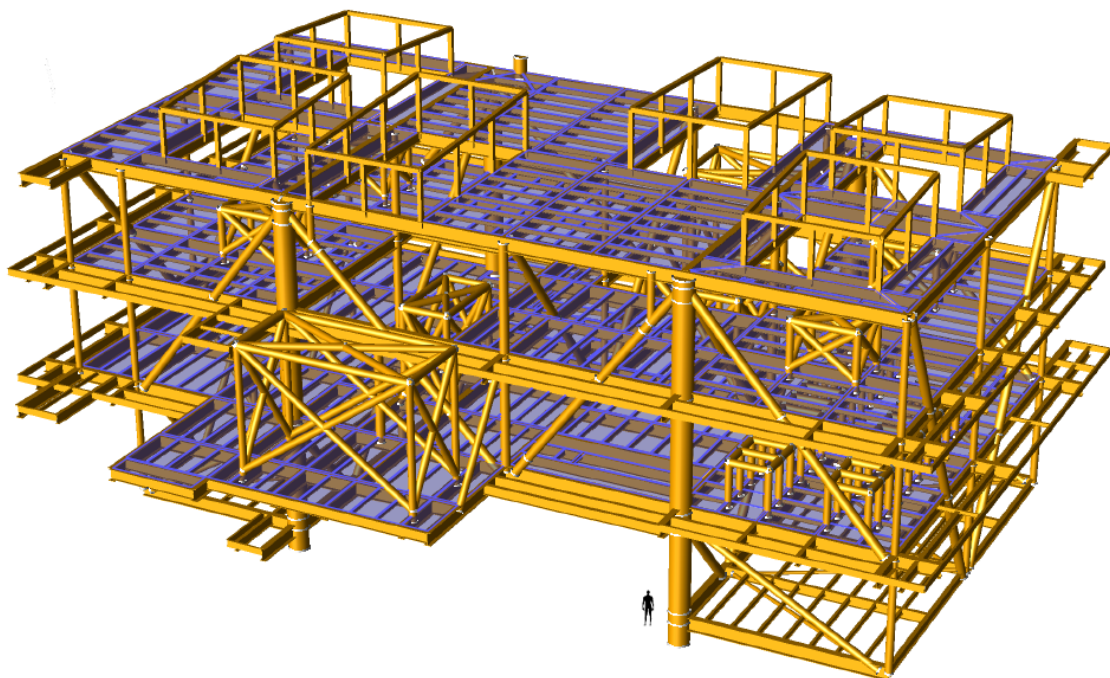


Figure 1.9: Model as designed by Iv-AGA [1]

1.4. Thesis outline & boundary conditions

In this section, the overall outline of the report is presented and the scope of this thesis is clarified.

The design of the Thornton bank substation consists of a topside weighing in the order of $2000mT$ (Metric tonnes), which can be considered an average weight for a HVAC topside servicing a moderate wind farm with an energy output of around $300MW$. The general applicability of this thesis lies in the weight range of around $1000mT$ to $4000mT$. Above and below these values, the concept of the design is subject to change: for structures below $1000mT$ a monopile foundation could be more efficient, for structures above $4000mT$ the number of legs becomes likely to increase. In both cases, the distribution of forces and stresses are bound to change and the proposed conclusions cannot be drawn in these situations.

In section 2, an overview is given of the state-of-art in steel plate technology in the format of a literature study. Part of this literature study is an introduction to the phenomenon of plate buckling. Section 3 deals with the software that is used in the thesis. The software package of choice when analysing beam-column type of structures is the SACS suite of software. As the SACS suite is typically not used for the analysis of plated structures, the Ansys suite of software is required for the modelling of the stressed skin design. The working of both of these software packages is evaluated and procedures that are used are demonstrated.

The design requirements for the purpose of this thesis are given in section 4. This involves a simplification of the basis of design that is produced by Iv-AGA [1]. The latter is made including all specifications that are required to design the structure. These include many elements that are considered to be too detailed for the purpose of this thesis, e.g. the exact locations of the equipment loading, which are used to design the equipment support beams. In this thesis, the focus is on the overall structural concept and therefore the basis of design is generalised.

The model that is built up from the simplified design requirements is presented in section 5. This model is more uniform than the design by Iv-AGA. Therefore, the conclusions that are drawn from this model can be generalised to be applicable to the overall concept of the design methodology. As this model is highly generalised, the behaviour of the overall structure can be consolidated to the behaviour of its elements. In order for the structure to then be a system in which the design methodology fulfils its purpose, a structural frame is chosen to base the comparison on. In section 5, the considered frame is chosen and the loading on this frame is determined.

Section 6 introduces the different designs. In section 6.2, the beam-column design set up using the SACS software is considered. The stressed skin design in Ansys is presented in section 6.4. Herein, the considered plating solutions that are looked at are the stiffened flat plate and the corrugated panel. As these models are built up using different software packages, the software is compared by modelling the beam-column design also in Ansys. Here, a comparison is made on the output of the different software packages in terms of level of safety. This Ansys design is provided in section 6.3.

The designs are then compared on steel mass and welds in section 7. Herein, the mass is compared directly. The welds are subdivided in categories that indicate the labour that is required to complete the welds. Combining the two parts results in an overall score of the design.

The results from the comparison are presented in section 8. In addition to the main conclusions that are drawn from the mass and weld comparison, some conclusions are drawn from modelling and designing the different variants. All of these conclusions are stated.

2

Literature review

For the analyses in the following sections to be carried out, some research has to be done in order to provide with a decent background in the topic. This is done in the format of a literature study. In the following, a summary is given to this research. The full analysis of the literature is given in appendix A.

2.1. Books & theses

The most complete format of the reference to the project can be found in books. Few specialistic books on the subject of steel plated elements in the offshore industry exist. One of these is Ultimate Limit State Design of Steel-Plated Structures by Paik and Thayamballi [2]. Herein, all aspects of steel plate design are addressed. A more detailed overview can be found in appendix A.1.

Timoshenko and Gere [3] provides an introduction into plate buckling, as well as a range of other relevant topics. The clear steps in the book are generally applicable for a wide variety of load conditions. In appendix A.5, plate buckling under various types of loading is described mathematically by the help of this book.

This thesis is an extension of the masters thesis of Jianping Xu [4]. In the report, a substation module is designed that is transported offshore. A small module, the original beam-column type structure was replaced by a stressed skin design. Herein, the plating served purely as a replacement of the bracing. Due to harsh weather conditions in the case study project area, some additional requirements were posed to the insulation of the substation. Therefore, in addition to the stiffened flat plate and the corrugated panel, sandwich panels were considered in the design. Overall, the corrugated panel yielded the best results for application in this type of substation. A more in-depth analysis of the thesis can be found in appendix A.2.

Aberkrom [5] poses an introduction to plate buckling. Several parameters of influence are analysed in combination with prescriptions from the codes. Herein, the Allowable stress design (ASD) codes of the American Bureau of Shipping and Det Norske Veritas are used. It is stated that the parameters that are applied in these codes are sufficient to determine the buckling capacity of simple models. For more complex models, however, additional parameters need to be considered. The full procedure is provided in appendix A.2.

2.2. Papers & codes

In the literature review, papers concerning the subjects that are covered in the thesis are considered. Mainly, the state of art in steel plate structures is covered. The focus herein lays on both stiffened steel plates and corrugated panels. As the structure has to comply to the governing codes, these are looked at to find what flexibility in the design is allowed and the limits of their application. The full extracts of the papers described below can be found in appendix A.3.

Paik and Thayamballi [6] introduces several failure modes for steel plated structures. Also, methods are given for determining the bearing capacity of the structure by hand. For each of the failure modes, an indication is given for when to expect such failure. This way, a certain feeling for the behaviour of the plated structure is obtained and measures to reduce the sensitivity for each of the failure types can be introduced accordingly.

One of the failure modes described by Paik and Thayamballi [6] is also regarded by Paik et al. [6]. This paper deals with the occurrence of global plate buckling, in which the stringers are too weak to prevent the buckling of the entire plate. A representative unstiffened plate is proposed that takes into account the orthotropic properties of the stiffened steel panel.

The removal of the hot rolled sections in the design calls for an application in the direction of plate girders. The behaviour of these plate girders is considered in Abspoel [7]. In the study, the bending moment capacity of the plate girder is investigated. The maximum bending moment capacity for a certain steel mass is determined.

the plate girders can be extended by involving different steel grades, the so called hybrid girders. Veljkovic and Johansson [8] investigate the applicability of such girders. In codes valid elsewhere, the use of different steel grades in a single profile is common practice. This paper introduces the phenomenon to the European industry. In the following thesis, only one steel grade is assumed to be present.

A plate configuration that by its nature shows reasonable stiffness, the corrugated panel is investigated by Hosseinpour et al. [9]. The geometry of the panel is investigated and it is found that it depends on several factors if the sinusoidal or trapezoidal corrugates score better. El-Amin et al. [10] adds that for relatively large corrugations, it is not particularly necessary to provide lateral stiffening.

The use of corrugated panels in offshore applications is considered in Sun and Spencer [11]. Herein, mainly the use of the corrugated panel in offshore living quarters is addressed. The research is done in light of the ABS standards and therefore should be converted to the LRFD standards used in this thesis. In the paper, some definitions are given that the ABS standards use for determining the local buckling of the corrugated pane. Using these definitions on a case study, it is concluded that the corrugation angle should be as large as possible and that a deep corrugate with thin plating is more efficient than a small corrugate with thick plating.

In the designs, the post buckling behaviour of the steel plates were used. The applicability thereof is considered in Alinia and Dastfan [12] for plated elements loaded in shear. The support condition (simply supported or clamped) is investigated. For loads under the shear buckling load, a 80% clamping of the supports is found to be best matching the test results. For loads that exceed the shear buckling load, the support conditions do not have any influence.

Rhodes [13] discusses the post-buckling behaviour of thin walled structures. Herein, the notion of effective width is also considered and it is shown that the structure possesses a significant additional strength after the plate field has buckled. The influence of support conditions is also investigated.

In order to prevent the occurrence of global plate instability, Sabouri-Ghomi et al. [14] introduce requirements for the stiffeners, such that the buckling pattern will be local. An analytical derivation poses the area moment of inertia that the stringers should have to induce the local type of buckling. This derivation is supported by a FEM analysis.

The designs are complying to the codes. In section 4.1, the codes that are used are elaborated. Herein, Load and Resistance Factor Design (LRFD) codes are used. These codes utilize an effective width of the plate field to simulate the buckled shape. This effective width is dependent on the geometry and the loading condition on the plate. Alternatively, a method using reduced allowable stresses is posed. However, the method using effective width is recommended. Full details are found in appendix A.4.

The methods described above originate from the original derivations of plate buckling under several types of loading. These are well described by Timoshenko and Gere [3]. In appendix A.5, the applicable derivations for plate buckling are given in a concise manner.

3

Numerical modelling

Since the introduction of Finite Element Methods (FEM) for the analysis of engineering problems, its value to the engineer has grown steadily. In the last decades, the occupation of an engineer has shifted from executing the calculations manually to modelling and interpreting finite element results. As the computational power of present day computers has increased exponentially, the complexity of the models and software packages is also increased.

In the FEM, the structure to be analysed is subdivided in a mesh of small elements, called finite elements. Then, instead of analysing the structure as a whole, the structural behaviour of the individual elements is checked. Using boundary conditions on the interfaces between these elements, the entire structure is considered.

In section 3.1 and 3.2, the modelling using FEM is elaborated. First, the use of the FEM program SACS is considered. Thereafter, the program of Ansys is looked at.

3.1. Numerical modelling in SACS

At Iv-Oil & Gas, the SACS suite of software is primarily used as a line element software. In this application, the models composed are generally less complex when compared to the models made in Ansys, as the line element modelling is computationally less intensive than the FEM. A drawback of this simpler design is that particular care has to be taken in the assumptions that are used to form the model. The most important aspects are covered in section 3.1.1.

3.1.1. Member modelling

The SACS software, used as line element analysis software, consolidates the physical properties of the members into their centreline. Also, for the stability check of the members, it conservatively assumes that the elements are connected by hinges. To provide a more realistic result in the analysis, some additional information is to be entered manually. At Iv-Oil & Gas, it is customary to use conservative values in an early design stage. These values are adjusted in later stages, should it be necessary. Since not applying the measures can lead to unrealistically high design verifications, these measures are included in present design.

Reduced member lengths

In the line modelling, all elements are defined by their centreline. At connections with other members, this means that there is an overlap in the elements. The appending members can therefore be offset to the connection with the main member (at a distance of $\frac{D}{2}$ from the centre of the member). The part of the member that is omitted may be considered to be rigid by section 12.3.3.3 of ISO19902 [15]. This omitted part is shown in red in figure 3.1.

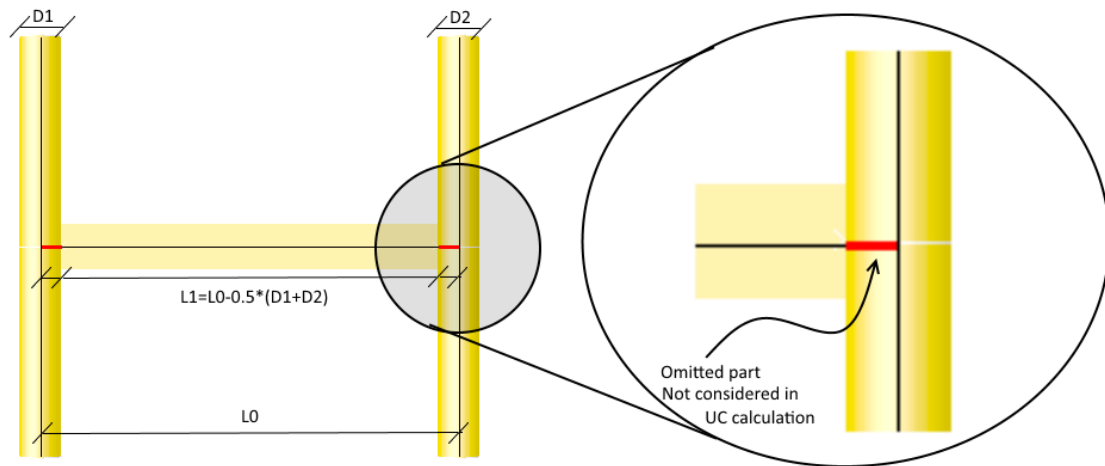


Figure 3.1: Member length L_1 that is taken into account in the analyses

Disregarding this part of the member has several advantages:

- The software does not perform a design check on this part of the member, which is often the location of the critical cross section.
- The buckling lengths are reduced, which leads to a more realistic representation of the reality.

No loading is acting on the omitted member part. However, a loading on this piece coming from the surrounding plate is to be considered. The loading on this part is modelled as acting on the remaining part of the member. This value is therefore increased and gives a conservative result.

Moment resisting joints

The joints in the model are considered to be moment resisting when calculating the internal member forces. However, during the design verification, the influence of the moment resisting joints is not considered. For the verification of the member cross sections, this would not be an issue, since the cross section is verified directly from the occurring member forces. In the verification on buckling, the member length that is to be considered depends on the support conditions. This is accounted for by reducing the buckling lengths of all diagonal tubular members to $l_b = 0.7 \times l_{member}$, as is stated in ISO19902 table 13.5-1 [15].

Design verification

The SACS output consists of the occurring member forces and the accompanying design verifications. These verifications are based on the codes that are specified in the analysis. Documentation of the SACS analysis shows the outcome of the applied codes, from which the governing verification is chosen. In the thesis, the ISO19900-19906 [16] is used for the tubular members and the EN1993 [17] is used for the other sections. A sample calculation of the code checking is given in appendix E.

3.2. Numerical modelling in Ansys

In the modelling using Ansys, several assumptions have to be made: the element type, mesh size and shape, and analysis type have to be chosen. All of these aspects have to be adapted to yield optimal and realistic results. The requirements for these aspects are given in sections 3.2.1 to 3.2.4.

3.2.1. Element type

The element type is chosen based on the geometry of the structure and the desired analyses that are to be carried out. In the Ansys suite of software, the element type is indicated with a geometric description and a number specifying the mathematical properties.

In the analysis of the present structure, shell elements are used. Depending on the input, different element types are used. The element library of Ansys provides several shell type elements, each with its own characteristics. When looking for a non-symmetric, single layered element that has both in-plane (extensional) and out-of-plane (bending) stiffness, only the elements Shell63, Shell150, Shell181, and Shell281 are applicable. Herein, Shell63 is considered an outdated element (Shell181 being its replacement) and Shell150 is particularly applicable to curved elements. This leaves the Shell181 and Shell281 element type to be the most useful.

The Shell181 element type consists of a 4-node element which shows a linear interpolation scheme. At each of the nodes, the element has 6 degrees of freedom (3 translational DOFs and 3 rotational DOFs). The bending resistance of the element is achieved by a number of integration points through the thickness of the element. The default value of this number is 3, but it can be adjusted to 1, 3, 5, 7, and 9. The element is considered to have no out of plane shear stiffness. The behaviour is based on the Reissner-Mindlin plate theory. Figure 3.2a shows the integration scheme of the Shell181 element type. Herein, only the corner nodes are considered. Since no information is present for positions between the nodes, the element is interpolated linearly.

The Shell281 element type is an 8-node element that uses a quadratic integration scheme. The other specifications are the same as for the Shell181 element type. The nodes are visualised in figure 3.2b. As opposed to the Shell181 element, the Shell281 element determines the displacements on the corner joints as well as the mid-edge nodes. The deflection over the element edge is interpolated in a quadratic manner.

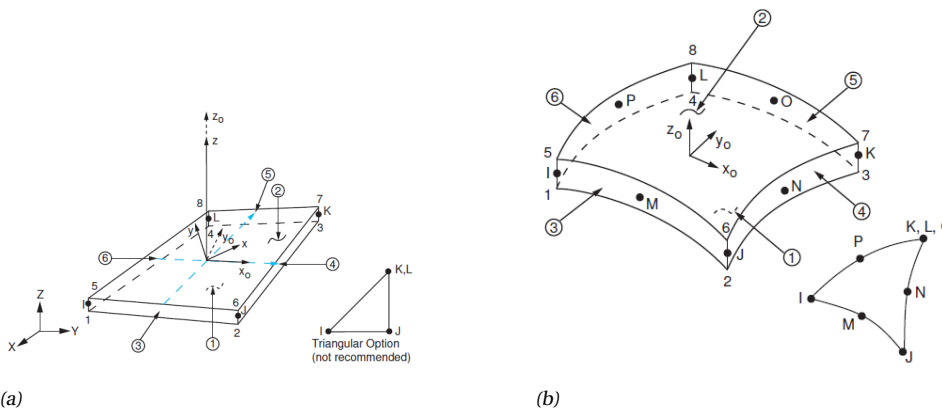


Figure 3.2: Integration scheme of the Shell181 (a) and the Shell281 (b) elements

3.2.2. Interface

The Ansys software is gradually switching from a scripting oriented model input (Ansys APDL) to an input using a more user-friendly Graphical User Interface (Ansys Workbench). As both of the interfaces are currently available, a decision should be made as to which one to use. Therefore, a sample calculation is made in both environments, which is then analysed on result accuracy, calculation time, modelling time, and number of elements.

The sample calculation consists of a flat plate of 15mm thick. The edges are 1.5m by 2m and are simply supported. The material used is structural steel with a Young's modulus of 210GPa and Poisson's ratio of 0.3. The yield strength is not relevant, since all of the analyses will be carried out in the elastic regime: only in the post-processing, it could be checked if the occurring stresses do not exceed the yield strength. The loading is applied as a constant pressure in one direction, normal to the edge. The loading is shown in figure 3.3. The calculation carried out is an Eigenvalue buckling analysis.

It is tried to find the buckling mode with the lowest buckling load for the loading direction indicated in figure 3.3. For the analysis, Eigenvalue buckling is considered and the first mode yields one half sine wave in both directions, which is visualized in figure 3.3. The Eigenvalue buckling analysis predicts the theoretical buckling strength of an ideal linear structure, and should therefore be in accordance with the theoretical textbook values. This theoretical value is determined and the approaches to the numerical modelling are given in this section.

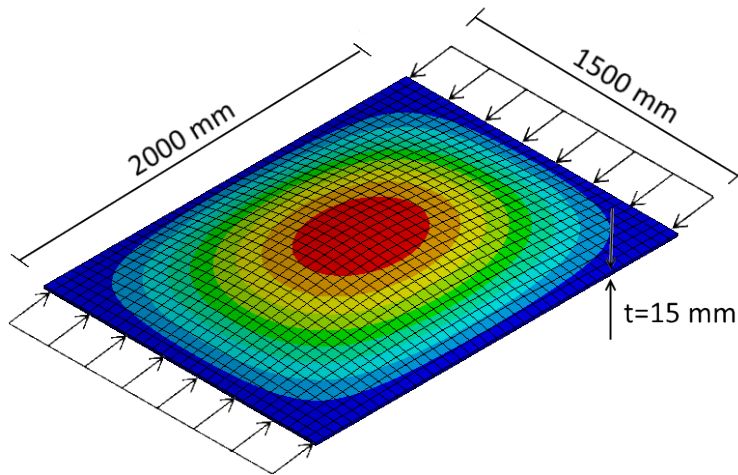


Figure 3.3: First buckling mode shape of a rectangular plate

Theoretical result

The expressions that are required to determine the buckling resistance of the rectangular plate shown in figure 3.3 are given in appendix A.5.1. From equation A.16, the following theoretical buckling resistance is determined:

$$n_{xx,el} = \frac{\pi^2 D}{b^2} \left(\frac{bm}{a} + \frac{a}{bm} \right)^2 = 1235.6 N/mm \quad (3.1)$$

using one half wave length in direction of the loading (as shown in figure 3.3), $a = 2m$, $b = 1.5m$, and D as follows:

$$D = \frac{Et^3}{12(1-\nu^2)} = 64.90 * 10^6 Nmm \quad (3.2)$$

Ansys APDL

In Ansys APDL, a distinction is made between a scripted input and a graphical input. Both of the input methods use the APDL language for their commands. For the purpose of the analysis, a script has been set up. This speeds up the analysis of the parametric study, as the entire script can be loaded instantly, only changing for the parameter considered. The script is given in appendix B.

Since the input is in the format of a script that contains the bare commands the software uses, the analysis will be carried out unobstructed and is therefore as fast as possible. The lack of automation of geometry and loading, however, calls for a complete tracking of element and node numbers. Especially for large assemblies, this can lead to inconsistencies and errors.

Ansys Workbench

In the Ansys Workbench interface, element selection is not as straightforward as in the Ansys Mechanical environment. Through several specific design inputs, the element type is determined. The settings used result in either Shell181 or Shell281 elements.

An advantage of the Workbench over Mechanical is the Project Schematic, which allows for a system of linked analyses in a comprehensive overview. This fact comes in handy when assembling several submodels.

Comparison results

The test structure presented in figure 3.3 is modelled in both Ansys Mechanical and Ansys Workbench. The results from this analysis are given in table 3.1 and compared to the theoretical result from section 3.2.2. Varying the number of integration points does not change the outcome of the Eigenvalue buckling analysis.

Table 3.1: Comparison of results from Ansys APDL and Workbench

		# of elements (linear)	# of nodes	Computing time [s]	Modelling time [min]	Resistance to buckling [kN/m]
Ansys APDL Shell181	Coarse	3	16	1	10	1566.2
	Medium	10	121	1	10	1259.1
	Fine	30	961	2	10	1235.1
Ansys APDL Shell281	Coarse	3	40	1	10	1218.1
	Medium	10	341	2	10	1226.1
	Fine	30	2821	3	10	1226.4
Ansys Workbench Shell181	Coarse	3	16	5	5	1457.4
	Medium	10	121	5	5	1250.9
	Fine	30	961	8	5	1233.3
	Extra fine	100	10201	15	5	1227.8
Ansys Workbench Shell281	Coarse	3	40	5	5	1193.9
	Medium	10	341	5	5	1201.8
	Fine	30	2821	10	5	1202.0
	Extra fine	100	30401	60	5	1202.0
Ansys Workbench Solid186	Coarse	3	96	5	5	1242.8
	Medium	10	803	5	5	1221.3
	Fine	30	6603	10	5	1221.0
	Extra fine	100	71003	100	5	1222.9
Analytical Solution						1235.6

It is seen that for greater number of elements, the results of the shell element models tend to converge to a value that is close to the value obtained theoretically. Figure 3.4 shows this convergence. The quadratic elements converge at a much faster rate than the linear elements. However, the increased accuracy comes at a cost of computational time. It is seen that the Shell281 elements show an Eigenvalue buckling load that is somewhat smaller than the theoretical buckling load, whereas solid elements tend to give unreliable results by the simple integration points through the thickness of the element. Therefore, it is chosen to use the linear elements of Shell181 and a medium mesh in subsequent analyses.

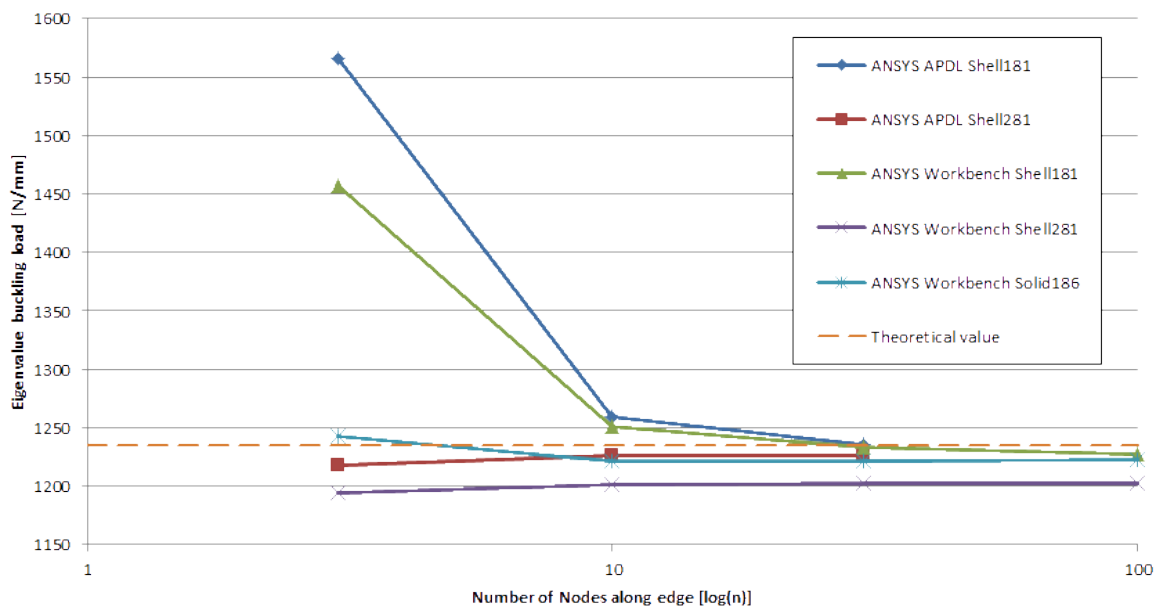


Figure 3.4: Eigenvalue buckling load plotted against number of nodes and element type

3.2.3. Analysis type

It is important to use a suitable type of analysis in order to get accurate results. The comparison in section 3.2.2 is carried out using an Eigenvalue buckling analysis, which is a non-conservative analysis method for determining the buckling strength. Geometric imperfections prevent the structure to attain the buckling load determined above.

In order account for the influence of these imperfections, a non-linear buckling analysis should be performed. For this purpose, an incremental load is applied to the structure.

Under incremental loading, a perfect flat plate will remain in its original shape until the buckling load is reached. If the loading is then increased, the plate will show excessive deformations in the out of plane direction. A residual strength is obtained via the boundary conditions of the plate. In figure 3.5, the loading of a perfect plate is plotted against the lateral deflection.

If an initial imperfection is applied, the occurrence of a sudden buckling is not observed. Instead, the deflection occurs much more gradual. By the absence of a specific bifurcation point, it is said that buckling occurs when the loading-deformation curve is flattened by an arbitrary degree. The deflection that a plate structure under small imperfections shows is plotted in figure 3.5.

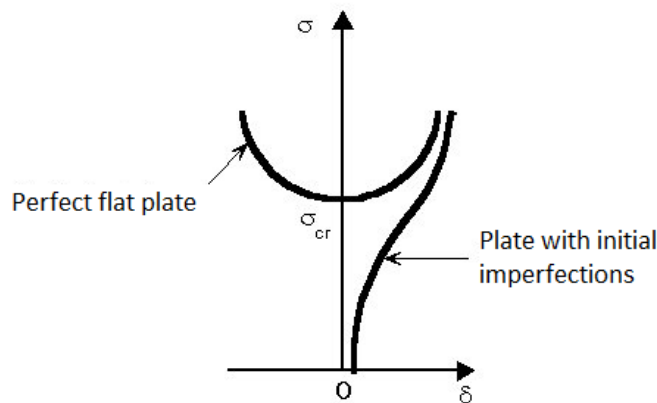


Figure 3.5: Applied loading plotted against lateral deflection (image from ESDEP lecture 6.2)

Finite Element software is quite unable to deal with sudden transition points. A perfect flat plate, for the software, is in unstable equilibrium, and therefore shows no buckling behaviour. This poses an additional incentive to apply initial imperfection.

Non-linear analysis

The same plate as described in section 3.2.2 is regarded for a non-linear buckling analysis. Under several values for the initial imperfection, the buckling of the plate is analysed. In order to achieve this level of initial imperfection, a small initial deflection in the range of several micrometres to 2 millimetres is applied to the plate by a lateral pressure. In figure 3.6, the deformation of the plate is plotted against the applied loading on the plate edges.

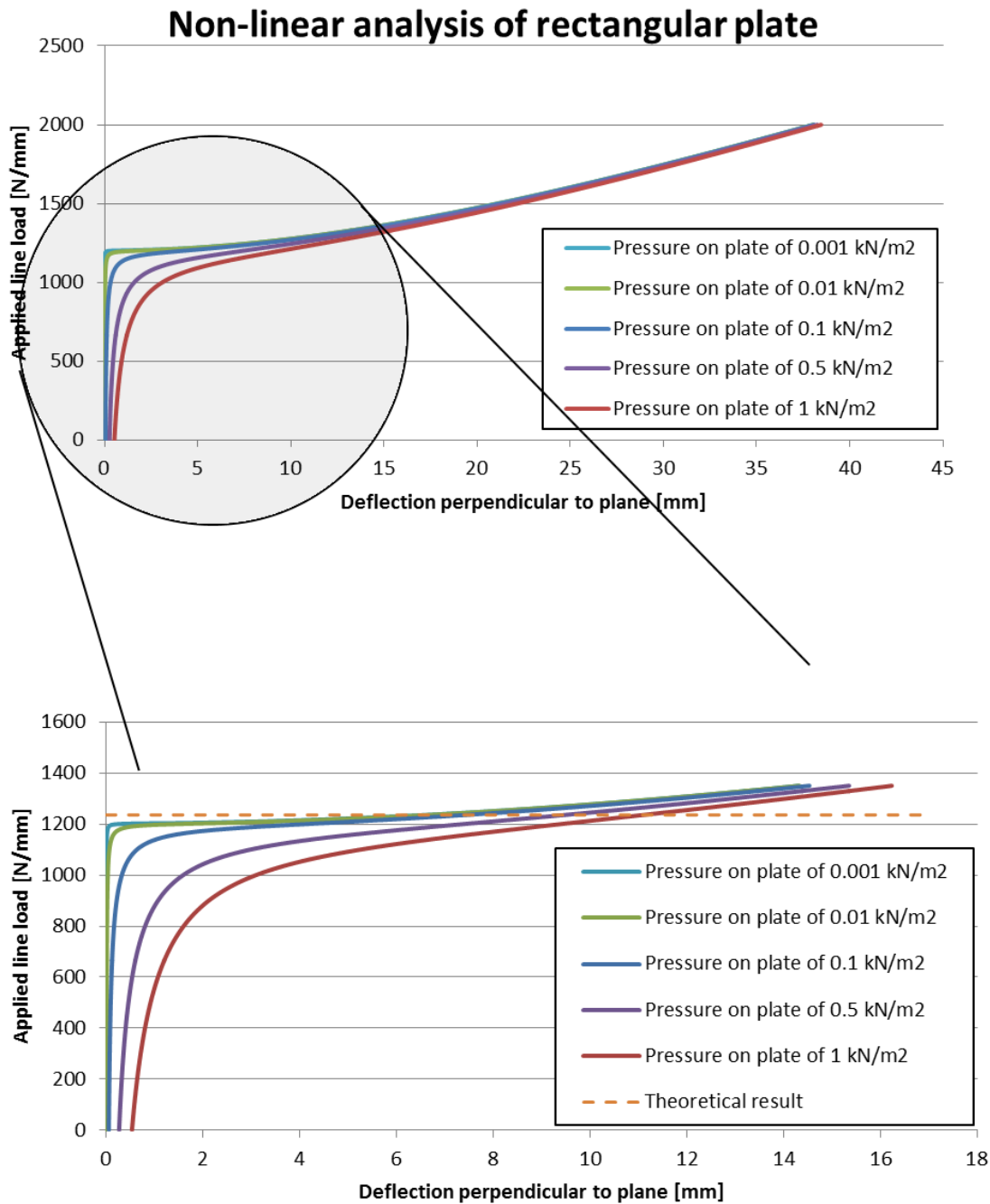


Figure 3.6: Applied loading plotted against lateral deflection of the non-linear analysis

In the upper graph of figure 3.6, it is seen that the structure shows a substantial post-buckling strength. The value of the initial imperfection is of little influence on the results in the post-buckled regime. It is noted that the material used in this analysis is linear elastic, and therefore the structure behaves elastically during the entire analysis. Because of the geometric non-linearities, the load is not distributed uniformly. It is therefore required to assess the actual stress distributions in the post-processing.

The lower part of figure 3.6 zooms in on the buckling of the structure. Here it can be seen that for the smaller initial imperfections, the structure shows behaviour that resembles the graph of a perfect flat plate in figure 3.5. Increasing the initial imperfection shifts the loading-deformation curve to the graph with initial

out-of-flatness in figure 3.5.

For the smaller initial imperfections, it is shown that buckling will occur at a loading of around $1200\text{N}/\text{mm}$, which is just under the theoretical buckling load of $1235.6\text{N}/\text{mm}$, as calculated in 3.1.

Even for small values of the lateral pressure applied to the plate, the buckling phenomenon becomes a rather gradual process, in contrast to the sudden occurrence of buckling when a negligible initial deformation is applied. For a lateral loading of $0.5\text{kN}/\text{m}^2$ and up, buckling is observed by a reduction in stiffness similar to the post-buckling stiffness. This is opposed to the stiffness of a perfect flat plate during buckling, which is close to zero. Because of the occurrence of this phenomenon at relatively low initial deflection, the asymmetric nature of the loading on the structure and the geometry is expected to induce these imperfections.

3.2.4. Assembly

The geometry of the structure is set up in the DesignModeler program within the Ansys Workbench. The assumptions that are considered in the modelling are elaborated in this section.

Mesh sizing

One thing to keep in mind when constructing an assembly of parts is the validity of the applied mesh. The Shell181 element type prefers to use quadrilateral elements. Tetrahedral elements are also usable, but it is advised to use them sparsely. When connecting meshes consisting of different mesh sizes, it will be inevitable to use tetrahedral elements.

In order to achieve an accurate result, there are some limitations to the aspect ratio of the elements. As the judgement of sufficient accuracy of the result is arbitrary, no strict limitations exist on the dimensioning of the elements. Normally, an aspect ratio that does not exceed 1-to-5 is considered to be acceptable.

Stringer element type

The application of stringers can be done in multiple ways, ranging from a full modelling of the stringer plating to adjusted material properties of the parent plating. Implications of the choice of stringer modelling affect the computational time and accuracy. Generally speaking, methods that require less computational time yield results that are less accurate. In this section, the method of modelling the stringers is assessed.

Model definition The geometry of the model that is used for the analysis of the different methods of stringer modelling is given in figure 3.7. The structure consists of a square plate with edges of 6m . The plate thickness is 30mm . The one stringer is located halfway along the length and has the following dimensions:

Web height ¹	150mm
Web thickness	10mm
Flange width	200mm
Flange thickness	10mm

The plate is loaded with a distributed load of $1\text{kN}/\text{m}^2$.

Full modelling The method that is expected to yield the most accurate results is using plated elements to model the stringer. Because of the full modelling of the stringers, buckling modes that include the stringers are taken into account as well. The high degree of accuracy comes at the price of computational efforts.

Line element modelling In order to decrease the time taken by the computations, the stringers may be modelled as beam elements attached to the parent plating. In this modelling, the buckling modes involving the stringers are not taken into account. Therefore, the modelling loses accuracy to the benefit of computational time.

¹Measured from centreline of the parent plate to the extreme point in the flange

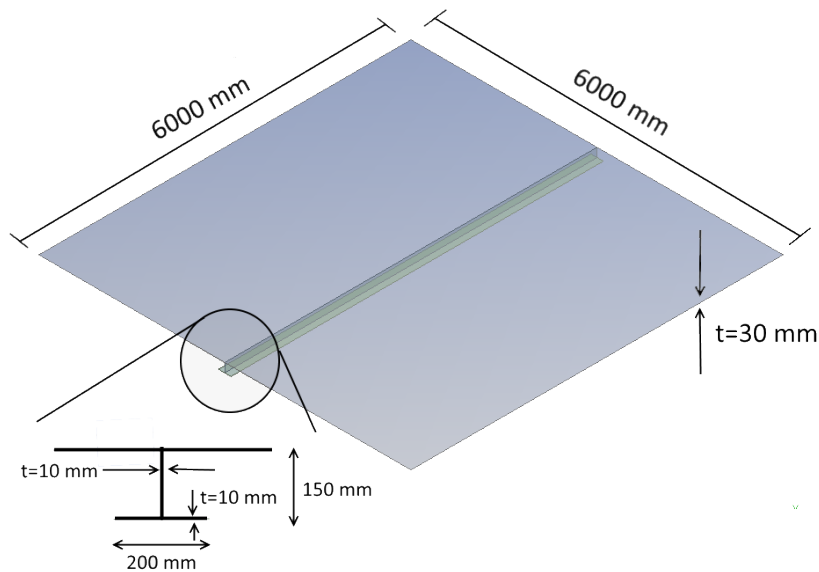


Figure 3.7: Plate with one longitudinal stringer for analysis

Comparison of results As is concluded in section 3.2.2, the mesh size used for the analysis of the structure will be in the order of 10 elements in any direction. For this structure, an element size of 300mm is therefore used. A distinction is made between linear and quadratic elements in the comparison. The values that are obtained via this way are compared to the results of the same analyses using element sizes of 100mm and one analysis using element size of 50mm for the full modelling. The latter is used as a reference to the accuracy of the former analyses.

It is chosen to compare the results of the analyses on the maximum deflection in the structure. In order to get workable results, it would have been better to use the maximum stress in the plating. However, the location of the maximum stresses in the full modelling is generally in the stringers, whereas there is no detailed stress calculation in the line modelling. Therefore, the maximum deflection is used.

In table 3.2 the results are shown.

Table 3.2: Comparison of full stringer modelling vs. stringer modelling using beam elements

	Element types	Element size [mm]	Computation time [s]	# of elements	# of nodes	Max deflection [mm]
Line elements	Linear	300	4	420	461	3.931
		100	12	3660	3781	3.964
	Quadratic	300	5	420	1301	3.989
		100	20	3660	11101	3.990
Full modelling	Linear	300	5	460	504	3.907
		100	15	3840	3965	3.950
	Quadratic	300	5	460	1467	3.957
		100	30	3840	11769	3.959
		50	>>60	15246	46233	3.960

It can be seen that, considering the variables taken into account, the results of the maximum plate deflection are quite accurate. The largest deviation to the reference analysis is $\frac{|3.931-3.960|}{3.960} = 0.73\%$. Therefore it can be said that all analyses conducted in this section are accurate enough.

In the analysis of the entire topside, modelling of the stringers using full element modelling is used. This is done in order to make the modelling easier to perform and computation time is not heavily impeded. In line

with section 3.2.2, the linear elements of Shell181 are used with a medium mesh sizing of 10 elements per edge or member cross section.

Applying the measures described in this section, a geometry as given in figure 3.8 is made. Herein it is seen that, opposed to the line element modelling used by SACS, the members consist of physical dimensions. Therefore, connection between members are automatically placed at the outer plane of the connecting members (for which in the SACS modelling additional measures had to be taken, see figure 3.1).

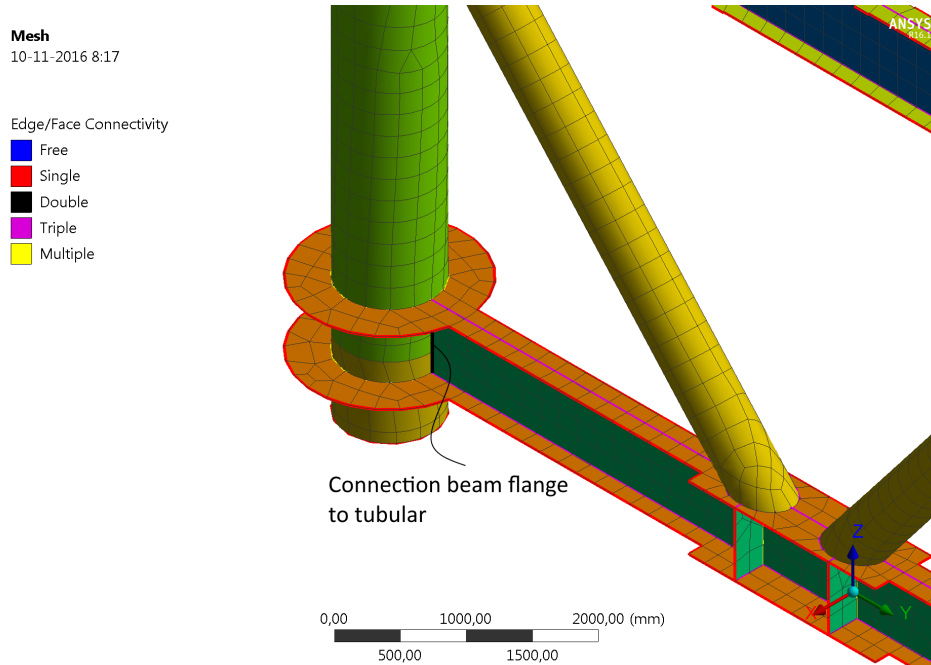


Figure 3.8: Detail of the node at the support: mesh for the beams and some strengthening measures (to reduce member distortion, see section 6.3) are visible; it is also seen that the beam web terminates at the interface with the tubular

3.2.5. Actual stress distribution

Because the flat plate shows a deformation when buckling, the stress distribution in the plate is not uniform. In the codes, this phenomenon is addressed by an effective width that has been taken into account. The Ansys software package is capable of determining the actual stress distribution in the plate when it is buckling. Comparing these two methods should verify their applicability.

In figure 3.9, the stress distributions in a cross section located halfway along the plate in loading direction is given for different stress levels with regard to the buckling strength. For a relatively low loading, the stresses in the cross section are close to the uniform level of $\sigma_x = \frac{N_x}{t} = \frac{450}{15} = 30 \text{ MPa}$ (see figure 3.9a). At the buckling level, the stresses in the centre are only $\frac{72.0}{100.4} = 71.7\%$ of the stresses at the supports (see figure 3.9b). In the post-buckling situation, this value decreases to $\frac{27.3}{340.4} = 8.0\%$ (see figure 3.9c). Therefore, it can be said that the middle section of the plate does not contribute in the strength if the plate has been buckled, which is the proposition in the effective width method.

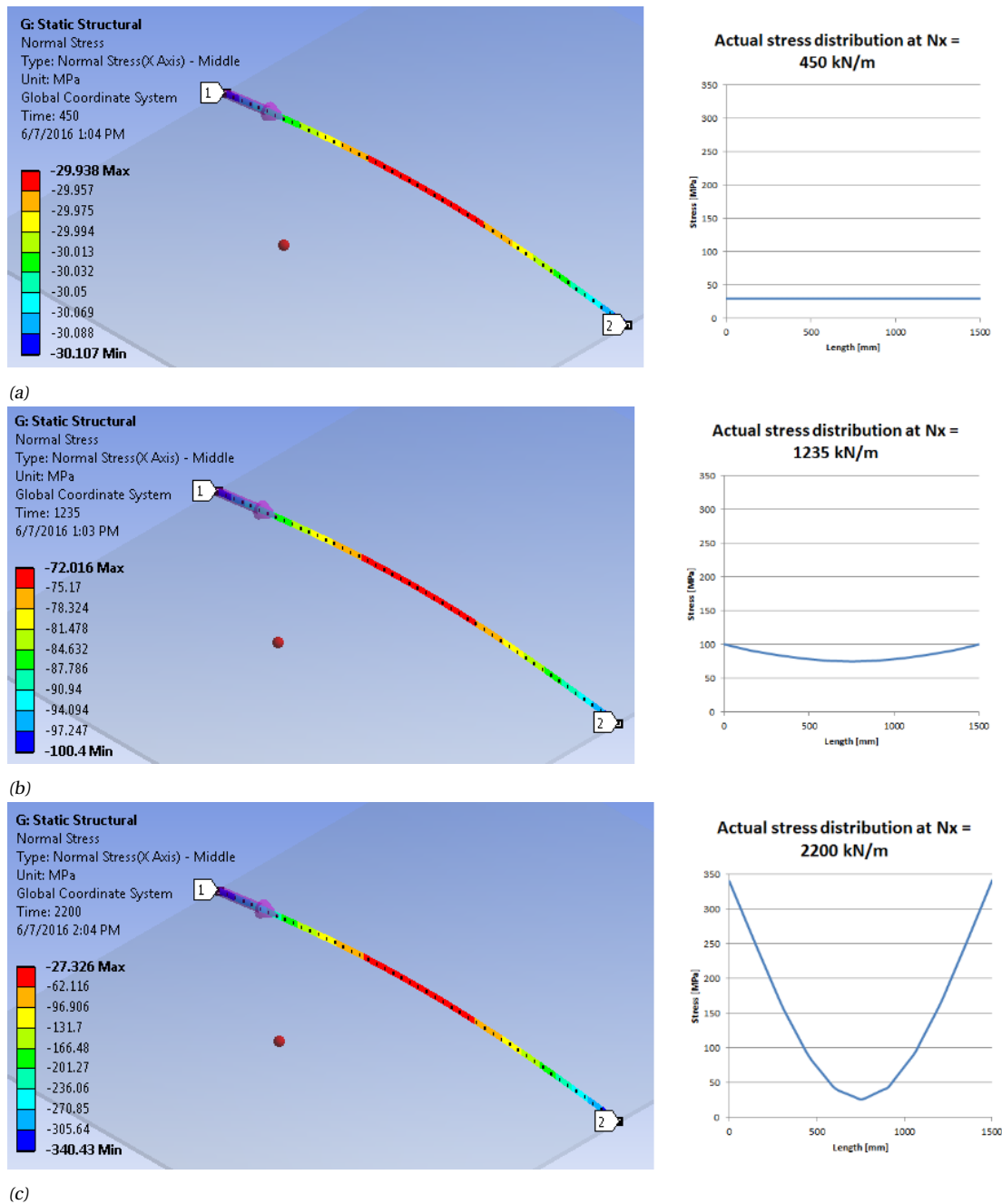


Figure 3.9: Stress distribution in the plate under different stress levels with regard to the buckling load: (a) at $N_x = 450 \text{ kN/m}$, well under the buckling load, (b) at $N_x = 1235 \text{ kN/m}$, at the buckling load, and (c) at $N_x = 2200 \text{ kN/m}$, well above the buckling load

Effective width in Eurocode

The reduction of strength in the centre of the plate is accounted for in the Eurocode by an effective width. The method used in section 4.4 of NEN-EN1993-1-5 [18] is compared to the outcome of the Ansys model of section 3.2.5.

Using the same plate dimensions as in section 3.2.2, the effective width can be determined under uniform compressive loading. NEN-EN1993-1-5 section 4.4 prescribes the following method to determine the effec-

tive width:

$$\text{EC3-1-5 eq. 4.1} \quad \rho = \frac{\bar{\lambda}_p - 0.055(3 + \Psi)}{\bar{\lambda}_p^2} \quad (3.3)$$

in which

$$\bar{\lambda}_p = \sqrt{\frac{f_y}{\sigma_{cr}}} = \frac{\bar{b}/t}{28.4\eta\sqrt{k_\sigma}} = 2.174$$

using $\bar{b} = 1500\text{mm}$, $t = 15\text{mm}$, $\eta = \sqrt{235/f_y} = 0.81$, and $k_\sigma = 4$ (for $\Psi = 1$).

Then the reduction factor for the effective width becomes:

$$\rho = \frac{2.174 - 0.055(3 + 1)}{2.174^2} = 0.413 \quad (3.4)$$

The value for the reduction factor ρ indicates the portion of the plate that can be loaded up to the yield stress, without the actual stresses in the plate exceeding the yield stress level. In effect, this means that an edge loading of $N_x = \rho f_y t = 0.413 \times 355 \times 15 = 2199\text{N/mm}$ can be supported by the plate. As shown in figure 3.9c, the maximum compressive stress in the plate under a loading of $N_x = 2200\text{N/mm}$ is 340MPa , which is reasonably close to the yield strength of 355MPa . Therefore, the application of the effective width method according to NEN-EN1993-1-5 is justified.

3.2.6. Design verification

The output of Ansys consists of stress distributions in the modelled geometry. In order to achieve a design verification that is ultimately comparable to the beam-column design, some processing is necessary. The stress outputs are compared to the yield strength of the material. Deformations are allowed up to a certain value, at which the structure is considered to have buckled. In this situation the largest stresses are expected to occur at the location that are restricted from buckling (e.g. near stringers). Therefore, this situation is governing.

4

Design requirements

The beam-column design has to comply to the same design requirements as the stressed skin design, this means that the assumptions made in this section have to comply to both beam-column and stressed skin designs. Also, the loading pattern is simplified to a certain extent from the reference design, since above a certain level of detail, the comparison doesn't benefit from it any more and more time lost modelling than additional value in the model is gained.

4.1. Codes

The reference design is based on the offshore codes of the Det Norske Veritas (DNV) and American Petroleum Institute (API). For a structure composed of beams and columns, these codes are valid and easy to apply. However, bearing in mind that the stressed skin variant has to comply to the same codes as the beam-column design for comparative reasons, the applied codes are changed.

From the beginning of development, the API code is based on trial and error design, so at the time, the mathematical background was somewhat more limited than one might wish for. This was expressed in the relatively easy way of modelling the considered structure, using one seemingly unfounded factor for the allowable stress in the steel section. This yielded an easy to apply set of codes, yet it was harder to explore what were the assumptions used to achieve such factors. This Allowable stress design (ASD) is still used today in the offshore industry. However, it is losing ground against the Load and Resistance Factor Design (LRFD). For this reason, LRFD codes are chosen to be applied.

The stressed skin design consists of steel plated elements, so a set of codes is applied that gives a clear insight in how to deal with these. This, combined with the fact that LRFD codes are preferred, leads to the application of the Eurocode 3 and ISO19900-19906 [16, 18]. As the structure is designed in the Netherlands, the Dutch national annex is used for the country specific definitions in the Eurocode.

4.2. Materials

The structure will be designed using steel grade S355. For the specific mass of the material, $7850\text{kg}/\text{m}^3$ is taken, and for the Young's modulus 210GPa . The Poisson ratio is taken as 0.3. For the structural calculations, partial factors of $\gamma_{M0} = 1.00$ and $\gamma_{M1} = 1.00$ are used, as stated in EN1993-2 section 6.1 [19]. It is assumed that plasticity can occur in the cross section.

The calculation in SACS will consist of a linear-elastic analysis, using grade S355 structural steel. As the ultimate design consists of steel elements with a thickness of $t \leq 40\text{mm}$, the yield strength can be taken to be $f_y = 345\text{MPa}$ for elements with $t > 16\text{mm}$ and $f_y = 355\text{MPa}$ for elements with $t \leq 16\text{mm}$, as indicated in table 7 of EN10025-2 [20].

For the Ansys analyses, the material is considered to be able to deform plastically. Therefore a bilinear stress-strain relationship is assumed. Figure 4.1 shows this relationship. Herein, the angle of the curve represents the Young's modulus and the tangent modulus, respectively. No strain hardening is considered in the material.

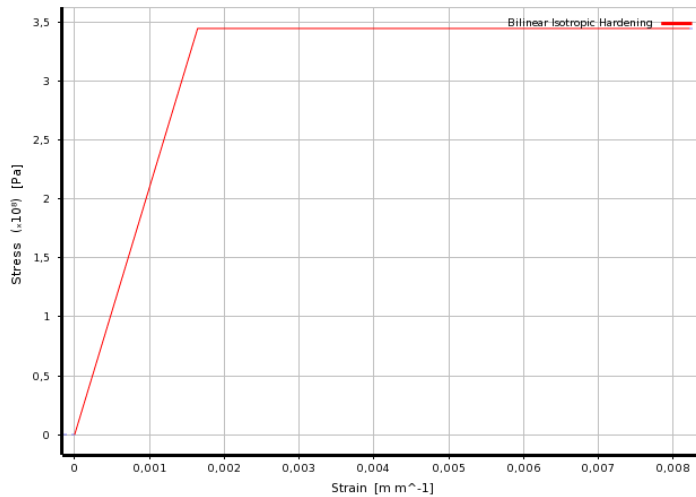


Figure 4.1: Stress-strain relationship considered in the Ansys analyses

4.3. Loading conditions

For every phase during the lifetime of the structure, the governing load combinations should be determined. Generally, for every one of the load conditions (in-place, transport, lifting, decommissioning, load-out) a separate analysis has to be performed. For the purpose of the comparison, some of the loading conditions are omitted, because these are too similar to other loading conditions. The loading conditions that are considered in the design are:

- In-place condition
- Transport condition
- Lifting condition

In order to make the designs best comparable, from each of the loading conditions one load combination is composed. Therefore, a total of three combinations are considered.

4.4. Loads

During each of the loading conditions, the structure is subject to specific loads. These loads can be induced by the equipment, environment, the structure itself, and dynamics/motions. Of these load cases, the equipment and environment will be practically equivalent for both the beam-column and stressed skin design. The self-weight, and thus the dynamics, will be different over the designs and is thus determined in the specific design.

4.4.1. Self weight

The self weight of the modelled steel is calculated by the FEM software. Additionally, the outer walls of the structure have to be considered as an additional loading on the topside of the beam-column design. Therefore, a loading of $0.6\text{ kN}/\text{m}^2$ is applied. This loading is not present in the stressed skin design, because the walls are modelled herein. On top of that, a grating loading on the cellar deck is considered of $0.6\text{ kN}/\text{m}^2$.

Additionally, design simplifications are also accounted for by an additional permanent floor loading. The value for this floor loading is taken the same for the different designs at $3.4\text{ kN}/\text{m}^2$. This value is computed by comparing the modelled steel weights to the structural weight obtained from the reference design by Iv-AGA [1].

4.4.2. Equipment loads

The equipment loads are extracted from the reference model and simplified. The values of these loads are provided in table 4.1 and the according locations in figure 4.2. In order to simplify the model further, the

equipment loading is distributed over its full deck. The original locations of these loadings are presented in order to show the simplifications made in the loading.

Table 4.1: Equipment loading on the structure

Equipment ID	Load [kN]	Location in reference model
REACTOR	565.1 (2x)	Mezz deck (see figure 4.2b)
	612.1 (2x)	Mezz deck (see figure 4.2b)
SW.GEAR	563.6	Main deck, 4 line loads on north side (see figure 4.2a)
TR-BIG	2391.4	Main deck (see figure 4.2a)
	422.0	Main deck (see figure 4.2a)
TR-SMA	1911.2	Main deck (see figure 4.2a)
	337.3	Main deck (see figure 4.2a)
Total	7979.9	

The equipment loading on the decks are given in table 4.2.

Table 4.2: Distributed equipment loads

Deck	Loading [kN/m^2]	
Main Deck	$\frac{563.6+2391.4+422.0+1911.2+337.3}{18 \times 38}$	8.22
Mezzanine Deck	$\frac{2 \times (565.1+612.1)}{18 \times 38}$	3.44

4.4.3. Floor live loads

In the reference design, a distinction is made in regular floor area and floor area that is used as a lay-down area for bigger equipment. For the simplification, a uniform floor load of $5kN/m^2$ is considered over the whole floor area. On the roof, a live load of $2kN/m^2$ is considered.

4.4.4. Environmental loads

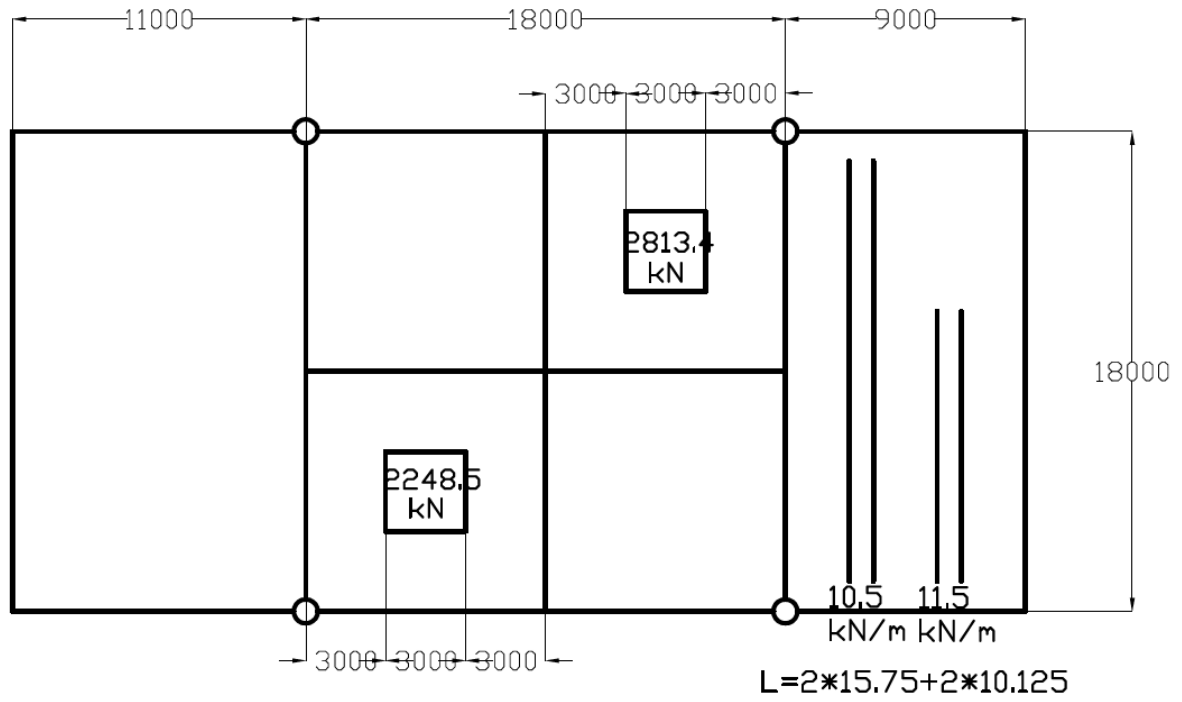
The environmental loads on a topside structure consist for the most part of the wind loading. For the wind loading, the extreme 100-year condition is considered. Herein, the 10-minute average wind velocity at a reference elevation of $10.0m$ above mean sea level is given as $33.4m/s$. The 15-second gust velocity at $35.8m$ above mean sea level is $43.8m/s$ in storm conditions and $36.1m/s$ in operating conditions. These velocities exert a pressure of $1.76kPa$ in the Ultimate Limit State (ULS) and $1.17kPa$ in the Serviceability Limit State (SLS) (via ISO19901-1 and ISO19902). These values are obtained using a wind shape factor of 1.5 (ISO19902 table 9.7-1).

4.4.5. Transport motions

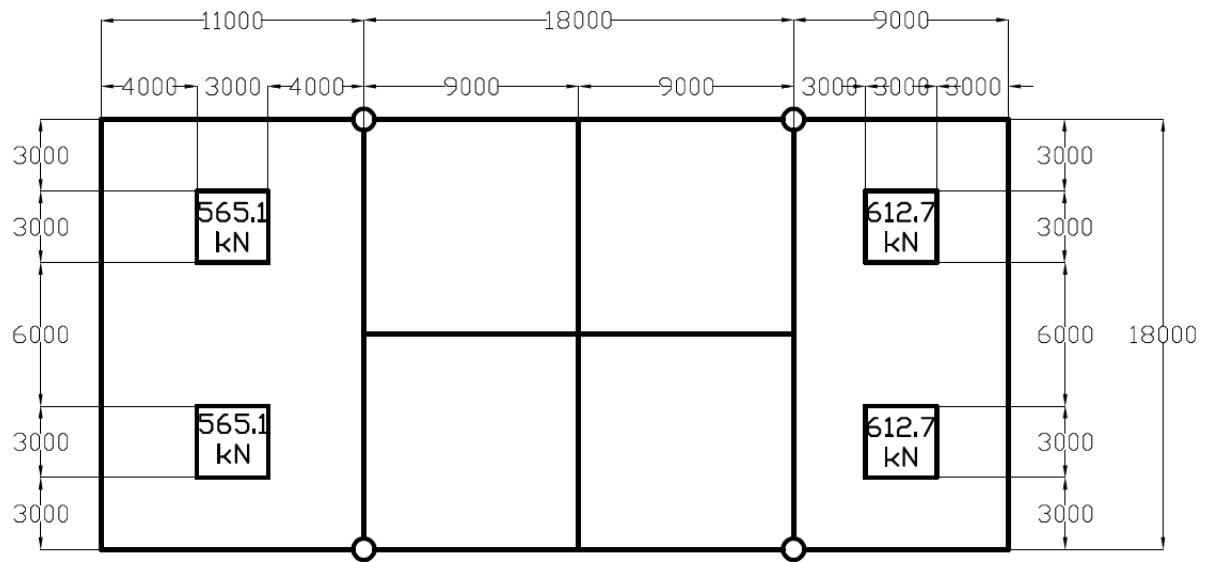
The forces on the structure induced during transport are due to the sea motions. These are taken from the Noble Denton criteria [21]. The loads taken into account are (Noble Denton 0030/ND table 7.1):

- Pitch: 12.5 degrees in 10 seconds
- Roll: 20 degrees in 10 seconds
- Heave: 0.2 G

The TOW procedure from SACS is used to convert the motions to inertial forces acting on the structure. The inertial loading can be validated manually and applied to the stressed skin design.



(a)



(b)

Figure 4.2: Equipment loading locations: (a) for loading on the main deck, (b) for the loading on the mezzanine deck

4.4.6. Rigging loads

In addition to the equipment loads, in the transport condition, an additional rigging load of $12kN/m^2$ is considered on a $3.0m$ wide strip at the roof deck.

4.4.7. Load case indication

The load cases as defined in section 4.4 are used in the finite element packages under abbreviated form. The abbreviations used are given in table 4.3.

Table 4.3: Load indications in finite element packages

Load case	Indication FEM
Self weight	DEAD
Equipment load	EQPT
Floor live load	LIVE
Environmental load	WIND
Transport motions	Applied as inertial loading
Rigging loads	RIG

4.5. Load combinations

The loads determined in the previous section are combined in the load combinations using an appropriate factor.

4.5.1. In-place condition

For the in-place condition, the loads are acting on the structure are given in table 4.4. Hereby, both an SLS and an ULS load combination are used. The environmental loading is considered to consist of the wind loading acting in the negative Y-direction and the positive X-direction.

Table 4.4: Load combinations for the in-place condition

	DEAD	EQPT	LIVE	WIND(-Y)	WIND(+X)
SLS	1.0	1.0	1.0	$1.0 \times 0.71 = 0.71$	$1.0 \times 0.71 = 0.71$
ULS	1.35	1.35	1.5	$1.5 \times 0.71 = 1.06$	$1.5 \times 0.71 = 1.06$

4.5.2. Lifting condition

In the lifting condition, several effects have to be taken into account. This is done in order to comply to the requirements posed in ISO19902 [15]. The factors that have to be taken into account are:

- Dynamic amplification factor 1.30 (ISO19902 section 8.3.2)
- Effect of tolerances 1.15 (ISO19902 section 8.3.3)
- Dual lift factor 1.10 (ISO19902 section 8.3.4)
- Shift in centre of gravity 1.10

All of the structure has to be able to withstand the loading taking into account the above factors. For the elements framing onto the lifting points, an additional local factor of 1.25 has to be taken into account (ISO19902 section 8.3.5). The total load factors in the combination now become:

- 2.30 for elements framing onto the lifting points
- 1.80 for other elements

The design load combination taken into account during the lifting are given in table 4.5.

In here, the load case CGCH complies a moment applied to the bottom of the topside legs in order to correct for the eccentricity of the loading.

Table 4.5: Load combinations lifting condition

	DEAD	EQPT	CGCH
LIF1	1.80	1.80	1.80
LIF2	2.30	2.30	2.30

4.5.3. Transport condition

During transport, the characteristic loads are considered on the topside. Due to the transport motions elaborated in the previous section, inertia loadings are active on the structure. The transport motions are applied to the structure as an inertial loading. This is done in order to facilitate the calculations on the stressed skin model. A loading on the beam-column design according to table 4.6 is found to be applicable.

Table 4.6: Resulting inertial load in transport condition

	Positive [G]	Negative [G]
x-direction	0.35	-0.35
y-direction	0.50	-0.50
z-direction	1.20	0.80

The combination that is considered involves a negative roll (acceleration in negative y-direction) and a positive heave (increased gravity). The combination considered is given in table 4.7. In the combinations, a partial load factor of 1.20 is used, according to section 8.6.1 of DEP 37.91.00.30 [22].

Table 4.7: Load combination in the transport condition

		DEAD	EQPT	RIG
TRNS	SLS	1.00	1.00	1.00
	ULS	1.20	1.20	1.20

4.6. Support conditions

Since the jacket structure is assumed not to change and its design is not in the scope of the thesis, the support conditions of the topside for the in-place condition are kept the same as in the reference design. The substructure consists of a four-legged jacket structure, with its supports spaced 18m in both longitudinal as transverse direction.

For the lifting condition, the support locations are more flexible. Due to possible eccentric support conditions, the centre of gravity could be needed to be adjusted.

During the transport, additional supports are required for the resistance to horizontal loads induced by barge motions. It is assumed that the vertical support is provided by the same columns that provide the support in the in-place condition. The horizontal forces are taken by the additional sea fastening.

4.7. Failure criteria

For the structural design to be complete, the occurring stresses and deformations should not exceed several criteria. In the ULS, the criteria generally consist of strength checks; in the SLS, the criteria are mostly deflection or vibration checks. In the present design, only the load combination SLS in the in-place condition is considered for the SLS criteria, all other combinations are considered for the ULS criteria.

4.7.1. ULS

The failure criteria in the ULS take into account the strength of the materials. An element is considered failed if yielding occurs in the cross section. In the elastic regime, the general requirement for the structure is as

follows:

$$\frac{E_d}{R_d} \leq 1.0 \quad (4.1)$$

in which E_d is the design effect of the loading, taken into account partial factors and combination factors, R_d is the design resistance of the structure, taking into account partial safety factors and reduction factors.

4.7.2. SLS

Failure conditions in the SLS generally consist of deflection or vibration criteria. These are often client-specified, as opposed to the hard requirements in the ULS. ISO19901-3 poses some requirements that have been adopted to serve as the SLS requirements in this structure. These are given in table 4.8.

Table 4.8: Requirements for deflection in the SLS (ISO19901 table 1)

Structural component	Maximum deflection	
	Δ_{max}	Δ_2
Floor beams	$\frac{l}{200}$	$\frac{l}{300}$
Cantilever beams	$\frac{l}{100}$	$\frac{l}{150}$
Deck plate thickness	—	2δ or $\frac{b}{150}^a$

l span
 δ deck thickness
 b stiffener spacing
 a Whichever is smaller.

in which Δ_{max} is determined as w_{max} in figure 4.3, Δ_2 is determined as w_3 (the additional deflection resulting from the variable loads).

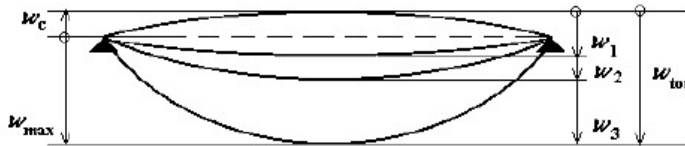


Figure 4.3: Occurring beam deflections (EN1990 figure A1.1)

The horizontal deflection of wall plates should be limited to not impede the serviceability of the structure. This imposes a rather subjective criterion. The maximum allowable deflection is set to be 20mm under characteristic loads.

4.8. Fatigue

In the design of the topside, fatigue is not considered. For several reasons, the fatigue loading can be an important element in the analysis of the topside. Examples include tall flares that induce a large bending moment at the base due to wind loading, or crane loads inducing a bending moment to the crane base. However, these loadings act on a local basis, while in present thesis, the overall behaviour of the topside is considered.

5

Simplified Beam-Column Design

The design requirements as elaborated in section 4 are used in the design of the complete topside structure. This structure bears similarities to the structure designed by Iv-AGA [1]. However, it is taken care of that the design is structure is designed in a simplified manner. This is done in order to conserve the overall overview of the structure and make the project more general applicable.

The design composed in this section serves as the connection between the full design of the topside and the designs that are made upon which the comparison is made. Therefore, this model is used for determining the loads on the structure and providing some of the geometries for the comparison designs.

5.1. Geometry and loading

The geometry of the topside is simplified from the reference design made by Iv-AGA [1]. Non-structural elements, i.e. external walkways, are removed. The weight of the steel that is not modelled is added as a uniform deck load. Member dimensions are taken as closely as possible to the dimensions of the members in the reference design. The geometry considered is given in figure 5.1. The structure is designed complying the design requirements given in section 4.

The floor plates are modelled as shear plates. Therefore, the plates are only capable of transferring shear stresses and are considered to have no resistance to normal stresses. As in reality these plates, in combination with stringers, show some resistance to normal stresses, it is assumed that the modelled beams cannot deflect in the plane of these plates.

The load combinations that are considered during each of the load conditions, are kept as given in the design requirements (see section 4). Load conditions that have been considered are the in-place, lifting, and transport condition.

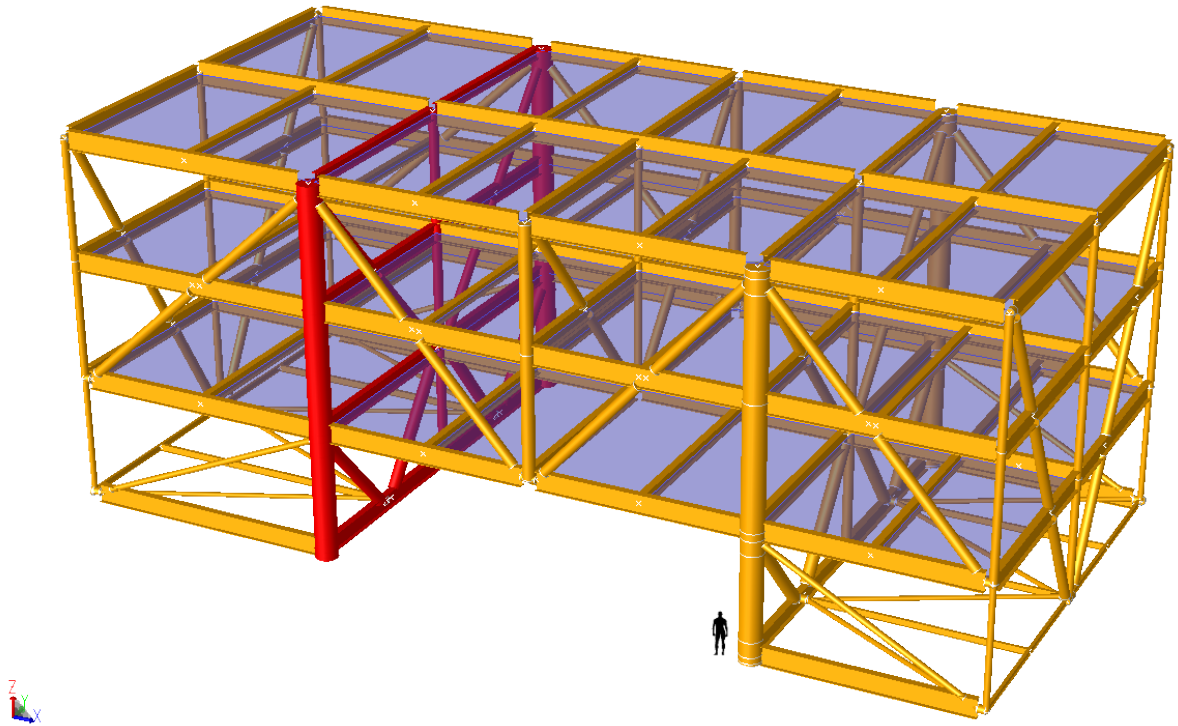


Figure 5.1: Geometry of the beam-column design

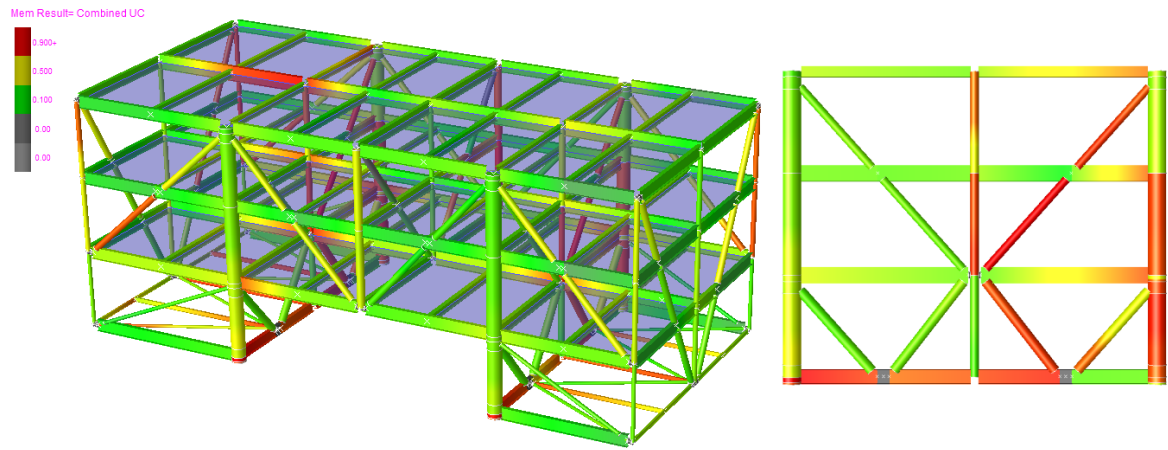
5.2. Member results

The design is made such that the maximum design verification in general does not exceed 0.8. However, due to the reduced number of different cross section, this condition is not met in all members (in total, 3 members show a design verification that is larger than 0.8). The resulting design verifications of the full SACS-model are presented in table 5.1. In the table, all of the 25 members that show a design verification in excess of 0.7 are given. The last column indicates the mode that leads to the maximum design verification of the considered member. The full SACS-output of the simplified beam-column model for members showing a design verification larger than 0.7 is given in appendix C.1.

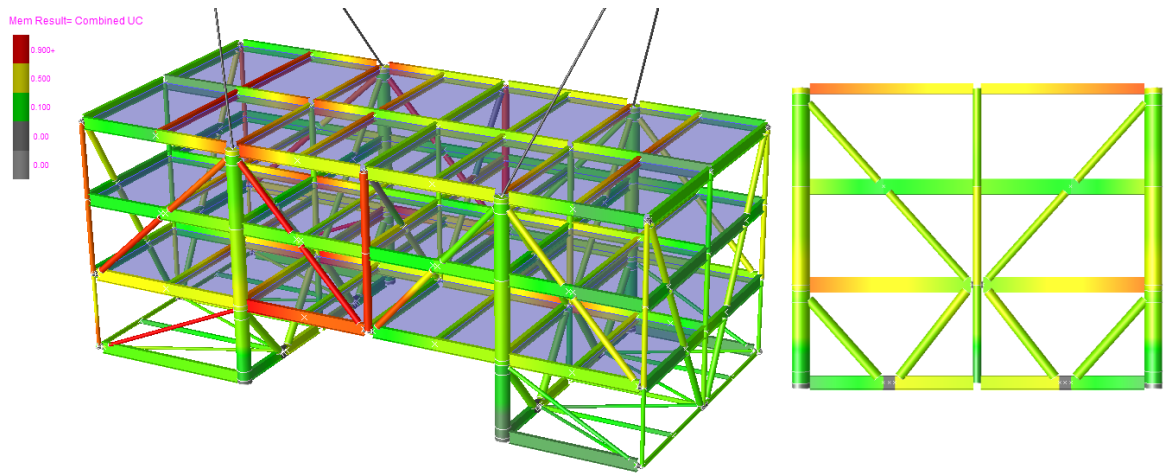
Table 5.1: Unity checks above 0.7 in the line model

Location	Member	Group	Type	Verification in SACS			Highest verification due to
				In-place	Lift	Transport	
Cable deck	0026-0237	I30	IPE300	0.24	0.30	0.76	Bending and axial force (cross section)
Cable deck	0309-100D	M70	HE700M	0.44	0.10	0.72	Bending and compression (buckling)
Cable deck	0328-100C	M70	HE700M	0.42	0.13	0.80	Bending and compression (buckling)
Main deck	0048-0028	M10	HE1000M	0.79	0.74	0.66	Bending and axial force (cross section)
Main deck	0494-0028	M10	HE1000M	0.84	0.89	0.67	Bending and axial force (cross section)
Mezz deck	0044-0029	A80	HE800A	0.83	0.66	0.59	Bending and axial force (cross section)
Mezz deck	0702-0029	A80	HE800A	0.84	0.69	0.57	Bending and axial force (cross section)
Mezz deck	0038-0044	MES	HE450A	0.77	0.56	0.47	Bending and axial force (cross section)
Mezz deck	0044-0046	MES	HE450A	0.77	0.57	0.47	Bending and axial force (cross section)
Roof deck	0030-0090	M10	HE1000M	0.47	0.59	0.71	Bending and axial force (cross section)
Roof deck	0030-0019	M10	HE1000M	0.45	0.52	0.85	Bending and axial force (cross section)
Roof deck	0007-0019	ROS	HE550A	0.46	0.77	0.46	Bending and compression (buckling)
Roof deck	0019-0022	ROS	HE550A	0.46	0.77	0.34	Bending and compression (buckling)
Wall row 2	0035-0037	16C	406x12.7 CHS	0.74	0.50	0.76	Axial, combined bending interaction
Wall row 3	1254-1268	20D	508x12.7 CHS	0.75	0.69	0.44	Axial, combined bending interaction
Wall row 3	1271-1237	20D	508x12.7 CHS	0.74	0.68	0.63	Axial, combined bending interaction
Wall row 3	1268-1111	20E	508x19 CHS	0.78	0.70	0.41	Axial, combined bending interaction
Wall row 3	1271-1060	20E	508x19 CHS	0.80	0.77	0.78	Axial, combined bending interaction
Wall row 4	0002-0057	16C	406x12.7 CHS	0.22	0.33	0.76	Tension and bending
Wall row 4	0028-0029	16D	406x19 CHS	0.55	0.41	0.76	Axial, combined bending interaction
Wall row 4	0057-0334	20G	508x30 CHS	0.36	0.27	0.79	Axial, combined bending interaction
Wall row 4	0245-0246	36G	914x25.4 CHS	0.47	0.17	0.71	Axial, combined bending interaction
Wall row 5	3002-2002	12C	324x14 CHS	0.59	0.53	0.73	Axial, combined bending interaction
Wall row A	103-100C	36M	914x30 CHS	0.47	0.00	0.70	Axial, combined bending interaction
Wall row B	0204-0050	16C	406x12.7 CHS	0.52	0.70	0.43	Tension and bending

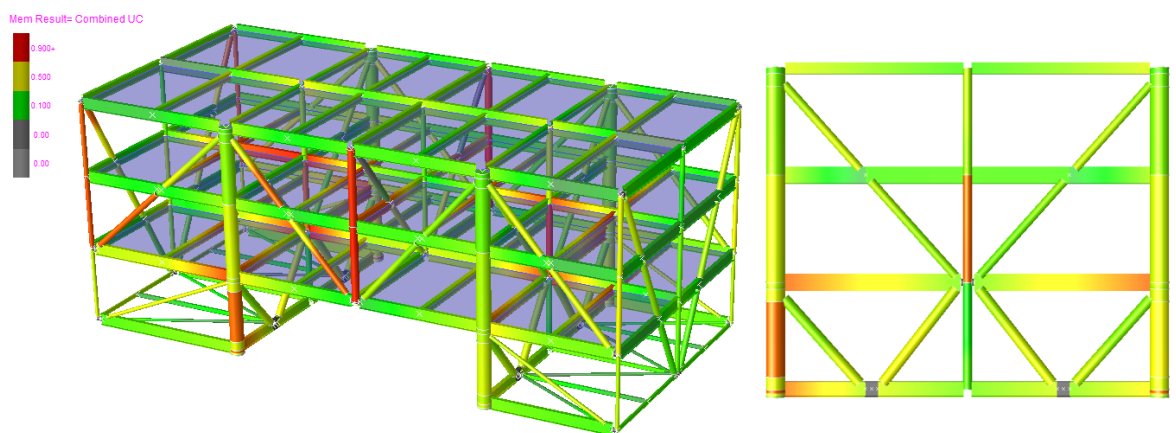
The numerical results from table 5.1 are visualised in figure 5.2. Herein, it is seen that for all of the loading conditions, different unity check distributions are obtained. In subsequent analyses, a part of the structure is considered. This is done with respect to the computation time, that would increase dramatically if the full structure would be considered in Ansys. The substructure that is considered consists of the most heavily loaded frame found in this analysis, which is the part of the structure indicated in red in figure 5.1. As is seen in figure 5.2, the transport condition provides the heaviest loading on this part of the structure. Therefore, this condition is considered in the subsequent analyses. The internal force distribution in this frame in the transport condition is given in figure 5.3. An external load distribution on the frame is determined to obtain the same internal load distribution as in the simplified full model in section 5.3.



(a) Transport condition

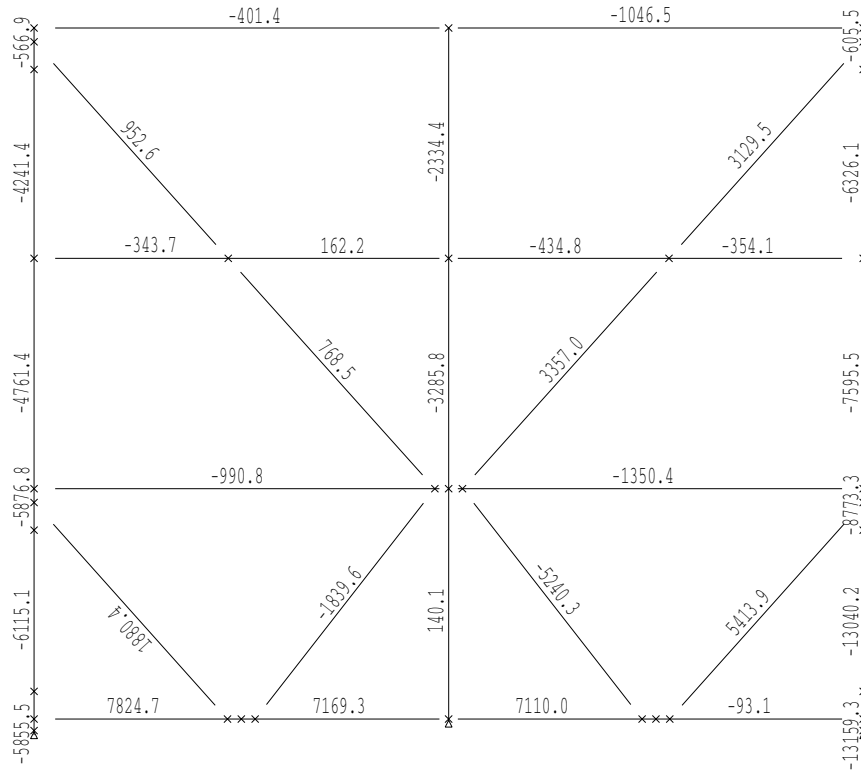


(b) Lifting condition

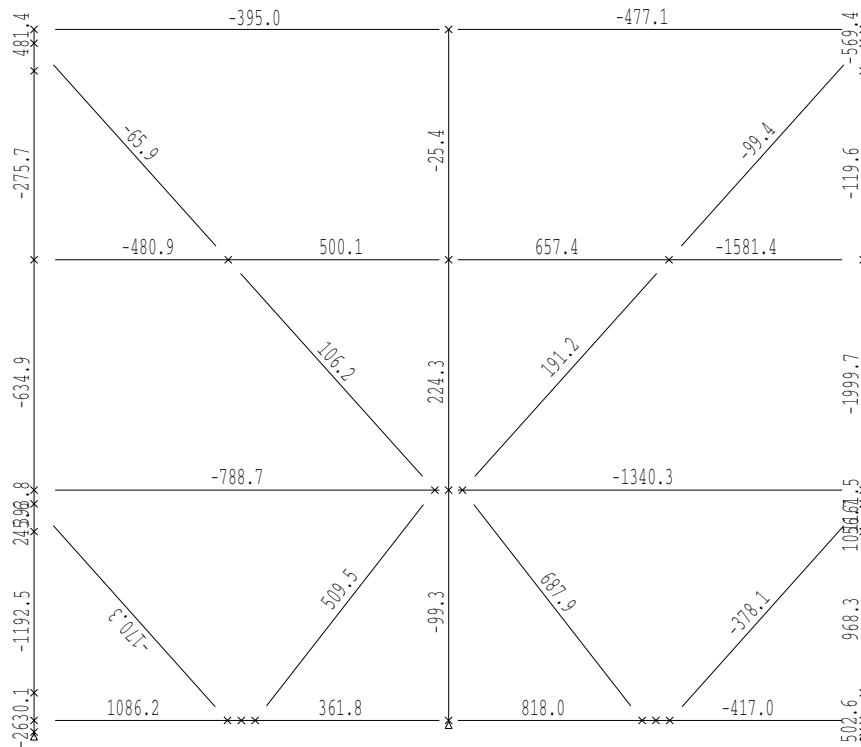


(c) In-place condition

Figure 5.2: Visualisation of the member results of the simplified beam-column design: (a) for the transport condition, (b) for the lifting condition, (c) for the in-place condition



(a) Axial force [kN]



(b) Bending moments [kNm]

Figure 5.3: Internal forces in the frame: (5.3a) shows the axial force in the members in kN, (5.3b) shows the in-plane bending moment in the members in kNm

5.3. Frame loading

In the analyses carried out in section 6, only a part of the structure is analysed. This means that the loadings on the omitted parts of the structure need to be transferred to the part that is considered in the analysis. These loadings consist of concentrated loads in the nodes of the structure and distributed loads on the members.

Table 5.1 and figure 5.2 show that the transport loading is the most governing on the considered frame. Therefore, this load condition is considered during the analyses carried out in section 6. The transport load consists of horizontal and vertical loads. According to table 4.6, the vertical component of the inertial loading is multiplied by a factor 1.2, while the horizontal loading is determined to be 0.5 times the vertical loading. The ratio of horizontal to vertical loads then becomes about $F_h = \frac{0.5}{1.2} \times F_v = 0.416 \times F_v$. Keeping in mind this ratio, the loading on the frame structure is determined iteratively to match the internal force distribution of the frame in the full model.

The loading is determined to be as indicated in figure 5.4. Herein, both the concentrated loading on the nodes and the distributed loading on the members consist of a vertical and horizontal component.

The self-weight of the structure is considered in the given loadings. Therefore, in the subsequent analyses, the self-weight is not separately included in the loading.

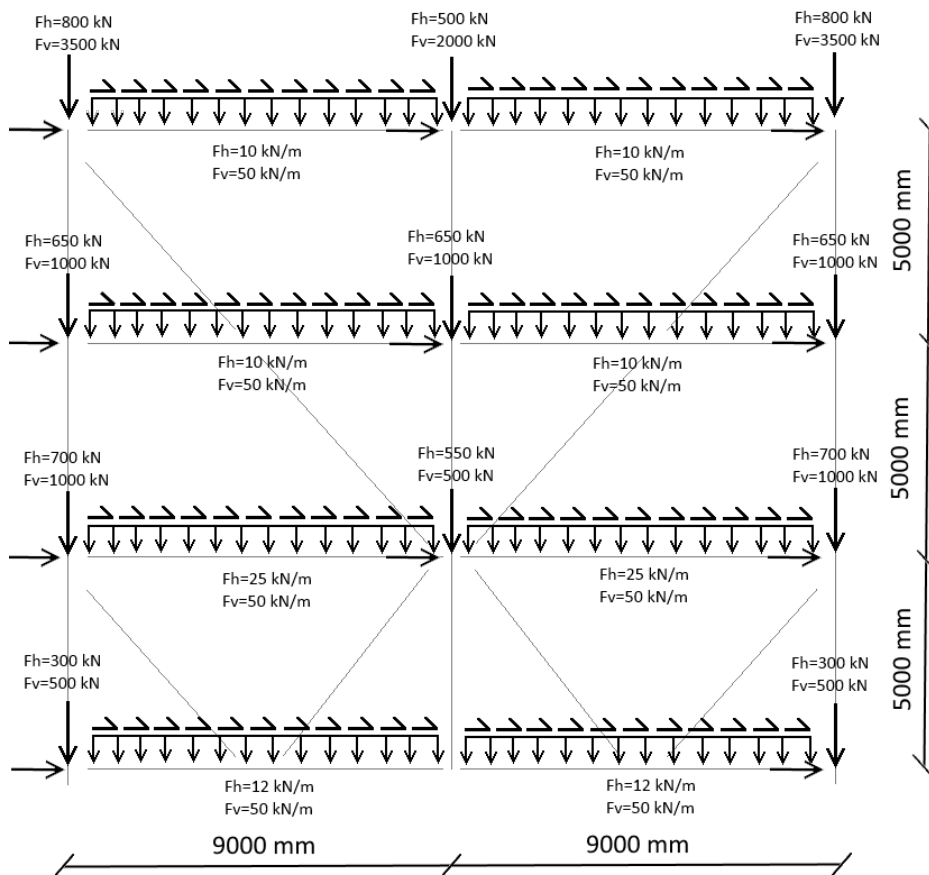


Figure 5.4: Loading locations and values on the frame

6

Variant study

In this section, the models that are made for the purpose of the comparison (in section 7) are presented. Different software packages are used for the different designs (SACS for the beam-column design and Ansys for the stressed skin design) and therefore, an additional model is made for the beam-column design in Ansys. The beam-column model in both SACS and Ansys are built up using the same design, which means that the results of the software packages can be compared using the designs.

6.1. Input for all models

The three designs are complying the design requirements (see section 4) with respect to use of materials and applied codes. The loadings on the structure are given in section 5.3, consisting of concentrated nodal loads and distributed line loads along the horizontal members.

6.1.1. Geometry

For all three of the designs, the geometry consists of the frame indicated in red in figure 5.1. In figure 6.1, the original geometry (and thus the geometry of the beam-column model) of the frame and the accompanying node numbers are given. These node numbering will also be considered in the stressed skin design. However, due to the more continuous nature of the design topology, these will not stand out as much as is the case in the beam-column designs.

The models are supported at the lower nodes (node 10 and 12) in vertical direction and horizontally in node 10. In the out-of-plane direction, the SACS model is supported at the four corners (which is sufficient due to the linear elastic calculation only determines deformations in the direction of loading). The Ansys model does take into account eccentric loading and as a result, out-of-plane displacements occur. This is prevented by attached wall and floor plating. At these locations, the Ansys model is supported in the out-of-plane direction.

6.2. Beam-column design in SACS

As explained in section 3.1, the SACS software package, as used by Iv-Oil & Gas, is focused on the evaluation of line models. Therefore, the frame that is considered is built up with relative ease. Hereby, all modelling assumptions made in that section are taken into account.

In figure 6.2, the geometry, including the member cross sections, of the analysed frame is given, which is built up according to the design requirements (see section 4). The geometry is considered in two dimensions (it is supported in the out-of-plane x-direction at the four corners), and is simply supported (lower left corner is restrained in the y- and z-direction, the lower right corner is restrained in the z-direction).

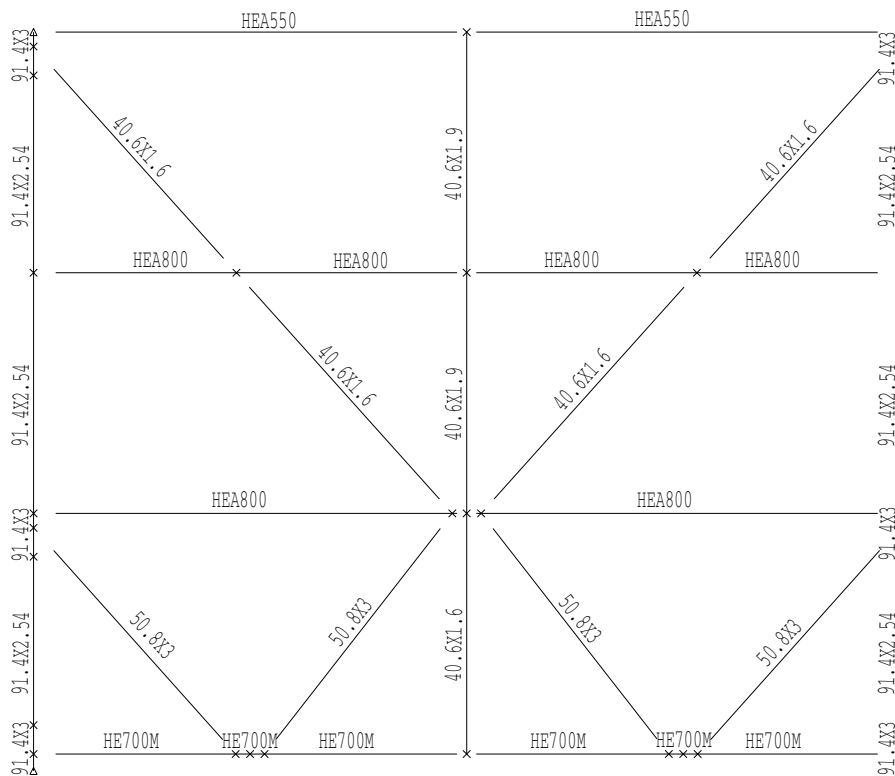


Figure 6.2: Frame analysed in SACS for the comparison with Ansys (sizes of tubular hollow sections are given in centimetres)

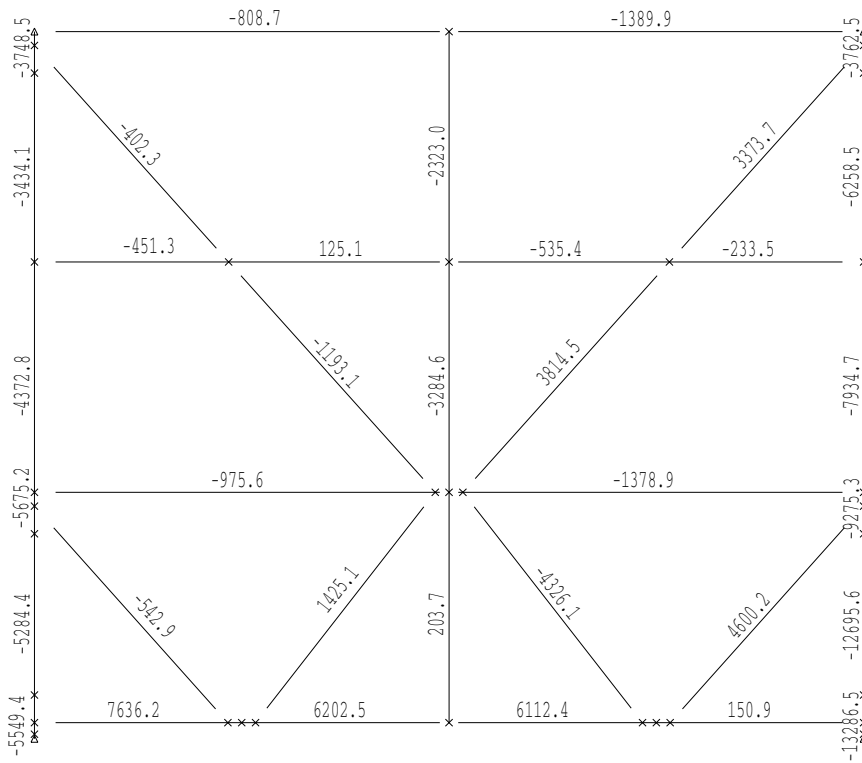
In line with the statements in section 3.1, the members are considered up to the point of intersection with the connecting member. Additionally, short members that are introduced to prevent overlap in joints are not considered in the analyses, as in reality, the members are strengthened at these locations.

The loading on the structure is taken as indicated in figure 5.4. These loads are applied to the respective nodes and the horizontal members of the frame.

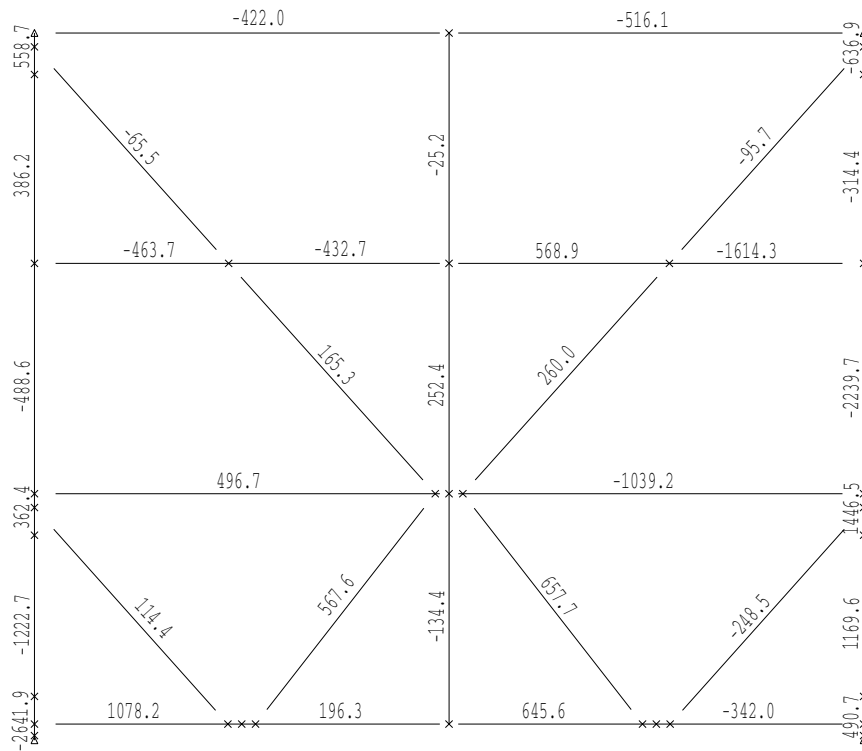
6.2.1. Results

The SACS analysis yields a set of member internal forces that serve as input for the design verification. This verification is included in the software, so no hand calculations are necessary. The occurring internal member forces are shown in figure 6.3. The output of the SACS software in terms of the design verifications is given in appendix C.2.

The results of the SACS model in terms of design verifications are verified by hand. In order to do so, four



(a) Axial forces [kN]



(b) Bending moment [kNm]

Figure 6.3: Internal forces under equivalent loading: axial force [kN] in (a) and in-plane bending moment [kNm] in (b)

cross sections have been selected that each show a different mode with the highest unity check. The hand verification of the SACS calculations is given in appendix E.

Deflections

The deflections of the beam-column model in SACS come forth from the linear elastic calculation. Herein, no higher order effects are considered. The SACS software takes into account the nodal displacements and integrates for the member to provide the deflections of members. Figure 6.4 shows the displaced structure under SLS loading.

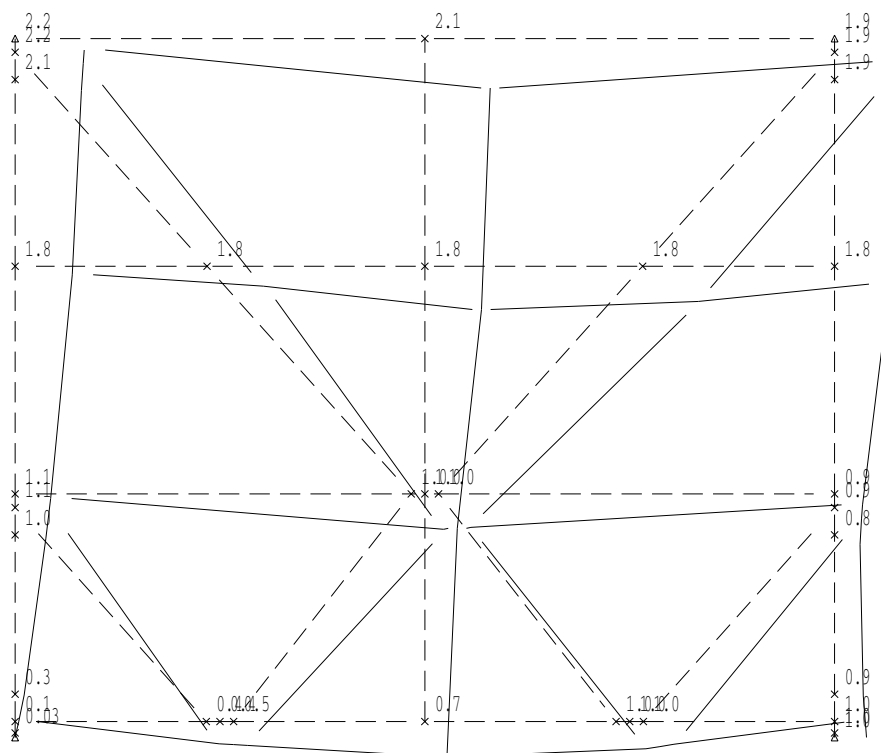


Figure 6.4: Horizontal deflection [cm] of the beam-column model in SACS under SLS loading

Mass

The structural mass of the beam-column model is determined by the software. The total structural mass of the beam-column model becomes $46.3mT$. In addition, an internal wall is present in order to enclose the volume in the topside. The characteristic value for the mass of this wall is $0.6kN/m^2$, which represents a mass of $M_{wall} = \frac{0.6 \times 15 \times 18}{9.81} = 16.5mT$. The total weight of the structure including the wall now becomes $46.3 + 16.5 = 62.8mT$.

Weld length

The welds in the beam-column model make up for a substantial part of the manufacturing. Therefore, these will be considered when comparing the different designs to each other. For the design to provide general conclusions, the main welds are considered. In the beam-column design these welds are mostly situated around the joints of the members and therefore need to be manufactured by hand. The welds in the design consist mostly of butt welds and tubular to tubular welds.

The member sections are considered to be available in the lengths that span the full member. In the design, the maximum member length is around $8m$. Therefore, it is considered that longitudinal butt welds are only necessary at joints and transitions in cross section (e.g. joint cans and joint strengthening).

The full breakdown of the welds in the design is given in the comparison of section 7.2.3.

6.3. Beam-column design in Ansys

The models of the beam-column design in SACS and the stressed skin design in Ansys cannot be compared directly. Therefore, the beam-column model is also modelled in Ansys.

The Ansys model is composed using the same cross sections as the SACS model from section 6.2. Figure 6.5 shows the considered geometry of the model, in which the plate thickness is given in mm in the legend. The model is built up from Shell181 elements.

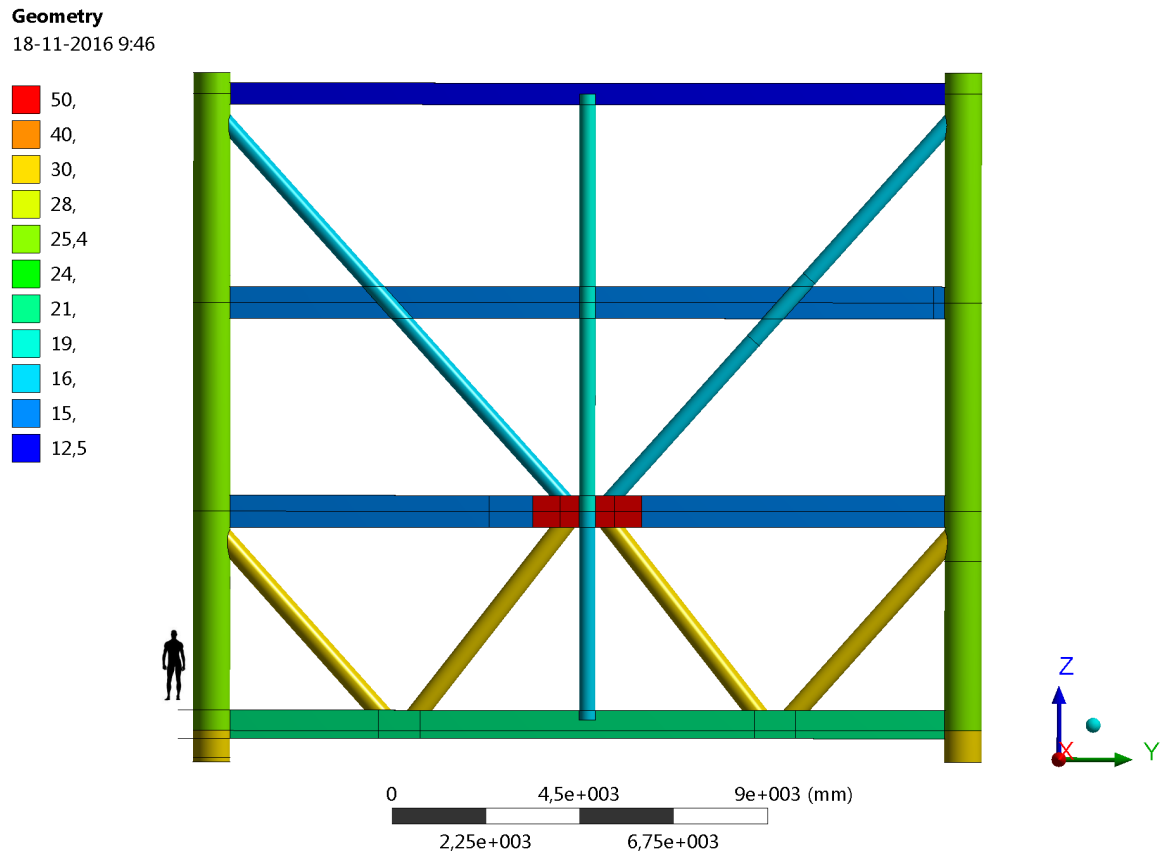


Figure 6.5: Frame analysed in Ansys for the comparison with SACS

6.3.1. Strengthening measures

Due to the different modelling approaches in the software, some parts of the Ansys model have to be strengthened in order to be able to resist the loading. The model is strengthened to such extent that the load in the ULS is resisted without considerable loss in stiffness compared to the initial stiffness.

Strengthening measures are implemented in the following manners:

- In order to prevent cross sectional deformations in the CHS at the supports, a diamond plate is simulated at node 10 (see figure 6.1) by a circular plate with thickness $40mm$ and radius $0.8m$, concentric with the CHS beam axis. This measure is applied only at node 10, because at this node, the structure is horizontally restrained. At node 12, no horizontal load introduction is present.
- The force introduction from tubular member to hot rolled sections is provided by widening the flanges of the latter section locally and applying a vertical stiffener at the connection of the tubular. These stiffeners have a thickness of $21mm$.
- The web of the beam at node 8 (see figure 6.1) has an increased thickness. This is done in order to prevent the beam to fail to shear. The web at the node has a thickness of $50mm$, as opposed to the rest of the beam, that has a thickness of $12.5mm$.

- The main columns are extended at the top for $0.5m$, this is done in order to provide a force introduction to this column from the roof beam.

The measures noted above are made visible in figure 6.6. It is made sure that the measures taken allow the structure to show a global failure mechanism, rather than local. This way, the structure shows the actual level of safety as it would be with properly designed details.

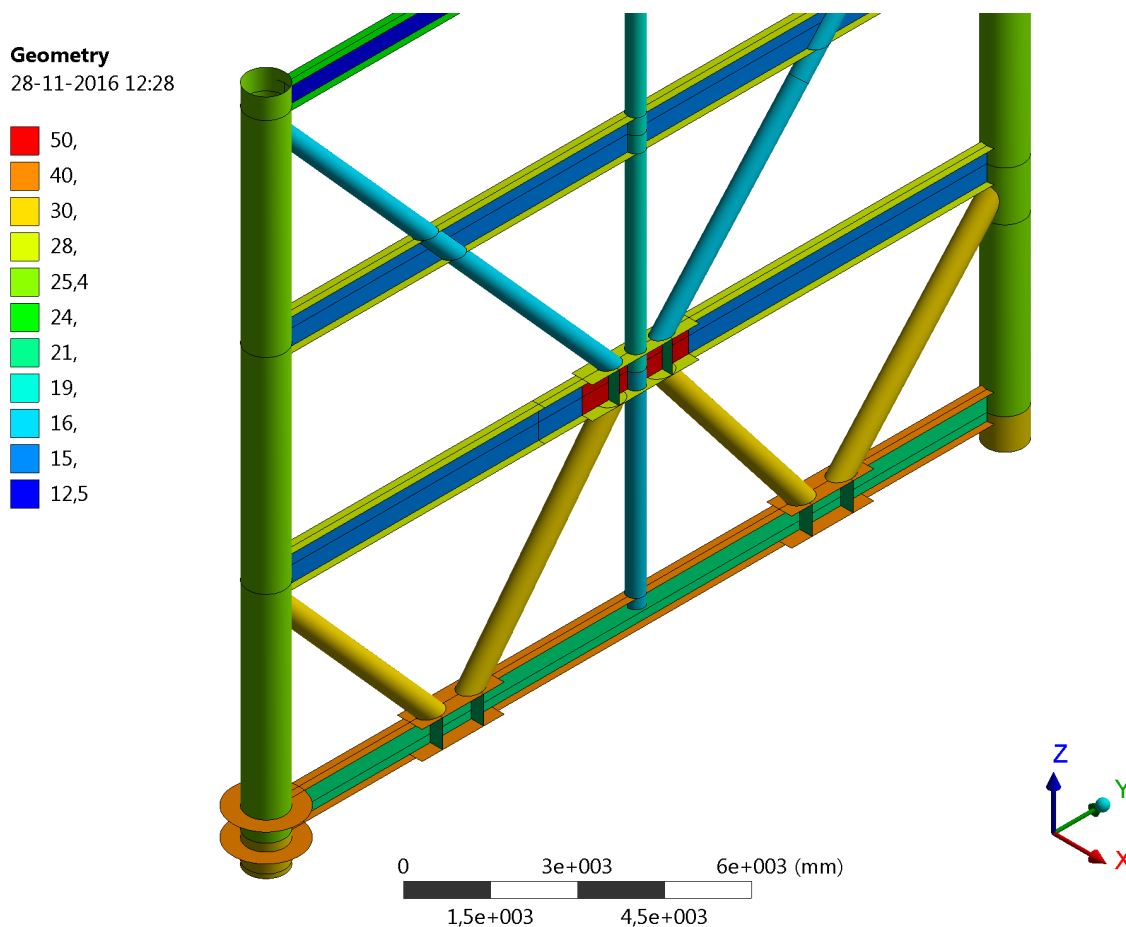


Figure 6.6: Joint details including the diamond plate and the widened flanges and stiffeners

6.3.2. Modelling

The modelling of the beam-column design in Ansys is carried out using Shell181 elements, with an average edge size of $200mm$. The material is considered to be bilinear as visualised in figure 4.1.

6.3.3. Results

Applying the measures discussed in section 6.3.1 leads to a model that represents the design such that the failure of the model is in a global mode. The level of safety that is present in the design is expressed in a maximum attainable load factor (i.e. the load that the structure is able to bear before failure). The load factor is defined as the portion of the ULS loading that is present on the structure:

$$\lambda = \frac{load_{actual}}{load_{ULS}} \quad (6.1)$$

The structure is found to fail upon reaching load factor $\lambda = 1.34$. Figure 6.7 shows the strain in the structure at the failure load level. It is seen that the highest strains are found in the lower left support. This part of the structure is considered to induce the global failure of the model. Also, the right upper brace is showing excessive deformations and stress levels close to failure.

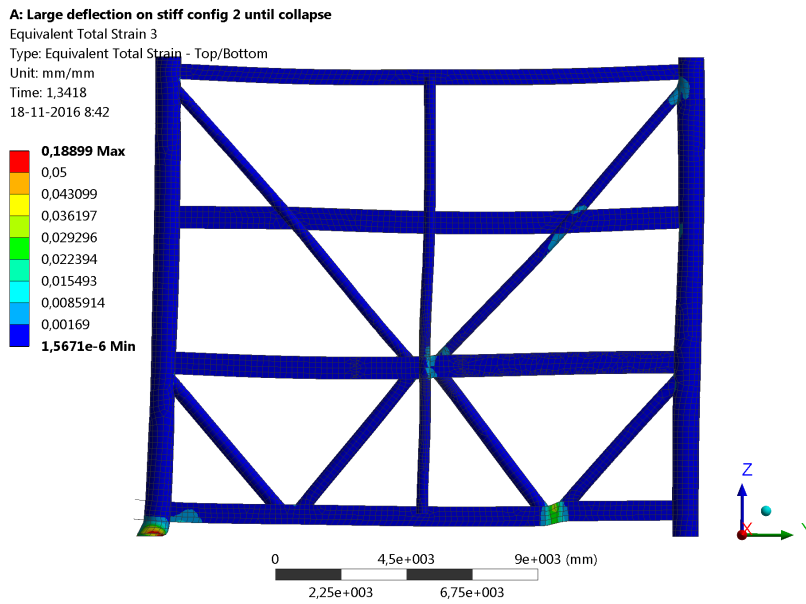


Figure 6.7: Strain of the beam-column model in Ansys under failure loading

Displacements

The displacements in the model are based on the elasto-plastic Ansys calculation. Herein, the effects of the structural deformations on the load distribution is taken into account. Therefore, the internal force distribution differs somewhat from the SACS results shown in section 6.2.1. The horizontal deflection of the members is calculated directly from the finite elements (as opposed to integrating the nodal results as is done in SACS) and is shown in figure 6.8.

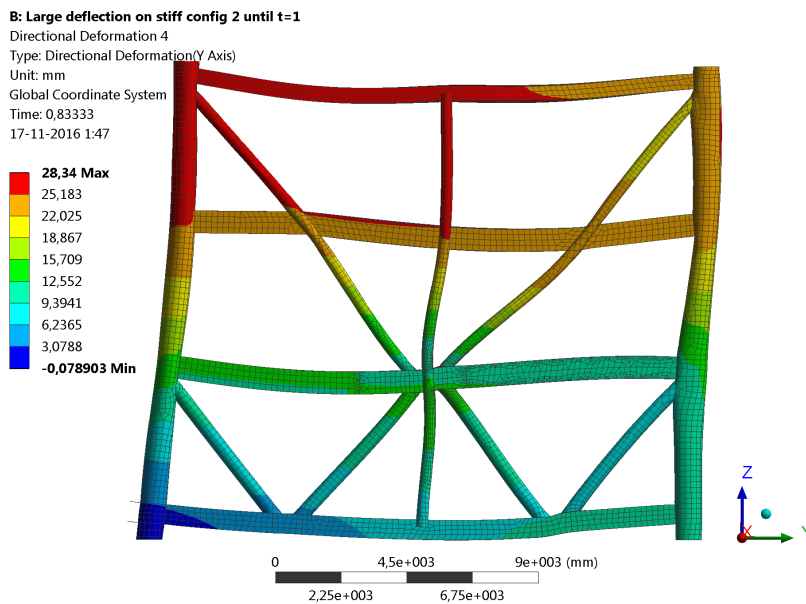


Figure 6.8: Horizontal deflection [mm] of the beam-column model in Ansys under SLS loading

Mass

The structural mass of the beam-column design in Ansys consists of two components. The bare structural steel has a mass of $46.8mT$ (which is similar to the mass of the model described in section 6.2), while the

strengthening measures add another $4.0mT$. This brings the total steel mass of the design to $46.8 + 4.0 = 50.8mT$. Additionally, the same separating wall as is considered in section 6.2.1 is applied. The total mass of the design now becomes $50.8 + 16.5 = 67.3mT$.

Welds

The model presented in this section is geometrically identical to the model described in section 6.2. Therefore, also the welds are identical. The full breakdown of the welds is given in table 7.2.

6.4. Stressed skin design

The stressed skin design represents the second design that is used for the comparison. This design is built up from plated elements. Because of the occurrence of plate buckling in the design, the Ansys software is used for the analysis of the design.

6.4.1. Geometry

The geometry of the stressed skin design is composed of steel plated elements. It consists of a main plate and a supporting edge beam. The main plate is stiffened by stringers and the effective width of plate fields attached to the frame (deck floors and outer walls) are taken into account. The considered geometry is shown in figure 6.9. Herein the geometry of the stringers is determined iteratively to obtain the most efficient configuration.

The design of the stressed skin model is made such that the structural safety is equivalent to the level of safety that is present in the beam-column design. This is verified by checking at which load factor λ the structure fails. When both models fail at approximately the same load factor and both show a global failure mechanism, the design are considered to show the same structural safety.

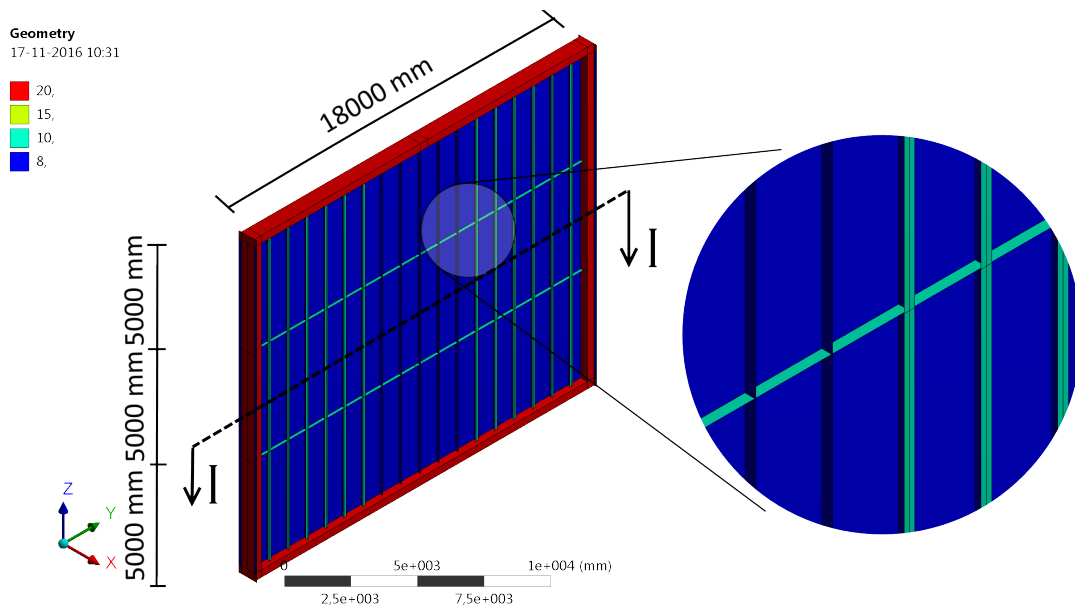


Figure 6.9: Geometry of the stressed skin design

The stringers are spaced one meter apart, whereby the middle 5 of the 17 stringers are rib stringers, the others are tee stringers. The webs of the rib stringers are 8 mm thick and have a total height of 150 mm. The tee stringers are considered to be built up as halves of an IPE300 hot rolled section. A cross section of the geometry of the stringers is given in figure 6.10.

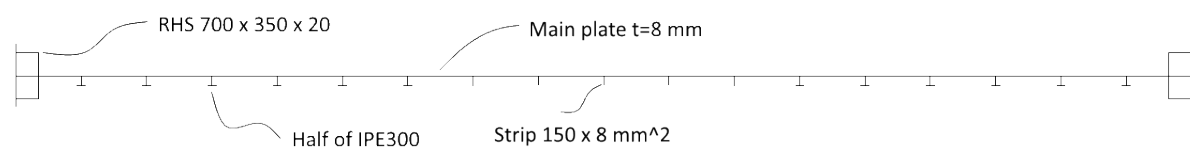


Figure 6.10: Cross section I-I of the geometry of stringers in the stressed skin design

The main plate is 8 mm thick. The edge beams are uniform around the plate and consist of a Rectangular hollow section (RHS). The RHS has a enclosed area of $350 \times 700 \text{ mm}$ and a thickness of 20 mm. The effective width of attached floor and wall plating is also considered and is taken to be 8 mm thick.

6.4.2. Loadings

The loading on the structure is taken equal to the loading used in the beam-column design. These loadings consist of in-plane horizontal and vertical loads and can be found in figure 5.4. Imperfections are introduced by the asymmetry of the model.

Self-weight is not separately applied, as it is considered in the nodal and distributed loading on the model (see section 5.3).

6.4.3. Modelling

The model is supported at the lower corners over a support area of $350 \times 700\text{mm}$, directly below the supporting edge columns. The support at node 10 (see figure 6.1) is constrained in all translational degrees of freedom, while the support at node 12 is constrained in x- and z-direction, effectively creating a statical determined system in-plane. Along all attached plating (deck floors and wall plates), the model is constrained in the out-of-plane x-direction.

Shell181 elements are used. These are made to have an edge sizing of around 100mm .

The material that is used in the analysis consists of structural steel with a bilinear stress-strain relationship. In the material, the partial factors $\gamma_{M0} = 1.00$ and $\gamma_{M1} = 1.00$ (as posed in section 4.2) are considered. Therefore, the calculations take place using a yield plateau of $f_{y,d} = 355\text{MPa}$, the Young's modulus is $E = 210\text{GPa}$.

At the supports, the material is assumed to remain linear elastic, even for high strain values. This means that in these parts, the stresses can build up to be much higher than the yield level of $f_{y,d} = 355\text{MPa}$. This is done in order to account for additional detailing that would be present in a full design of the structure and would assist in introducing the forces to the supports.

6.4.4. Results

Similarly to the beam-column design modelled in Ansys, the results for the stressed skin design consist of a deformation field and their accompanying stresses. It is made sure that the failure mode is global and that the level of safety is similar to the level of safety of the beam-column design in Ansys. The resulting load factor at which the structure fails becomes $\lambda = 1.37$. In addition to the results considered in this section, more in depth information is given in section D.

Deformations

For the deflections of the stressed skin design, both the in-plane and out-of-plane deflections are considered. The non-linear calculation takes into account the displacements in the internal force distribution and takes into account the (post) buckling capacity of the plated elements. Figure 6.11 shows the deformations in the model under SLS loading.

In figure 6.11b, the buckled shape can be seen to have already formed under SLS loading. The structure fails at a load factor of $\lambda = 1.37$, which indicates a considerable capacity in the structure after buckling.

Mass

The mass of the stressed skin design consists of the mass of the supporting frame and the mass of the structural wall. The omitted braces in the supporting frame reduce the mass to 22.7mT . Since the wall has an additional function to provide stability in the design, the mass of the wall is increased from the beam-column design and is now 22.0mT . The total mass now becomes $22.7 + 22.0 = 44.7\text{mT}$.

The replacement of the middle 5 Tee stringers in the centre area of the plate with rib stringers saves 824kg . This mass is considered to be significant enough to be included in the design. In the manufacturing, care has to be taken to where the Tee stringers and the rib stringers are applied.

Welds

The welds in the stressed skin design consist for the most part of long and straight welds with a relatively small thickness. These welds are suitable for an automatic welding procedure. In the design, most of the weld labour is going into the supporting beam and column, which consist of the thickest plate in the design.

A: Non-linear material properties until t=1

Directional Deformation 3

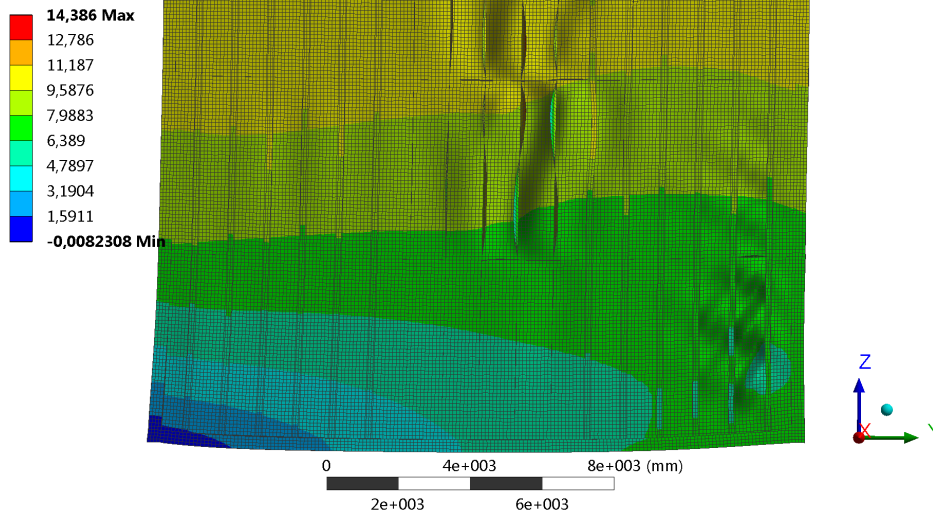
Type: Directional Deformation(Y Axis)

Unit: mm

Global Coordinate System

Time: 0,83333

17-11-2016 2:15



(a) Deformations in the in-plane horizontal direction [mm]

A: Non-linear material properties until t=1

Directional Deformation 3

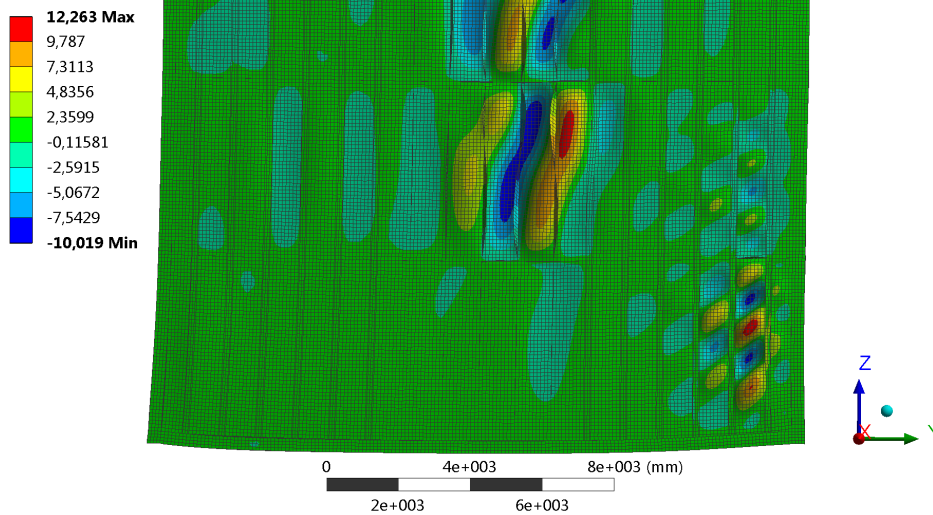
Type: Directional Deformation(X Axis)

Unit: mm

Global Coordinate System

Time: 0,83333

17-11-2016 2:16



(b) Deformations in the out-of-plane horizontal direction [mm]

Figure 6.11: Deformations [mm] in the stressed skin model under SLS loading: (a) for deformations in the in-plane horizontal direction, (b) for the out-of-plane horizontal direction

The full breakdown of the welds in the design is given in the comparison of section 7.2.3.

7

Comparison

The different designs are compared on steel mass and welds. In the designs presented in section 6, the geometry and loading of the design are simplified to be as general as possible. Also, in the design of the stressed skin model, it was tried to provide both of the designs with the same ultimate bearing capacity. In this section, the designs are compared: first the use of the different software packages is investigated, then the different designs are compared on their stiffness, steel mass and welds.

7.1. Software comparison

The two beam-column models are constructed in different software packages. Since the geometry and loading on both of the designs is equal, the software can be compared. The deformations at the nodes are taken at node 3 in horizontal direction (see figure 6.1), and in node 11 in vertical direction (see figure 6.1).

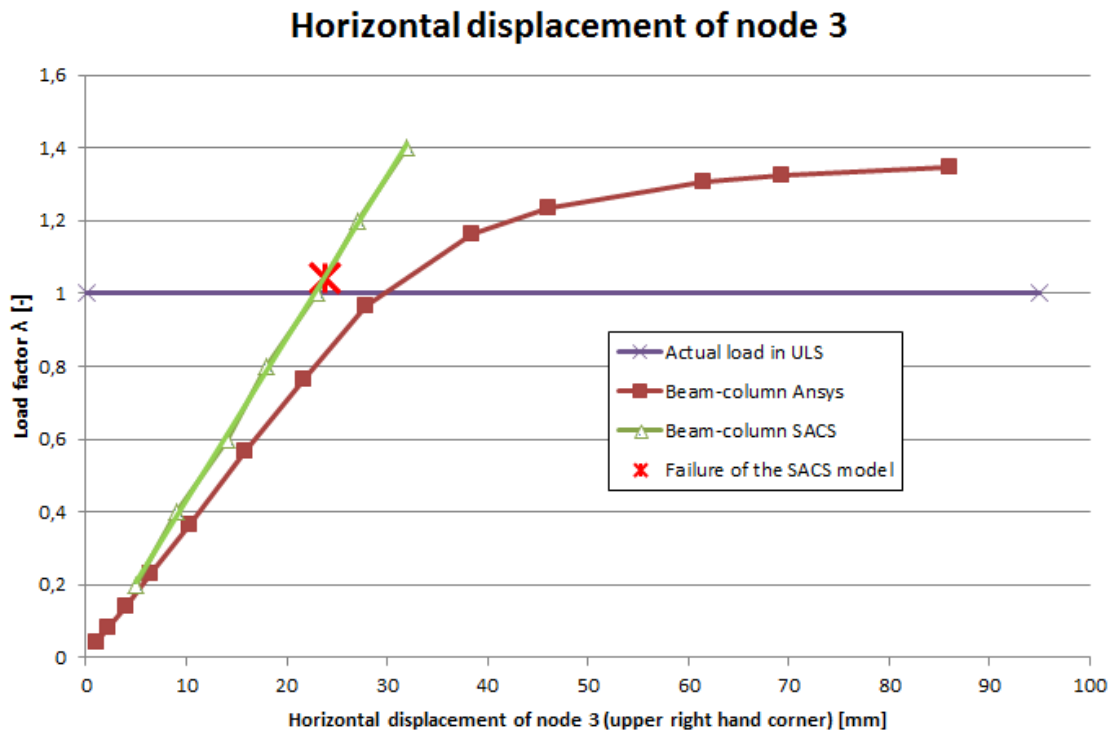
Figure 7.1 shows the effects of the linear elastic calculation that is performed by SACS. The load-deformation diagram of this model is linear, even after the point of failure. This point is shown to be at a load factor of $\lambda = 1.04$, at which one of the design verifications exceeds unity. Because of the linear elastic calculation that does not take into account the failure of said member, it is not clear whether the structure has any capacity left, and is thus considered to fail at that stage.

The Ansys model, however, takes into account the redistribution of internal forces in the separate members upon reaching the yield in one or more members. In figure 7.1, this is seen by the reduced stiffness for the Ansys model of the beam-column at a load factor of around $\lambda = 1.0$. Herein, it is seen that a considerable amount of residual capacity is present in the structure, as it ultimately fails at a load factor of $\lambda = 1.37$.

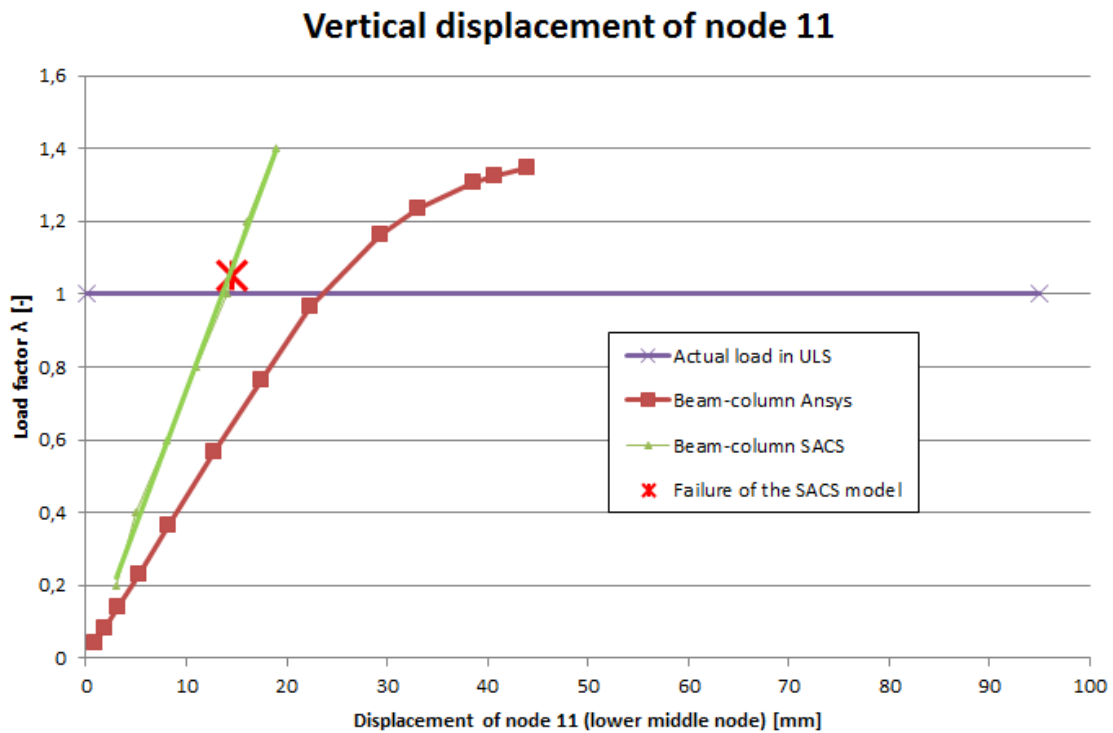
In the elastic regime, the beam-column model made in SACS shows a stiffer behaviour than the model made in Ansys. This is due to the cross sectional deformation in the CHS that the Ansys model takes into account, whereas in the SACS model, the cross section remains circular. Therefore, only the part of the joint that is attached to the beam is contributing to the rotational stiffness in the Ansys model, as opposed to the line model in SACS, which takes into account the whole cross section in determining the rotational stiffness. The differences in the deflection field of the Ansys and SACS models are presented in figure 7.2.

In the figure, the deformed shape of the SACS and Ansys models are compared. The comparison is made at different load factors, for which the frame deflection at node 3 is identical for both of the models. This load factor is chosen to be in the elastic domain for the Ansys model, so the deformations are linear and the displacement field is compared.

It is seen that the overall displacement of both models is roughly equivalent, with the joints of the members coinciding at most of the nodes. The SACS-software determines these displacements considering the beams as a single element, while the Ansys-software determines the nodal displacements by integrating the results of all separate elements. Therefore, the members of the SACS-model remain straight, while the Ansys-model has members that are deflected internally. This is also the reason for the cross sectional distortion discussed in section 6.3.1.



(a) Horizontal displacement in node 3 for the beam-column designs



(b) Vertical displacement in node 11 for the beam-column designs

Figure 7.1: Displacement of the beam-column designs made in SACS and in Ansys: (a) for the horizontal displacement in node 3 (upper right hand node), (b) for the vertical displacement in node 11 (centre bottom node)

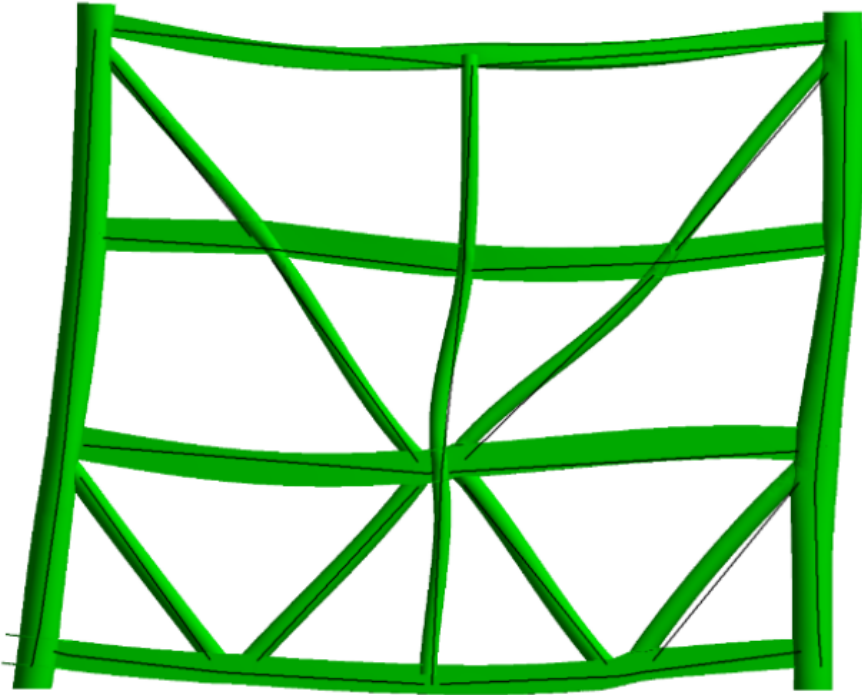


Figure 7.2: Comparison of the deformed shape in SACS and Ansys under the same horizontal deflection in node 3: the green shape represents the Ansys model and the black line represents the SACS model

Both of the models of the beam-column design fail on shear in the lower left support: the SACS model shows the highest unity checks and the Ansys model shows the highest strains at this location.

7.2. Comparison of designs

The beam-column design and the stressed skin design are compared on their displacements, steel mass and welds. Herein, the displacements are compared to analyse the structural performance of the designs respective to the load bearing capacity. The steel mass and welds are compared in order to find the design that is economically most attractive.

7.2.1. Deformations

The designs are compared on the displacements of distinct nodes in the designs. The horizontal displacements at right upper hand node (node 3 in figure 6.1) and the vertical displacements at the middle bottom node (node 11 in figure 6.1) are considered. These are given in figure 7.3.

In figure 7.3, it is seen that the stressed skin model behaves stiffer than both of the beam-column models. Also, it is seen that the designs have a similar level of safety: both of the designs can attain a load factor of around $\lambda = 1.37$. This is a direct consequence of the designing of the stressed skin design, which is made to show a similar load bearing capacity.

7.2.2. Mass

The primary factor that is used for comparing the designs is the structural steel mass. The mass of the designs is given in table 7.1.

Table 7.1: Structural masses of the models

Design	Frame mass [mT]	Wall mass [mT]	Total mass [mT]	Percentage of stressed skin
Beam-column	50.8	16.5	67.3	150.6%
Stressed skin	22.7	22.0	44.7	100%

The entries in the table are subdivided in their location in the design. The division is made to include elements that are part of the supporting frame and parts of the wall. Herein, the wall for the stressed skin design is considered to be a structural element, as opposed to the same wall in the beam-column design, which is a purely architectural seal.

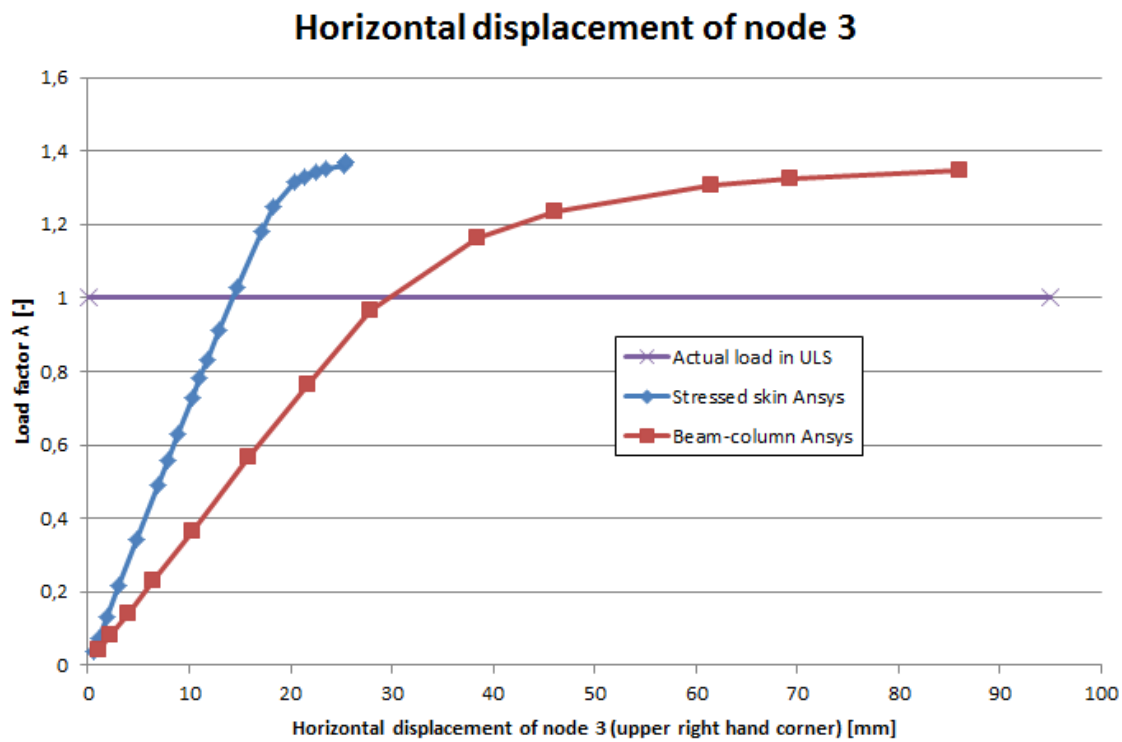
When comparing the total weight of the designs, the stressed skin design performs better than the beam-column design; the latter of these having a total weight of $\frac{67.3}{44.7} = 151\%$ of the stressed skin design. The reduction in steel mass for the structural steel frame in the stressed skin design is partly compensated by the increased mass of the separating wall. However, the combination of the structural and architectural system in the stressed skin design proves to reduce the steel mass in the design.

When the design of the structure was made without the necessity of the separating architectural wall, the mass of the beam-column design would have been $50.8mT$. If this value is considered, the beam-column design would only contain $\frac{50.8}{44.7} = 114\%$ of the mass of the stressed skin design.

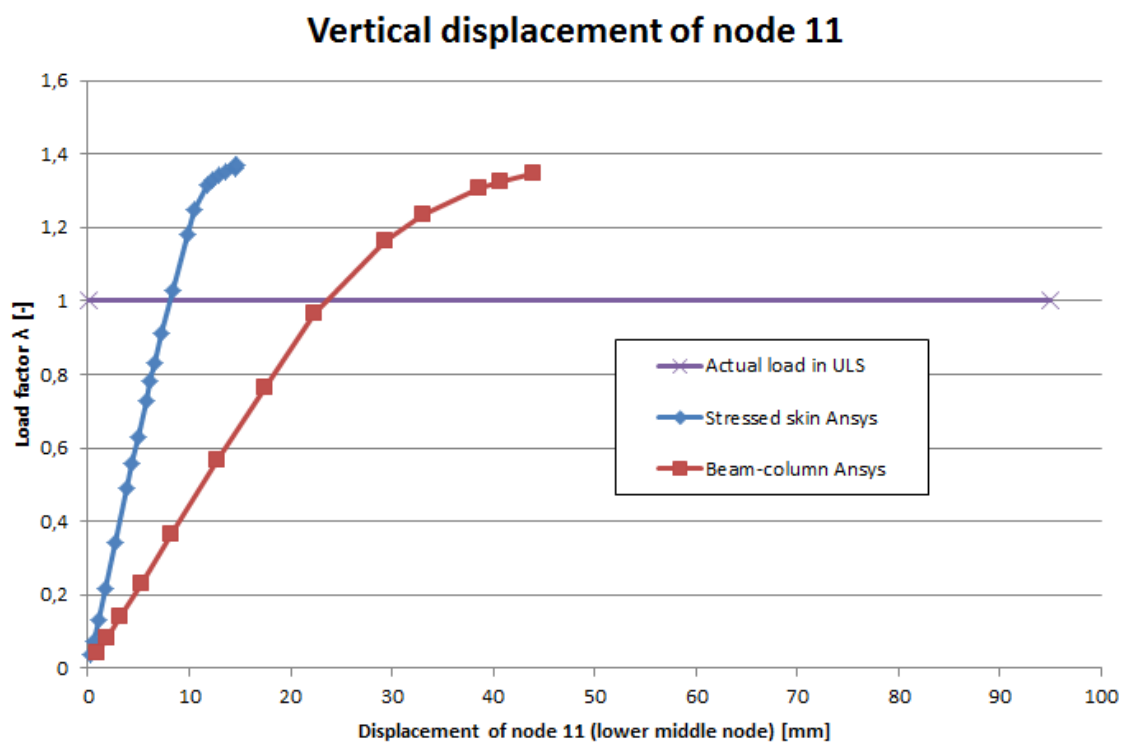
7.2.3. Welds

In addition to the (structural) mass, the designs are also compared on the welds. As the welds make up a significant part of the manufacturing process, these are taken to be representative for this. The labour intensity of the welds is dependent on the number of weld passes that is needed to complete the weld. Based on the geometry and volume of the weld, the number of weld passes is determined by appendix F.

The welds can be constructed in one of two ways. For the long and straight welds, a mechanised welding method may be used. For the more complex joint welds, manual welding might be necessary. The application of a mechanised welding method contributes to some advantages over hand-welding: by the automated nature, thicker weld passes may be used and the number of weld passes is reduced and because of the automation, less human labour is required. Therefore, a distinction is made between hand-welding and mechanised welding.



(a) Horizontal deflection in node 3



(b) Vertical deflection in node 11

Figure 7.3: Load-deflection diagram at distinct nodes (see figure 6.1) for the different designs: (a) displacement in horizontal direction at node 3 and (b) displacement in vertical direction at node 11

In the comparison, the connections between the considered structure and its surroundings (walls and deck floors) are not considered, as these are not part of the design.

The standardized geometry of the welds is shown in figure 7.4. Herein, figure 7.4a represents the butt weld of two elements with thickness $t \leq 8\text{mm}$, with a gap width of $b = 6\text{mm}$. Figure 7.4b shows the butt weld of two elements with thickness $t > 8\text{mm}$ and accessible from both sides, using a gap width of $b = 2\text{mm}$ and bevel angle of $\alpha = 60^\circ$. In figure 7.4c, the butt weld of two elements with a thickness $t > 8\text{mm}$ and accessible from only one side is shown. Herein, a gap size $b = 2\text{mm}$ and a bevel angle of $\alpha = 60^\circ$ is assumed.

In figure 7.4d, the geometry of a fillet weld connecting the stringers to the main plate is given. Herein, the total throat thickness is made sure to be larger than the plate thickness of the attached element. Figure 7.4e shows the geometry of the weld connecting two orthogonal elements, which are positioned with a gap of $b = 1\text{mm}$. Figure 7.4f represents the weld between a brace to the chord. Because of the complexity of this weld geometry, it is considered separately.

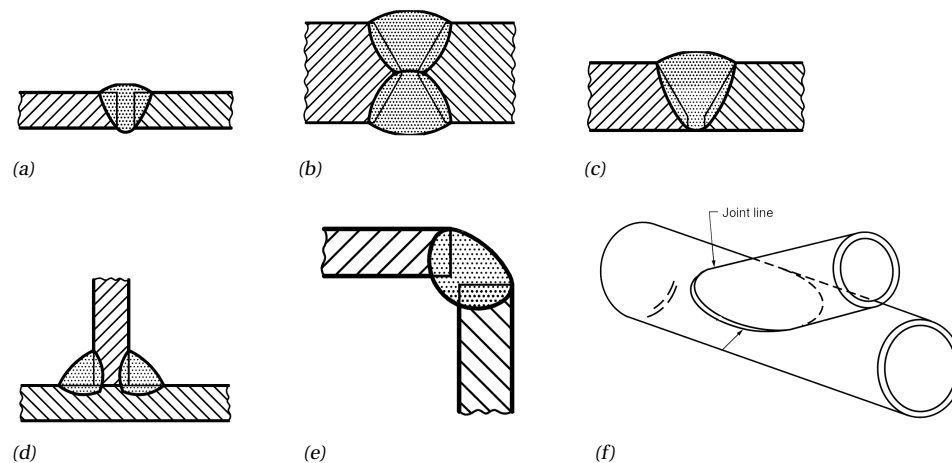


Figure 7.4: Standardized geometry of the welds: (a) for small butt welds accessible from only one side, (b) for large butt welds accessible from both sides, (c) for large butt welds accessible from only one side, (d) and (e) for fillet welds, and (f) for connections between tubular braces to chords

In tables 7.2 and 7.3, the welds are determined under the assumption that the welds have a higher resistance than either of the attached elements. For the butt welds, this means that the weld thickness is determined using a weld thickness equal to the thinnest attached element; for the fillet welds, the throat thickness is equal to the thickness of the attached element. Therefore, it is said that the welds are not a critical element in the design.

In the tables, the volume of the welds is given for each of the welds. Also, the number of weld passes per weld is given, determined using an example calculation given in appendix F. This value is integrated over the length of the welds to get a total length that is welded. The weld volume and weld pass length is used for the comparison of the designs.

It is seen that the beam-column design consists of a substantially lower welded volume than the stressed skin design: $2.59 * 10^7 \text{mm}^3$ for the beam-column design, and $6.85 * 10^7 \text{mm}^3$ for the stressed skin design. This means that the stressed skin design has $\frac{6.85 * 10^7}{2.59 * 10^7} = 264\%$ as much welds as the beam-column design by volume.

When the total weld pass length is considered, the beam-column design is more efficient. The total length of the weld passes is 1257.4m , as opposed to the stressed skin design, which totals to 5081.8m . This means that the stressed skin design consists of $\frac{5081.8}{1257.4} = 404\%$ as much weld pass length as the beam-column design.

Apart from the weld volume and total weld pass length, the ease of welding has to be taken into account. The stressed skin design consists mostly of long and straight fillet welds, as opposed to the beam-column design, in which the complex nodes require more difficult welding procedures. The amount and level of automation may vary between the different manufacturers, depending on the available equipment and other resources.

In the stressed skin design, a significant portion of the welds are present in the build up of the supporting

Table 7.2: Decomposition of the welds in the beam-column design

Weld	Weld type see figure 7.4	Number of welds	Weld length (per weld) [mm]	Weld thickness [mm]	Weld volume [mm ³]	Number of passes (per weld)	Passes × length [m]
Hot rolled sections							
Butt weld HE550A web	b	4	492	12.5	$1.38 * 10^5$	6	11.8
Butt weld HE550A flange	b	$2 \times 4^\dagger$	300	24	$5.14 * 10^5$	12	28.8
Butt weld HE800A web	b	8	734	15	$5.58 * 10^5$	6	35.2
Butt weld HE800A flange	b	$2 \times 8^\dagger$	300	28	$1.36 * 10^6$	16	76.8
Butt weld HE700M web	b	6	636	21	$6.46 * 10^5$	10	38.2
Butt weld HE700M flange	b	$2 \times 6^\dagger$	304	40	$1.98 * 10^6$	40	145.9
Tubulars							
Main columns	c	12	2791.6	25.4	$1.42 * 10^7$	16	536.0
Vertical upper decks	f	1	1218.8	19	$1.73 * 10^5$	9	11.0
Vertical lower decks	f	2	1225.2	16	$2.60 * 10^5$	7	17.2
Diagonals upper decks	f	6 at 48.1°	1502.6	16	$9.55 * 10^5$	7	63.1
	f	2 at 41.9°	1608.5	16	$3.41 * 10^5$	7	22.5
Diagonals lower decks	f	4 at 52.0°	1816.9	30	$2.32 * 10^6$	18	130.8
	f	2 at 48.2°	1878.3	30	$1.20 * 10^6$	18	67.6
	f	2 at 41.8°	2015.2	30	$1.29 * 10^6$	18	72.5
Total weld volume [mm³] & weld passes [m]					$2.59 * 10^7$		1257.4

† All I-sections have 2 flanges to be welded

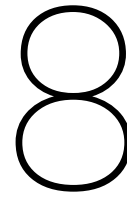
Table 7.3: Decomposition of the welds in the stressed skin design

Weld	Weld type see figure 7.4	Number of welds	Weld length (per weld) [mm]	Weld dimension [mm]	Weld volume [mm ³]	Number of passes (per weld)	Passes × length [m]
Main plate				Thickness			
Horizontal welds	a	5	18000	8	$1.44 * 10^6$	3	270
Vertical welds	a	1	15000	8	$2.40 * 10^5$	3	45
Stringers				Leg length			
Tee stringers	d	$2 \times 12^*$	15000	6	$6.48 * 10^6$	2	720
Rib stringers	d	$2 \times 5^*$	15000	6	$2.70 * 10^6$	2	300
Supporting column				Leg length			
Weld to main plate	d	$2 \times 2^*$	15000	6	$1.08 * 10^6$	2	120
Corner welds	e	8	15000	20	$2.57 * 10^7$	9	1620
Supporting beam				Leg length			
Weld to main plate	d	$2 \times 2^*$	17300	6	$1.25 * 10^6$	2	138.4
Corner welds	e	8	17300	20	$2.96 * 10^7$	9	1868.4
Total weld volume [mm³] & weld passes [m]					$6.85 * 10^7$		5081.8

* The fillet weld geometry consists of 2 welds at both sides of the attached plating

beam and column. In total, $\frac{2.57*10^7+2.96*10^7}{6.85*10^7} = 81\%$ of the total weld volume and $\frac{1620+1868.4}{5081.8} = 69\%$ of the total weld pass length is present in the supporting beam and column.

As the beam-column design would fail on strength, the full penetration of the welds is a necessity. For the stressed skin design however, the welds might be overdimensioned.



Conclusions and Recommendations

This section presents the conclusions of the thesis, as well as recommendation for further study. All conclusions are based on the analyses performed in the previous sections and are directly or indirectly related to the objective stated in section 1.2.

8.1. Conclusions

The main conclusion is given in section 8.1.1, then the use of the different software packages is considered in section 8.1.2, after that, the conclusions about the designs are presented in section 8.1.3.

8.1.1. Objective conclusion

In the thesis, the research question that is answered is:

Will a design of an offshore module using steel plated elements be competitive in comparison to a design using beams and columns in terms of mass and weld labour?

The general conclusion to the research question is that a competitive design can be made for an offshore module using steel plated elements, given the requirement for the structure to be sheltered from the environment. The respective contributions to the conclusion are given in the following.

Mass

The mass of the designs is compared in section 7.2.2. Herein, it becomes clear that the stressed skin design behaves more efficiently in terms of overall weight. The removed necessity for an additional separating wall in the stressed skin design accounts for a significant part in the weight reduction: the mass of the beam-column design is 151% of the stressed skin design, when the architectural wall is not considered, the mass of the beam-column design is only 114% of the stressed skin design.

Welds

The welds in the design make up for a significant amount of the manufacturing costs. Therefore, the number of welds is minimized. These outcomes are summarised in section 7.2.3. From that, it is concluded that the beam-column design scores better with respect to the total weld volume and total weld pass length. In terms of weld volume, the stressed skin design uses 264% of the weld volume of the beam-column design. When the total weld pass length is considered, the value becomes 404%.

In determining the labour required for completing the welding in the design, it is also considered that in the beam-column design, all welds are to be performed by hand. This is in contrast to the welds in the stressed skin design, which can be automated for a significant part. Dependent on the fabrication yard performing the welds, the benefits of welding automation may vary.

8.1.2. Modelling

During the project, different software packages are used. Conclusions about the modelling in these software packages are given below:

- For the initial overall model, the line element analysis software of SACS and the FEM software of Ansys show similar results. The difference in the displacement field is seen in figure 7.2.
- In order to provide a stable design, some detailing needs to be modelled in the Ansys software (as shown in figure 6.6). The SACS software assumes moment resisting joint and members that retain their shape under loading, and therefore these detailing does not need to be taken into account.
- A good understanding of the software is necessary to build up a model and analyse it in a correct manner. When dealing with software without thorough knowledge, certain functionalities can be overlooked and default settings might be unwillingly applied.
- Calculations in the Ansys models tend to be more time consuming than the calculations in the SACS models. This is due to the analysis type that is used: for Ansys, a full FEM shell analysis is performed, while in SACS a much lighter line element analysis is used. Therefore, modelling the full topside cannot be readily done in Ansys, while this is no problem to do in SACS.
- Because of the difference in the analysis between SACS and Ansys, the different designs cannot be compared while modelled in the different software packages. Therefore, the third model is made to obtain comparable results for the designs.
- The linear elastic calculation in the SACS software provides conservative results with respect to the ultimate load bearing capacity ($\lambda_{max} = 1.04$) when compared to the results from the Ansys model ($\lambda_{max} = 1.34$, see figure 7.1). The stiffness of this SACS model is non-conservative when compared to the Ansys model, as the angles of the load-deflection diagrams in figure 7.1 of the models show that $k_{SACS} \approx 2 \times k_{Ansys}$.

8.1.3. Designs

The conclusions that are drawn on the different designs that have been made are presented in this section.

- The stressed skin design behaves much stiffer than the beam-column (see figure 7.3).
- The transport loading is the most governing load condition, because of the effects of the motions during transport. Locally, however, any of the other load conditions may be governing. In a detailed design, these cannot be omitted.
- Both of the designs in Ansys show an additional load bearing capacity after local yielding or buckling. This is seen in the load-deflection diagram of figure 7.3 as the curves for the Ansys models flattening out above a certain load factor.
- The structural mass of the stressed skin design of the frame is somewhat smaller than the structural mass of the beam-column design ($\approx 14\%$). The necessity for an additional separating (inner) wall in the beam-column design adds to the mass of this design. Therefore, the total mass of the beam-column design becomes approximately 50% higher than the stressed skin design (see table 7.1). It is noted that the mass reduction holds for the walls of the design, as the floors of the design already use the stressed skin design methodology.
- The welds in the supporting beam of the stressed skin design take up a considerable portion of the total welds of this design (81% of the volume, 69% of the weld pass length, see table 7.3). Using a hot rolled section might prove preferable over forming a column of steel plated elements.
- The Ansys model of the stressed skin design buckles at an SLS loading, which is in this case taken as a load factor $\lambda = 0.833$ (see figure 6.11). This is inherent to the structural concept of the stressed skin design, which activates the post-buckling strength. Making use of the post-buckling behaviour increases the strength, but in the post-buckled regime, the stiffness greatly decreases as opposed to the situation prior to initial buckling.

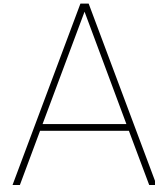
8.2. Recommendations

The main conclusion to the research question is that a competitive design for offshore modules can be made in steel plated elements, given that the structure need to be sheltered. The differences in the comparison of the beam-column design methodology and the stressed skin design methodology, however, are relatively small. Therefore, the resources with respect to welding at the fabrication yard and the experience in suitable software packages will be a deciding factor in determining which design methodology to use.

8.2.1. Further study proposal

During the thesis, choices are made to which aspects to consider. Several options on continuing on this thesis are found below.

- The design is set up in steel grade S355. For higher steel strengths (e.g. S460 or S690), the results will differ. Increasing the yield strength of the material increases the load bearing capacity of elements that are critical on strength. For elements that are critical on stability, increasing the steel grade has little to no influence on the bearing capacity. As such, it can be investigated whether the conclusions hold when steel grade S460 or S690 is applied.
- The stressed skin design is set up using stiffened steel panels. Herein, the welds play a large role making the conclusions. It can be investigated whether corrugated steel panels can add to the value of the design.
- As the welds are considered to be full penetration, it can be investigated if this is necessary. In the beam-column design, the members fail primarily on strength, which validates the full penetration of the welds. The stressed skin design, however, fails on instability. Therefore, some profit could be made to the stressed skin design not using full penetration welds of interrupted welds.
- Openings will be necessary in the stressed skin wall (e.g. for the purpose of doors, ducts). At these places, the structure will be weakened. It can be investigated to what extent the structure is weakened by the openings and what measures can be taken to prevent failure.
- The architectural sheltering wall that is present in the beam-column design has to be seal welded too. This is not considered in the thesis and it could have an influence on the total weld labour. This can be looked into.
- In the analyses, only one heavily loaded frame is considered. For a complete overview of the structural behaviour, in particular of the stressed skin design, the full topside should be modelled.
- The SACS software is capable of analysing plated elements. At Iv-Oil & Gas, this functionality is rarely used, and it may therefore be interesting to check whether the stressed skin design can be made with SACS, and how this compares to models created in the Ansys software.
- A combination of the beam-column design and the stressed skin design might be applicable, see figure 1.3. It might be interesting to investigate how a design that combines these methodologies compares to the designs presented in this thesis.



Literature review

In the effort of achieving a competitive design regarding offshore structures, the state of art in several topics should be investigated. The overall thesis scope includes a complete design of an offshore substation module topside, which is carried by either a beam and column type of structure or a steel plated structure. Since at Iv-Oil & Gas the former of the two methodologies is commonly applied, the focus will be on steel plated structures in the literature review.

In section A.1, the books used in the thesis are considered. Previously conducted theses are presented in section A.2 and used papers are found in section A.3. In section A.5, a mathematical derivation to plate buckling under different types of loading is presented.

A.1. Books

During the thesis, information is collected by several means. One of the most important sources of information are books. In this section, the books that have been used in the thesis have been elaborated.

A.1.1. Ultimate Limit State Design of Steel-Plated Structures [2]

In an effort to collect and arrange all knowledge regarding offshore steel plating design, Paik and Thayamballi wrote a book on the limit state design of steel-plated structures. It embraced the whole range of topics connected with plated steel elements. Starting with the principles of limit state design, going through the buckling and post-buckling behaviour of several steel plating topologies and the methods used to numerically analyse the considered structures.

Usefulness

This book is one of the best elaborations of offshore steel plate design, so its value is of incredible importance. It is used as the reference of choice when considering plated structures. The fact that the book is written keeping limit states in mind only contributes to its usefulness.

A downside of the book is that it is not always clear if the derivation of a certain formula is based on theoretical or empirical data.

A.1.2. Guide to Stability Design Criteria for Metal Structures [23]

Ziemian (2010) collected a lot of information regarding steel structures and created a comprehensive reference to steel structure design. In light of [2], especially of interest during this thesis are the chapters that are not dealing with plated structures. Regarding the elaborateness of the book, all kinds of questions will be able to be answered by the book. Also of interest is the provided background information, which grants an additional sense of familiarity with the considered topics.

Usefulness

The book is used as a general reference to steel structure design. All that is not basic knowledge, nor specialist topics, can be found in this book. Especially for the topics not regarding plated steel elements, the book is of value, as those topics are not discussed in [2].

A.2. Previously conducted theses

A.2.1. Optimal design of a module structure with sheeting [4]

In 2012, Xu conducted her master thesis at the Delft University of Technology, investigating the application of steel plated elements to onshore substation modules. A project in northern Siberia was taken as reference in order to come up with a valid comparison. In this reference project, the substation itself was onshore, though the transport was by offshore means. The structure considered was a 300 tonnes substation, which was originally designed using a space frame for the load bearing function.

In this thesis, three plating systems have been considered, namely the stiffened plate, corrugated plate, and sandwich panel. Due to the harsh conditions at the project location, there were some requirements regarding insulation. The analysis is limited to a single wall, that represents the whole structure and conclusions have been drawn from this one comparison. In order to get a more accurate conclusion, the whole structure should be regarded.

Usefulness

Above thesis is the basic starting point of this thesis: the problem at hand is quite similar, and so is the approach. However, the structure considered in this thesis will be much larger than that of Xu, and is an entirely offshore structure, as opposed to offshore transportation only. As the structure is more heavily loaded, the complexity increases, so understanding the fundamentals of above thesis is an important element of the preparatory works.

In the thesis of Xu, the care is taken for the structural modelling, which will bring a lot of information about the approach to tackle such a problem. The use of the FEM software is elaborated quite well. The Eurocode is used in the design of the structure, which is another aspect that proves the importance of the thesis.

A.2.2. Defining parameters for buckling checks in finite element software packages [5]

In his master thesis, Aberkrom (2014) investigates several plate buckling configurations and their appropriate buckling behaviour. His intention was to create a brief overview of buckling modes and the way they should be numerically modelled. The report is based on the ABS and DNV standards.

Aberkrom starts with explaining the general formulation of buckling. Herein the buckling factor is defined as the ratio between the critical plate buckling stress and the buckling stress as if the plate were considered a beam. Next, he elaborates on the plate buckling phenomenon. Applying the influence of the Poisson ratio on the buckling modes yields the general plate buckling expression shown in A.1. This expression is analogue to the expressions posed in Mathematical background.

$$\sigma_{cr(plate)} = \left(\frac{mL}{s} + \frac{n^2s}{mL} \right)^2 \frac{\pi^2 E}{12(1-\nu^2)} \left(\frac{t}{s} \right)^2 = k \frac{\pi^2 E}{12(1-\nu^2)} \left(\frac{t}{s} \right)^2 \quad (\text{A.1})$$

in which σ_{cr} is the critical buckling load of the plate, k is the buckling factor dependent on the support and loading conditions, E and ν are the material properties of Young's modulus and Poisson ratio, respectively, and t and s are geometric properties of plate thickness and span, respectively.

After this derivation, the geometry of the plate panels considered is explained, also the buckling modes are elaborated. It is noted that the buckling modes influence each other and that searching for one of the modes is difficult. However, it can be said that the mode that yields the lowest buckling strength is governing.

Further information is given on the buckling behaviour of unstiffened plate panels, including the influence of boundary conditions and adjacent plate fields. For this application, the effective width method regarding plate buckling is introduced, in which the centre of the plate is assumed to have no strength, while the

supported edges carry a load of up to the yield stress. Experiments have proven this method to be generally applicable. Figure A.1 illustrates the this method, the effective width S_e can be determined according to A.2.

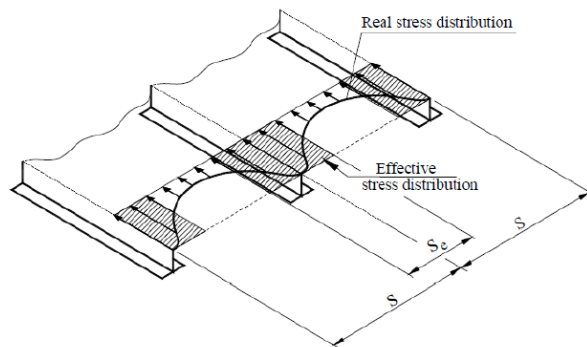


Figure A.1: Effective width regarding plate buckling of a uniformly loaded stiffened plate

$$S_e = \frac{\sigma_{cr}}{\sigma_0} S \quad (\text{A.2})$$

in which σ_{cr} is determined in A.1, σ_0 is the yield strength of the material and S is the plate span in transverse direction.

After the unstiffened plate panel buckling, the stiffeners are considered. The failure modes that have been identified in the flexural regime are the buckling and crippling of the stiffener webs and the beam-column type buckling of the entire stiffener. In the latter, the stiffener is considered in combination with the plate as to obtain a built up plate girder. Two important parameters for analysing this buckling mode are length and slenderness. Standards indicate reductions on the beam length as a result of certain support conditions. As long as the model does not specify these conditions, the lengths should be modified manually in order to arrive at an accurate buckling resistance.

Plastically, stiffeners can buckle due to lateral torsional buckling. Due to the plasticity of this failure mode, the structure shows no post-buckling behaviour and thus has no additional ultimate strength. The DNV includes a lateral torsional buckling check in their standards.

It is noted that in all of the buckling modes considered, the lateral pressure, although it has an inevitable influence on the buckling behaviour, is not considered in this thesis.

The main part of the thesis consists of a numerical research of a stiffened box girder. In this effort, two models are set up: one built up entirely from plate elements, the other built up with plate elements and stiffeners made of beam elements.

Then Aberkrom compares the prescriptions from the codes to the calculation methods in the FEM packages. In most software, the Poisson ratio is applied in order to achieve an accurate stress result in the structure. The codes, however, tend to require an additional stress component due to this Poisson ratio. Thus, care should be taken whether there should be a factor taking into account this discrepancy.

The next item in his thesis is the linearization of the stresses occurring at the plate edges. Codes specify a linearized input on the edges, while the FEM generally provide a pronounced and probably more accurate stress distribution. Aberkrom proposes four stress linearization methods:

- based on the corner stresses
- based on all stress results
- based on all stress results and shifted up to the level of the maximum stress
- based on the Eurocode (EN1993-1-5 4.6(3))

The stresses of the first three methods are then to be averaged over opposite edges, since these stresses should be in equilibrium in order to prevent rigid body motion.

Thereafter, the influence of shear stress is investigated. Figure A.2 shows some possibilities of shear stress along the edge of the plate. Due to this shear stress, σ_{min} and σ_{max} can differ from each other. If this shear stress is to be taken into account in the differential equations, a tedious equation is obtained. Therefore, the behaviour of the plate under combined in-plane loading and shear stress is described in an empirical way.

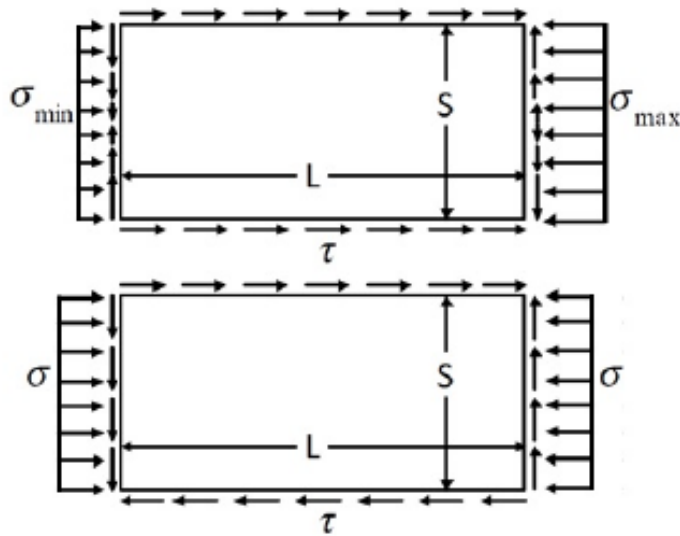


Figure A.2: Influence of shear stress on in-plane stress distribution

Using the theory mentioned above, the numerical analysis is started. The general flow of the analysis is as shown in figure A.3. The model is checked under the actual loading on the structure and under linearized loading. After that, it is checked by the use of standards.

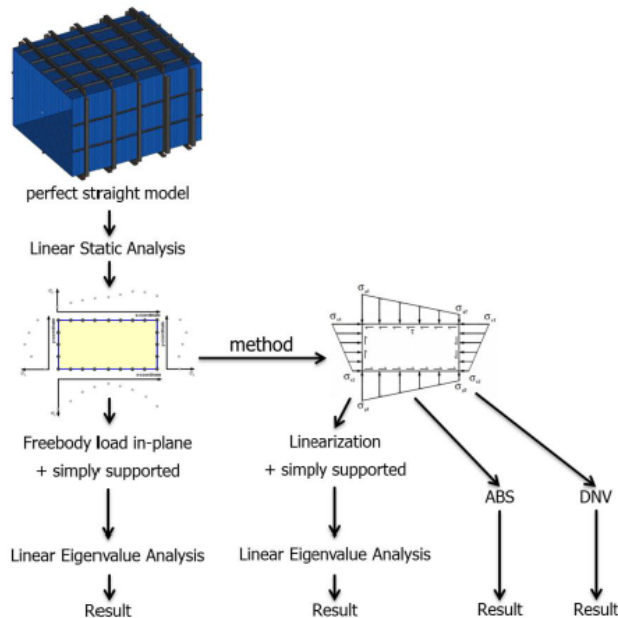


Figure A.3: Flowchart of analysis as performed by Aberkrom

In the numerical analysis, it is made clear that not all simplifications are validated. Aberkrom shows this fact by comparing the results obtained from the linearised model with the same model disregarding the shear stresses. An unbalanced result is obtained in which the chosen support conditions have a large influence on

the stress distribution. Aberkrom then formulates a method in which a summation of shear stresses and in-plane (compressive) stresses leads to the linearised in-plane stress distribution with according shear stresses.

Aberkrom uses 7 implementation methods for stress input on the plate, ranging from an average linear stress distribution to a free-body load including the complete actual stress distribution. Surprisingly, the simplest of the implementations yields exceptionally accurate results when compared to the more complicated stress distributions. However, the results might be unconservative. Using the Eurocode clause, the results of this method become conservative and hence is a better implementation.

The influence of mesh size on the shear stress results vary substantially. No conclusions can be drawn from that, so additional research has to be carried out. In the end, it is not really clear what method to use for stress linearization; a combination of implementation methods is proposed, which should be investigated some more.

After this, attention is given to the buckling behaviour of stiffeners. It is noted that in the ABS and DNV standards, there are certain limits posed to the geometry of stiffeners such that local buckling of these stiffeners would not occur. However, if these stiffeners are modelled as plated elements, the buckling check would become the same as that for the parent plate. Additionally noted is the fact that in stiffener web or flange, usually there is a section that is not supported by four supports.

In case the stiffeners are checked using the same plate element analysis described above, the results would be quite comparable, yet somewhat more non-conservative (at least, in this case). Regarding the few analyses done, no conclusions can be drawn.

Next, Aberkrom indicates the derivation for the effective width based on a beam-column type of collapse. For the plasticity correction, the Perry-Robertson formulas is used when considering the DNV codes and the Johnson-Ostfeld formulas when applying the ABS standards. Also, a magnification factor for taking into account additional bending stresses due to the deflection is also considered. Using these notions, the maximum allowable bending moment in the plate-beam is derived. After that, the implementation method is validated using FEM calculations.

After the beam-column type of collapse, the torsional buckling limit is considered. As a starting point, Aberkrom indicates that the occurrence of lateral torsional buckling of the stiffeners is closely connected to the plate buckling phenomenon, and as such, should be extensively covered in the codes. However, the ABS code does not incorporate a check on this buckling mode, as it only considers the uniform pressure compared to the allowable stress. The DNV utilises a buckling check covering both torsion and warping.

Concluding, Aberkrom says that most of the influencing parameters are already covered in the standards, but that the derivations in the thesis are applicable whenever complex models are considered. Since for some models, the implementation of the proposed linear regression of stresses lead to increasing deviations, also a gradient in transverse and shear stress is proposed.

Usefulness

The entire thesis is made using the ABS Guide and DNV standards. As in present thesis the LRFD standards of the Eurocode are used, some parts of Aberkrom's thesis might not be fully applicable. However, the mode in which a structure buckles does not depend on the applied codes, but on the geometry. Applying the same geometry will yield the same FEM results, independent of applied standards.

The expressions for the lateral torsional buckling in the Eurocode are derived from the Perry-Robertson formulations, so having these explained is beneficial.

A.3. Papers

A.3.1. Stiffened plate

Since a great part of the thesis is carried out using stiffened steel plating elements, these should be considered as a basis in this literature review. In elaboration of the books of section A.1, Paik and Thayamballi [6] and Paik et al. [24] consider plate buckling and in particular the buckling of the overall stiffened panel. Additional information is given on the occurrence of the buckling modes and the physical background of the modes that are mathematically explained in their book [2].

Since the plated structure will not contain any hot rolled sections, the application of plate girders (Abspoel [7]) is investigated. These composed plate beams and columns can be utilised at locations that show high stress concentrations, such as the supports. For an economic design, these plate girders could be built up from different steel grades, which is the topic of Veljkovic and Johansson [8].

The support conditions of shear wall systems are investigated by Alinia and Dastfan [12], who state that the support of a shear wall system can be considered neither clamped or simply supported. They provide with some design criteria and evaluating analyses. The authors refer to Rhodes [13], who derives the formulae regarding the post-buckling behaviour of thin-walled structures.

For the stiffened panels, Sabouri-Ghomi et al. [14] derive expressions that limit the number of buckling modes. They provide with requirements for the stiffeners that lead to the local buckling mode, which is considered to achieve a more reliable post-buckling behaviour.

Some recent developments on ultimate limit state design technology for ships and offshore structures [6]

In the paper Paik and Thayamballi (2006) wrote on the developments of ultimate design technology, several interesting aspects regarding the design of steel plated structures were discussed. Most of the topics discussed hereafter can also be found in the book on Ultimate Limit State Design of Steel-Plated Structures [2], by the same authors.

Design methodology Firstly, they commented on the shift in use of design standards from the allowable stress methods to limit state design, like the Eurocode. The main reason for this shift was that in the allowable stress method the actual safety of a design was difficult to assess, as the value of the allowable stress is determined by results of practical works. This results in a single reduction factor imposed on the yield strength of the material. Instead, the probabilistic background found in the material and the consequent load factors used for the limit state design give a more pronounced overview of the actual situation. The additional insight acquired from the limit state design provides the opportunity to analyse the design to a greater extent than the allowable stress method. It is noted that no conclusions can be drawn as to which design methodology is more conservative than the other, which is shown in an example shown in figure A.4.

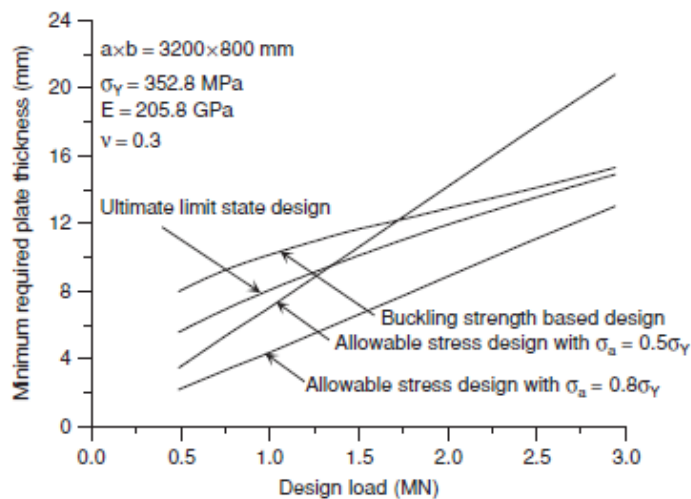


Figure A.4: Minimum required plate thickness of an arbitrary design situation on load and design methodology

Design idealisations In the design of steel plated structures, there is a multitude of ways to assess the strength of these plates. In the paper, three idealisations are presented, namely the plate-stiffener combination, the plate-stiffener separation, and the orthotropic plate model. Schematisations of these idealisations are given in figure A.5. Depending on the required speed or accuracy of the calculation, a (combination of) idealisation(s) can be used.

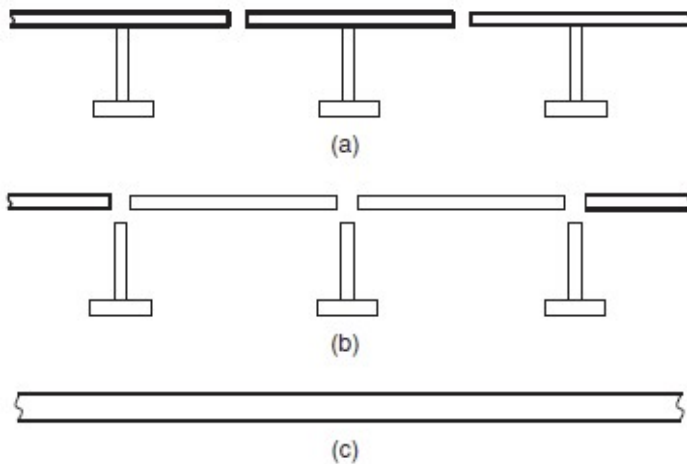


Figure A.5: Design idealisations: a. Plate-stiffener combination, b. Plate-stiffener separation, c. Orthotropic plate model

When considering the plate-stiffener combination, Poisson ratio, torsional rigidity and the effect of intersecting beams in the stiffeners are neglected, resulting in conservative designs that are relatively quick to achieve.

In the plate-stiffener separation model, more accurate results are obtainable. If the stiffeners are large, they can be considered as being a plated element in their own, so local buckling of the web needs to be investigated.

The orthotropic plate model can be used if stiffeners are relatively small and numerous, which can lead to a buckling mode in which the entire plate field including the stiffeners between the primary support beams buckles. In the paper, this is referred to as overall grillage buckling. Thereby, the stability of the stiffeners needs to be guaranteed. It is important to consider a combination of the above models in order to analyse the actual behaviour.

Several collapse pattern types have been investigated in this study:

- column or beam-column type collapse
- buckling of stringer web
- lateral-torsional buckling
- gross yield

The buckling behaviour of the stiffener webs is also considered, and it is stated that normally stiffener buckling and plate buckling interact in such a way that it can occur in any order. It is particularly undesirable for the stiffener to buckle first, so this has to be restricted. Local buckling of the plate decreases the rotational restraint of the plate-stiffener intersection, so the effective width of the stiffener has to be taken into account. After that, the lateral-torsional buckling is covered. Under the influence of low torsional rigidity of the stiffener, the combination of plate and stiffener will buckle together.

A distinction is made between elastic and inelastic buckling. The difference design-wise is that in elastic buckling, generally post-buckling capacity may be considered as opposed to inelastic buckling, which is regarded as ultimate failure. The stress level at which this ultimate failure is reached depends on the presence of geometric or material inconsistencies, corrosion, fatigue damage or local damage.

After this, the membrane method is explained, including redistribution of stresses and bending moments being carried via membrane action in largely deflected plates. The support conditions and derived formulas, considering in-plane and transverse loading, are given, indicating the location of the yielding part. These analytical formulas are complemented by empirical data, from which expressions are compiled that can be used in the preliminary (hand)calculations.

A strength reduction factor is introduced to take into account the presence of openings. This factor is determined empirically and does not take into account residual stresses present in the material. The author has derived a design formula that does consider residual stresses.

Usefulness The paper gives a lot of background information on failure modes and design methods. In the paper itself, there are not much expressions, but in the works cited, sufficient mathematical and mechanical derivations are provided.

The consideration of perforated plates is particularly of interest, partly because of the necessity of doorways and other access features of the structure, but also in case construction workers need to have a undocumented temporary hole for their construction activities. For this second case, some randomly placed holes need to be considered.

Large deflection orthotropic plate approach to develop ultimate strength formulations for stiffened panels under combined biaxial compression/tension and lateral pressure [24] In this paper, Paik et al. (2001) derive the expressions needed to analyse the orthotropic plate approach mentioned in section A.3.1. The expressions include large deflections and post-buckling effects, but no non-linearities in materials is considered, i.e. the section fails as soon as there is yielding somewhere in the cross section. The results in this paper are compared to non-linear FEM analyses. Further background of topics discussed in this paper is found in Ultimate Limits State Design of Steel-Plated Structures [2], written by the authors of this paper.

Orthotropic plate buckling occurs when the stiffeners are relatively weak in comparison to the master plate. In this case, the stiffeners will buckle along with the plate. If the stiffeners are very weak, the buckling failure will take place in the elastic regime. The normal approach to calculating the buckling resistance is to consider all of the buckling modes and selecting the one with the lowest buckling resistance value for the selected load pattern. The paper thus presents one of the buckling modes.

The material strength in the whole plate has not to be taken equal. However, all stiffeners in one direction are taken to be from the same strength class. The yield strength can then be taken as the average strength over the areas. The boundary conditions are taken to include a simply supported plate panel, which will give slightly conservative results over the actual occurring situation.

The derived formulas incorporate parameters that are normally assigned as material properties to be geometric properties. This means that the Young's modulus, which is usually a material property, in the orthotropic deck idealisation becomes both a material as a geometric property, which depends on the original Young's modulus and the influence of the stiffener stiffness.

Usefulness The topics discussed in this paper are part of the book by the same authors [2], which is used as the standard reference for plated structures. As the orthotropic plate approach is considerably relevant to the thesis, above paper is proven useful to the extent of it being an extract to said book.

The maximum bending moment resistance of plate girders [7] Abspoel investigates whether there is a maximum bending resistance for plate girders with a given cross sectional area. The paper mainly focuses on the web slenderness, and the arising failure mode of flange induced buckling. The study has been carried out in compliance with the Eurocode.

The starting point of the report is the fact that for a higher moment capacity using the same cross sectional area, a bigger lever arm between the flanges is needed. This is obtained by either removing material from the flanges and applying it in the web or increasing the web's slenderness, making it longer and thinner. As removing material from flanges could ultimately decrease the moment capacity, the maximum web slenderness is investigated. The failure mode that is considered to be governing is the flange induced buckling, which limits the value of the web slenderness. Combining this maximum web slenderness and the given cross sectional area, an optimum in moment capacity can be obtained.

These results are compared to several other studies regarding the same topic. The common element in this comparison is that there is a maximum in bending moment resistance when the web slenderness (expressed as the area of the web divided by the area of the flange) is varied. If the height to thickness ratio of the web is considered, the bending moment resistances of the investigated studies is not consistent.

Usefulness Since the plated structure designed in this thesis is made using stiffener elements that can be considered as a plate girder, the derivations of this paper will be applicable. For the hand calculation and

FEM validation, the stability of the stiffeners can be assessed more easily. The check on the maximum web slenderness can be incorporated in the hand calculations.

The inconsistency of the studies with respect to the web slenderness is due to some boundary conditions included in the study (e.g. whether effective width methods or reduced yield stress is considered). Application of the theory provided in this paper should happen in a cautious way and the right model for the situation should be determined.

Design of hybrid girders [8] In search for more economic use of high strength steel, Veljkovic and Johansson (2004) investigate the use of different steel grades in a steel plate girder. In order to get to this economic solution, the built up plate girder has a higher steel grade in the flanges than in the web. The investigation has been carried out with the Eurocode in mind.

In the USA, hybrid girders are already used for some decades now, starting around the 1960s, and hence they are included in the building standards. In Europe, the use of these girders is very limited. According to the Eurocode, the girders need to be divided into cross section classes, based on the susceptibility of lateral torsional buckling.

If the flanges of the girder are composed of a higher steel grade than the web, the web will be yielded before the flanges reach the yield stress. For the cross section classes 1 and 2, the bending resistance is easily obtained by A.3.

$$M_{Rk} = f_{yf} A_f (h_w + t_f) + \frac{f_{yw} A_w h_w}{4} \quad (\text{A.3})$$

in which f_{yf} and f_{yw} are the yield strengths of flange and web, respectively, A_f and A_w are the cross sectional areas of flange and web, respectively, h_w is the web height and t_f is the thickness of the flange.

For cross section class 3 and 4, the method is somewhat more cumbersome. Since the web is prone to buckling, the effective width of this web should be taken into account in the calculations. Under yielding of the flanges, this induces a stress distribution that is not symmetrical. Applying Eurocode 1993-1-5 for the check, the results are conservative if the yielding and buckling of the web is added up.

It is said that the reduction factor for lateral torsional buckling is taken the same as for homogeneous girders. However, the bending resistance coming up in the formulas should be taken as the reduced resistance obtained by using the effective width method of the cross section.

The shear resistance can be approximated by the rules posed by the Eurocode, since these already incorporate different yield strengths in web and flanges. For the interaction between bending and shear, it is said that the general rules may be applied for class 3 and 4; for class 1 and 2, it is proposed to neglect the interaction, as this is the best practice in the USA.

The limitation to the stress interval in the girder is $1.5f_y$, which means that after the first loading, the element considered will be in the elastic regime. For the fatigue life, this has no influence, because of this elastic behaviour.

The derivations of above are checked through experiments carried out in several studies. Some of these tests lay outside the scope of Eurocode 3, so these are excluded from examination. The purpose of this comparative study was to determine a safety factor that can be used in order to cope with the hybrid girders. For the 30 specimens that were investigated, the safety factor of $\gamma_m = 0.995$ is obtained.

Usefulness The application of hybrid girders can make the design of these girders more economical. Since plated structures can be regarded as flat and smeared out girders, hybrid plates might give an economical design on plates too. Care should be taken, however, that the failure mechanism on the homogeneous plate should be strength-dominated. It might be necessary for the application of multiple steel grades into one plated structure to be investigated more elaborately for it to be relevant in this thesis.

Behaviour of thin steel plate shear walls regarding frame members [12] Alinia and Dastfan (2006) examine the influence of support conditions (simply supported, clamped) on the buckling behaviour, including surrounding member rigidity.

First, the torsional support rigidity of the plate panel is assessed. This is done since the edges of the shear wall are generally welded to the supporting members, which induces a certain torsional rigidity. The findings indicate that the support rigidity tends to lay closer to being clamped than that is simply supported, as most of the standards describe. However, assuming a clamped support condition yields non-conservative results. It is concluded that the rigidity can be assumed to be clamped for 80%. The paper examines the effect of the relative stiffness of the thin steel plate shear wall for the ultimate strength of the wall system.

In the finite element method part of the paper, the procedure in Ansys is described. The plate elements that make up the shear wall are supported to the surrounding members using torsional springs for the first part. The second part consists of the same model, only then the shear wall is connected to the surrounding members using a clamped interface.

After Ansys analysis, it is concluded that the buckling load heavily depends on the lateral support stiffness. However, the post-buckling behaviour does not depend on the bending stiffness of the shear walls, but rather on the extensional stiffness. The support condition is hardly of influence on the post-buckling strength.

Usefulness The research yields that the post-buckling behaviour of steel plate shear walls hardly depends on the support conditions, which can be benefitted from in case the post-buckling behaviour is accounted for. This way, the calculations performed can be simplified.

Some observations on the post-buckling behaviour of thin plates and thin-walled members [13] Rhodes (2003) executed an examination of the state of art research in post-buckling analysis of thin-walled steel structures, which serves as a resume and mathematical background of plate buckling analysis.

In figure A.6, the buckling behaviour of a profile steel section is shown. At the corners of the profile, it is visible that the deflections are much smaller than in the field sections. These geometrical conditions induce the post-buckling behaviour of this section. The structure loses some stiffness, but the strength of the column increases after the elastic buckling of the plate fields.

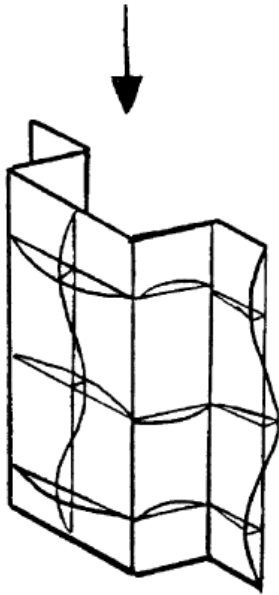


Figure A.6: Plate buckling and post-buckling deflection

The post-buckling behaviour discussed above is examined using energy equations. After some simplification, these formulas are compared to the widely known effective width method. Next, the differential equations taking into account initial imperfections (dubbed de “compatibility equations” and “equilibrium equations”) are posed. Due to the nature of these differential equations, only an analytical solution is obtained for the simplest of loading and support conditions. Ultimately, it is called for to introduce multiple effective widths

in the effective width method, one for the strength calculations and one for the stiffness calculations of the plated structure. This is because of the stress at the extreme fibre in the plate is not uniform due to changing stress distributions, as is seen in figure A.7.

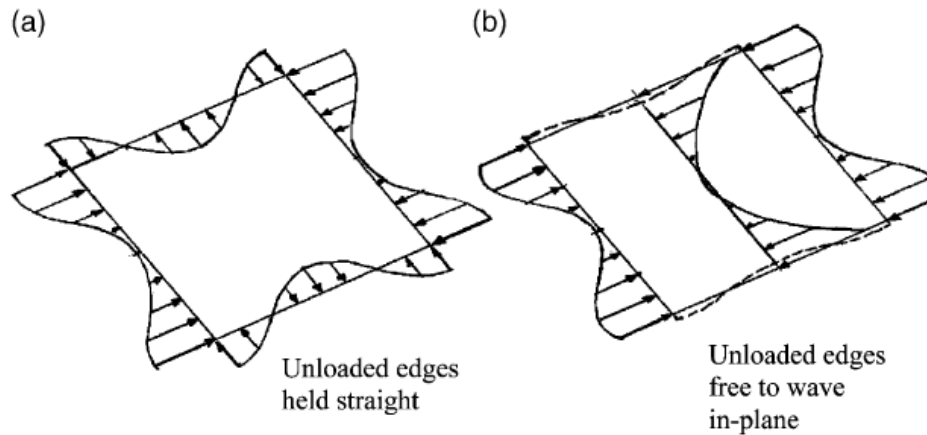


Figure A.7: Stress distributions on simply supported plates, in (b), non-uniformity is observed at the outermost fibres

Also, the behaviour far beyond buckling is considered by posing equations regarding strength and stability. A perturbation factor is introduced. In combination with the geometry of the plating, critical values for the stresses and strains are obtained. These equations are linked with the von Karman effective width equations.

Boundary condition for the above was a uniform loading condition. However, loading on steel plate structures is generally non-uniform. By applying a different expression for the strains to the equations that are indicated above, the (post-)buckling behaviour of the plates can be examined.

Lastly, plated columns are examined. Expressions are introduced for the buckling criteria and the post-buckling behaviour.

Usefulness In this paper, a great deal of equations is provided, which can be used to investigate (post)-buckling stability of plated structures under various loading conditions. Especially for hand calculations, these equations offer a good amount of help. The expressions that are considered in the paper offer a way for checking the outcomes of a finite element model.

Buckling behaviour improvement of steel plate shear wall systems [14] Sabouri-Ghomi et al. (2008) give requirements of the moment of inertia of plate stiffeners that is needed in order to force the failure mode of the system into local buckling of the infill plate. This way a more comprehensible structural behaviour is attained.

The equations for determining the strength regarding global buckling of the plate system are compared to the equations determining the local buckling strength. First, in the general case of stiffeners being equal in both directions and having an equal spacing, the required moment of inertia for the stiffeners is obtained. These boundary conditions eventually lead to a conservative result.

After the theoretical analysis, a FEM model was build and test specimens were loaded. All of these specimens showed large deformation capacities. Depending on the dimensions and spacing of the stiffeners, the test specimens failed on either global or local buckling.

The results from the analysis were quite straightforward: for thicker infill plates, a higher moment of inertia of the stiffeners is required to force the buckling mode into local plate buckling. Panels with double-sided stiffeners required a lower moment of inertia to attain the same phenomenon than the one-sided stiffened panels.

Usefulness The conclusions from the paper are almost directly applicable to stiffened steel plate design. It might be a good approach to force the panel in local buckling, eliminating some failure modes by the

boundary conditions set. Of course, attention should be given to the suppressed failure modes, but this could be accounted for by a check in the end, rather than a fundamental calculation during design.

A.3.2. Corrugated plate

Another means of stiffening a flat plate is by applying corrugations. The corrugation shapes of these plates can be sinusoidal or trapezoidal, of which the latter is mostly used. Application as wall elements generally consists of resisting the shear force as a so called shear wall. Their behaviour is assessed by Hosseinpour et al. [9] and is focused on the earthquake resistance of these panels.

A comparison is made between triangular corrugated panels and trapezoidal corrugated panels in the paper of El-Amin et al. [10]. Also, the influence of the number of transverse stiffeners in a steel panel shear wall is investigated. The trapezoidal corrugated panel is found to show better performance than the triangular corrugations.

As the corrugated panel is frequently used in shipbuilding, Sun and Spencer [11] investigate the buckling behaviour of these panels subjected to compressive and shear stresses, as well as lateral pressure. Attention is given to the possible buckling modes and after that, an FE-analysis is carried out.

Evaluation of steel shear wall behaviour with sinusoidal or trapezoidal corrugated plates [9] In this paper, Hosseinpour et al. (2015) investigate the behaviour of corrugated plate panels subjected to a shear load. The researchers continued an experiment on plate girder with corrugated webs, in order to come to a setup to investigate one-storey shear walls. An Ansys model is made and the results are compared to experiments, wherein non-linearity was used due to large displacements. The research targets earthquake loading, however, the applied loading in the test experiments is monotonic. The orientation of the used corrugation is horizontal.

It is concluded from the experiments that a plate geometry using trapezoidal corrugations leads to a higher ductility. On the bearing strength, the trapezoidal corrugated plate scores better for low thickness; for high thickness, the sinusoidal corrugated plate shows the highest bearing strength. On the stiffness, the sinusoidal corrugated plate shows a better behaviour than the trapezoidal corrugates. With increasing thickness, the stiffness increases at a rate that is less than proportional to the thickness.

If boundary members get stiffer, the overall system of the shear wall also gets stiffer. In the research, the boundary columns are held constant at a IPB180 cross section, the beam is varied between IPE180 to IPE300. Also, the bearing strength increases under increasing beam section.

The corrugation depth is also investigated. Under increasing corrugation depth, the bearing strength of sinusoidal corrugations increases significantly. However, the stiffness under shear loading decreases in the investigated range of corrugation depth of 19 to 60 mm. For the trapezoidal, the corrugation depth has insignificant effect on the bearing strength, ductility, and stiffness.

Lastly, the corrugation length is considered. In sinusoidal corrugations, for increasing corrugation lengths the ductility of the structure decreases, as the shear wall will be more prone to global buckling. The initial stiffness is unaffected. For trapezoidal corrugations, both the stiffness and bearing strength decrease for increasing corrugation lengths.

Usefulness The research was done primarily to investigate the performance of trapezoidal and sinusoidal corrugations against each other. The results regarding the structural behaviour of both types are quite inconclusive, since they both score better in different areas. The paper gives a good overview in which type is applicable in which case.

Elastic buckling behaviour of steel frames with corrugated steel shear walls [10] In this paper, El-Amin et al. (2005) investigate the buckling behaviour of corrugated shear walls in steel framing. By the use of a finite element model, the buckling strength of this plate configuration is assessed. The corrugation profiles that have been investigated are the trapezoidal and triangular corrugations with a constant corrugation angle and steel thickness, corrugation height and width were varied. These panels were oriented with the corrugations in the vertical direction. Also, the number of transverse stiffener is varied. The corrugation layouts that

have been researched are shown in figure A.8, figure A.9 shows the loading and the geometry of the applied stiffeners in the shear wall.

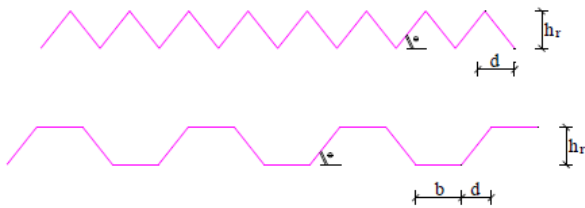


Figure A.8: Corrugation types considered in this paper

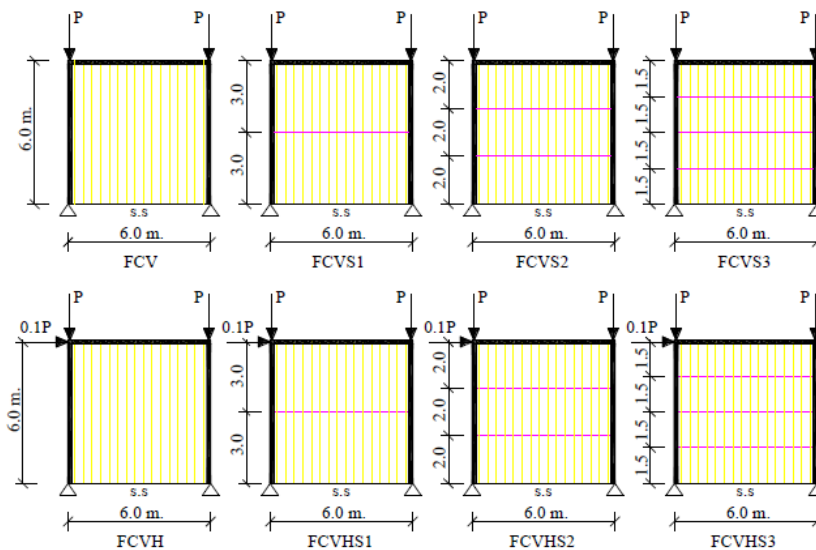


Figure A.9: Loading on the shear wall and transverse stiffener location

In the finite element analysis, the elastic buckling load is investigated. Therefore, an eigenvalue analysis has been performed. Herein, the lowest eigenvalue corresponds to the critical buckling load and the eigenvector indicates the buckled shape.

Before implementing the shear walls, the frame itself is checked on consistency. Applying the vertical loads on the frame yield the exact solution of the buckling load with an error of -1.67%. This frame is kept constant in the rest of the paper.

The results for the effectiveness of the shear wall is expressed as the buckling load of the system divided by the buckling load of the framing alone. It is found that generally, the resistance increases with an increasing number of transverse stiffeners. However, in case of a corrugation depth of 80 mm, this influence diminishes, which indicates a local buckling in the plate fields of the corrugated panel. Further, it is concluded that trapezoidal corrugations lead to a higher allowed increase of loading in comparison to the triangular corrugated panels.

Usefulness Insight is given to the corrugated panels when oriented vertically. It is also made clear that a higher resistance is obtained if trapezoidal corrugations are applied.

Buckling strength assessment of corrugated panels in offshore structures [11] Sun and Spencer (2005) investigate corrugated panel applied to offshore structures. Because of the low construction costs of corrugated panels, it is demanded for the buckling behaviour to be analysed in order to get more precise information about its behaviour. As the plates are available with corrugation angles ranging from 45° to 90° and may have unequal flange widths, shipping codes are inapplicable (these set a limit of 57° having equal flange width).

The considered buckling modes are the local face/web buckling, unit corrugation buckling, and entire corrugation buckling. It is noted that corrugated panels show hardly any post-buckling behaviour.

The derivations and expressions are based on the ABS standards. From earlier experiments, it is made clear that in examining the entire corrugated plate, a single unit corrugation can be considered, given that the end conditions of each through are the same.

For the local plate buckling, the general resistance formula can be adapted:

$$\left(\frac{\sigma_{x,max}}{\eta\sigma_{C,x}}\right)^2 + \left(\frac{\sigma_{y,max}}{\eta\sigma_{C,y}}\right)^2 + \left(\frac{\tau}{\eta\tau_C}\right)^2 \leq 1.0 \quad (A.4)$$

in which $\sigma_{x,max}$, $\sigma_{y,max}$, and τ are the maximum stresses in the corrugation, η is the allowable strength utilisation factor and $\sigma_{C,x}$, $\sigma_{C,y}$, and τ_C are the critical buckling stresses. The allowable strength utilisation factor is taken to be 0.6 in operating conditions and 0.8 in storm conditions.

In the unit corrugation buckling, the following expression is formulated:

$$\frac{\sigma_A}{\eta\sigma_{CA}} + \frac{C_m\sigma_b}{\eta\sigma_{CB}\left(1 - \frac{\sigma_a}{\eta\sigma_{EC}}\right)} \leq 1.0 \quad (A.5)$$

wherein σ_A is the axial compressive stress in the unit corrugation, C_m is a factor that can be taken as 1.5 for simply supported panels, η is taken as said above, and σ_b is calculated as:

$$\sigma_b = \frac{M_b}{SM_{a,b}}$$

in which M_b is the bending moment resulting from the lateral pressure, and $SM_{a,b}$ is the section modulus of either flange, whichever is governing. σ_{CA} is determined by taking into account the Johnson-Ostenfeld plasticity correction.

Now the critical buckling stresses can be derived as given in A.1.

For the entire corrugation buckling, a similar expression is found:

$$\left(\frac{\sigma_{x,av}}{\eta\sigma_{G,x}}\right)^2 + \left(\frac{\sigma_{y,av}}{\eta\sigma_{G,y}}\right)^2 + \left(\frac{\tau}{\eta\tau_G}\right)^2 \leq 1.0 \quad (A.6)$$

in which $\sigma_{x,av}$, $\sigma_{y,av}$, and τ are the average stresses in x- and y-direction and the shear stress, respectively, the $\sigma_{G,x}$, $\sigma_{G,y}$, and τ_G are the overall critical buckling stresses in corrugation and transverse direction, η as defined above.

Next, the geometric properties are linked to the buckling modes that are likely to occur for corrugated panels under axial loading: shallow corrugations are susceptible to column or entire corrugation buckling; if the individual plates are not considered compact, plate buckling should be considered. After that, the results from test specimens are compared to the outcomes of Finite Element Analyses. Mean and covariance of the modelling uncertainty were 1.11% and 8.35%, respectively.

For lateral pressure, it is stated that:

- The corrugation angle should be as large as possible
- A deep through with thin plating is more efficient than a shallow through with thick plating (under the same section modulus)

Also for the lateral pressure, test specimens are compared to the FEM analyses, which yields a mean and covariance of modelling uncertainty of 1.1% and 17.64%, respectively.

For the tests on the shear stress, all specimens failed under overall shear buckling. The mean and covariance modelling uncertainty were 1.1% and 12.62%, respectively.

Usefulness The paper is based in the principles stated by the ABS, since these design guides are based on the allowable stress methods, the exact formulas may not be useful. However, the general ideas posed in the paper can be used for the design of plated structures.

Also, the paper is focused on the relative lightly loaded plated structures used in offshore living quarters. For the heavier application, more research might be needed.

A.4. Codes

Before a comparison can take place, the most important requirement is that the design complies to the prevailing standards. In the design requirements, it is decided that the structures will be designed according to the ISO19900/EN1993-1-5 [16, 18], so the focus of this section is based on these standards. Some aspects of the basis of design have been copied one to one from the original structural design report [1].

Limit state design On plated structures, the Eurocode provides two methods to take into account plate buckling. The most predominant of those is the effective width method. The other method takes into account the critical plate buckling stress. Both of the design methods are elaborated below.

Effective width method The method that is elaborated most in Eurocode 3 part 1-5 [18] is the effective width method. The basic assumption of this method is that in a steel plate under compressive loading, the centre area is ineffective in resisting this load, while the edge parts are able to resist it. In figure A.10, the basis of the method is visually explained. After plate buckling, the edge region is capable of attaining additional loading, while the stress in the centre region is dropping. If loading is increased, the stress distribution will take the shape of part (b) in figure A.10, which is the basis effective width.

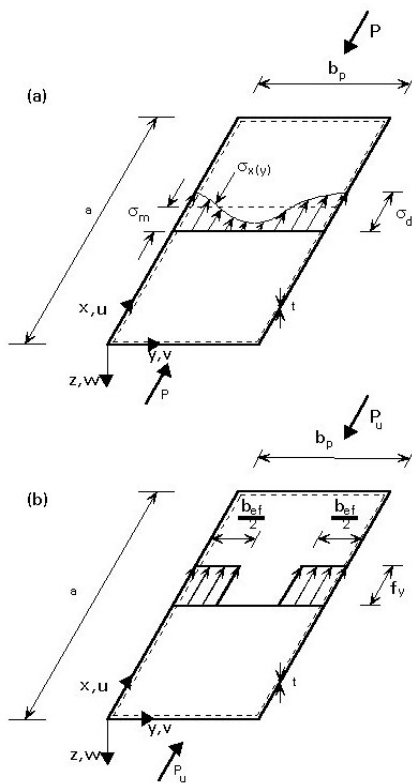


Figure A.10: Basis of effective width method (ESDEP Lecture 9.1)

The Eurocode provides expressions regarding the effective width of a plated structure, given the support and loading conditions. In table A.1 and table A.2, the values for the effective width have been elaborated. In these expressions, ρ is a function of the plate slenderness and loading conditions (EN1993-1-5 section 4.4).

Attached stiffeners can be analysed on the occurrence of plate buckling by the effective width method as well.

For the more complex loading configurations, such as combined compressive stress in multiple directions or combined compressive and shear stresses, the standards provide expressions that will approximate the buckling resistance. Derivations of these expressions are given in the mathematical background.

Table A.1: Buckling factors for plates simply supported on four edges under single loading

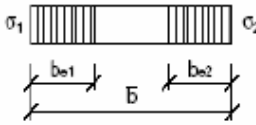
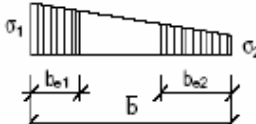
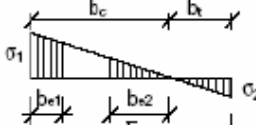
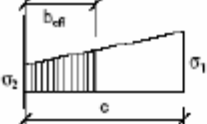
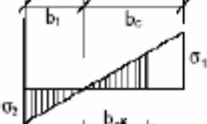
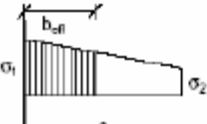
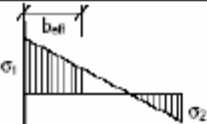
Stress distribution (compression positive)				Effective ^p width b_{eff}		
				$\psi = 1$: $b_{\text{eff}} = \rho \bar{b}$ $b_{e1} = 0,5 b_{\text{eff}} \quad b_{e2} = 0,5 b_{\text{eff}}$		
				$1 > \psi \geq 0$: $b_{\text{eff}} = \rho \bar{b}$ $b_{e1} = \frac{2}{5 - \psi} b_{\text{eff}} \quad b_{e2} = b_{\text{eff}} - b_{e1}$		
				$\psi < 0$: $b_{\text{eff}} = \rho b_c = \rho \bar{b} / (1 - \psi)$ $b_{e1} = 0,4 b_{\text{eff}} \quad b_{e2} = 0,6 b_{\text{eff}}$		
$\psi = \sigma_2 / \sigma_1$	1	$1 > \psi > 0$	0	$0 > \psi > -1$	-1	$-1 > \psi > -2$
Buckling factor k_{σ}	4,0	$8,2 / (1,05 + \psi)$	7,81	$7,81 - 6,29\psi + 9,78\psi^2$	23,9	$5,98 (1 - \psi)^2$

Table A.2: Buckling factors for plates simply supported on three edges under single loading

Stress distribution (compression positive)				Effective ^p width b_{eff}		
				$1 > \psi \geq 0$: $b_{\text{eff}} = \rho c$		
				$\psi < 0$: $b_{\text{eff}} = \rho b_c = \rho c / (1 - \psi)$		
$\psi = \sigma_2 / \sigma_1$	1	0	-1	$1 \geq \psi \geq -3$		
Buckling factor k_{σ}	0,43	0,57	0,85	$0,57 - 0,21\psi + 0,07\psi^2$		
				$1 > \psi \geq 0$: $b_{\text{eff}} = \rho c$		
				$\psi < 0$: $b_{\text{eff}} = \rho b_c = \rho c / (1 - \psi)$		
$\psi = \sigma_2 / \sigma_1$	1	$1 > \psi > 0$	0	$0 > \psi > -1$	-1	
Buckling factor k_{σ}	0,43	$0,578 / (\psi + 0,34)$	1,70	$1,7 - 5\psi + 17,1\psi^2$	23,8	

Critical plate buckling As alternative to the effective width method as elaborated above, the critical elastic buckling stress may be considered for determining the resistance of the structure. The expression for the critical buckling stress is given in A.7.

$$\sigma_{cr} = k_{\sigma} \sigma_E = k_{\sigma} \frac{\pi^2 E}{12(1-\nu^2)} \left(\frac{t}{b}\right)^2 \quad (\text{A.7})$$

in which the k_{σ} is the buckling factor depending on geometry and loading conditions. Table A.1 includes the values of this k_{σ} -factor for plates that are simply supported on four edges and loaded in one single direction. The same values in case of three simply supported edges are given in table A.2.

A.5. Plate buckling

The derivation of the plate buckling expressions is presented in this section. This is an important aspect in the stressed skin design and therefore cannot be omitted in the literature review. The symbols used in the expressions are given in figure A.11. The derivations in this section are for the most part obtained via the book "Theory of elastic stability" by Timoshenko and Gere [3]

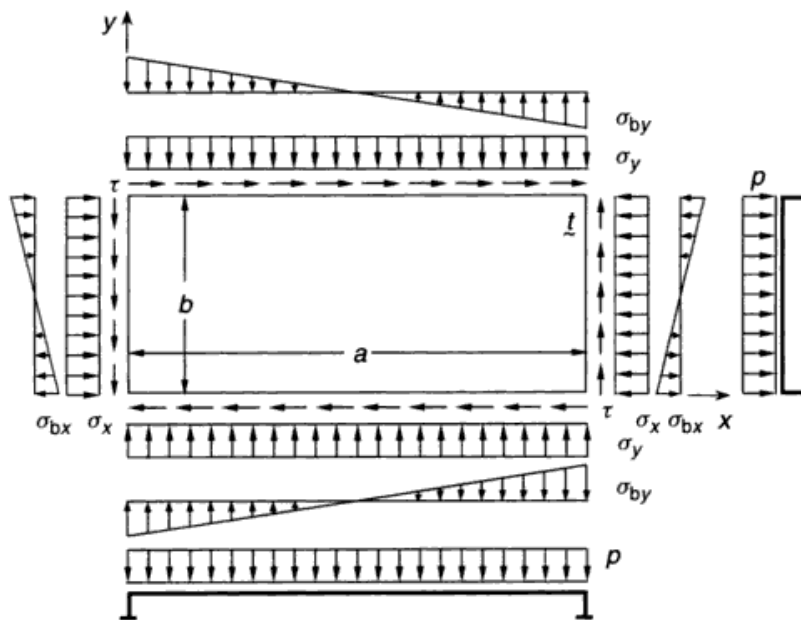


Figure A.11: Plate geometry and loadings on the plates as considered in the derivations

The derivations in this section are all done using the same assumptions and work flow. The general way to do this is as follows:

- A deflection field is assumed
- The deflection shape is inserted in
 - The expression for energy dissipated in bending
 - The expression for work done by the applied loading
- The expressions for internal energy and external work are equated
- The buckling strength is obtained when the external work exceeds the internal energy
- Depending on the assumed deflection, the buckling strength can be optimized

A.5.1. Compressive plate buckling

The expressions for the compressive plate buckling are derived from the classical Euler buckling expressions. The general plate buckling expression is as follows [25]:

$$\frac{\partial^4 w}{\partial x^4} + 2\frac{\partial^4 w}{\partial x^2 \partial y^2} + \frac{\partial^4 w}{\partial y^4} = \frac{1}{D} \left(p + n_{xx} \frac{\partial^2 w}{\partial x^2} + n_{xy} \frac{\partial^2 w}{\partial x \partial y} + n_{yy} \frac{\partial^2 w}{\partial y^2} \right) \quad (\text{A.8})$$

in which w is the out of plane deflection, x and y as indicated in figure A.11, t the plate thickness as indicated in figure A.11, D is the bending stiffness, p is the lateral pressure, and n_{xx} , n_{yy} , and n_{xy} are the distributed line loads on the plate edges, coinciding with the stress components σ_x , σ_y , and τ , respectively, indicated in figure A.11.

The above formula is derived from the expressions for internal bending energy and the external work exerted by the loading, obtained from Timoshenko and Gere [3]. The expressions are equated and a deflection field is assumed. The expressions are as follows:

$$\begin{aligned} \Delta U &= \frac{ab}{8} D \sum_{m=1}^{\infty} \sum_{n=1}^{\infty} a_{mn}^2 \left(\frac{m^2 \pi^2}{a^2} + \frac{n^2 \pi^2}{b^2} \right)^2 \\ \Delta T &= -N_{xy} \int \int \frac{\partial w}{\partial x} \frac{\partial w}{\partial y} dx dy \end{aligned} \quad (\text{A.9})$$

In these expressions, a general deflection field is assumed in a summation of sine terms. The applied expression is as follows:

$$w = \sum_{m=1}^{\infty} \sum_{n=1}^{\infty} a_{mn} \sin\left(\frac{m\pi x}{a}\right) \sin\left(\frac{n\pi y}{b}\right) \quad (\text{A.10})$$

In these expressions, it is considered that for a uniform stress in the x-direction only (σ_x) and a simply supported plate along all edges, a solution can be found in the form of:

$$w(x, y) = \sin\left(\frac{m\pi x}{a}\right) \sin\left(\frac{n\pi y}{b}\right) \quad (\text{A.11})$$

in which m and n are the number of half wave lengths in the x- and y-direction, respectively. At the boundaries, the proposed solution satisfies the displacement condition. For the bending moment, the following expressions are derived:

$$\begin{aligned} M_{xx} &= D(\kappa_{xx} + \nu\kappa_{yy}) = -D \left[\left(\frac{m\pi}{a}\right)^2 + \nu \left(\frac{n\pi}{b}\right)^2 \right] \sin\left(\frac{m\pi x}{a}\right) \sin\left(\frac{n\pi y}{b}\right) \\ M_{yy} &= D(\kappa_{yy} + \nu\kappa_{xx}) = -D \left[\left(\frac{n\pi}{b}\right)^2 + \nu \left(\frac{m\pi}{a}\right)^2 \right] \sin\left(\frac{m\pi x}{a}\right) \sin\left(\frac{n\pi y}{b}\right) \end{aligned} \quad (\text{A.12})$$

which satisfies the bending moment boundary conditions, being zero at the edges.

Expression A.8 is then simplified to include only n_{xx} on the right hand side and the proposed expression for the deflection is inserted. Now, the n_{xx} can be regarded as the elastic buckling stress $n_{xx,el}$. The expression then becomes:

$$\left[D \left[\left(\frac{m\pi}{a}\right)^4 + 2 \left(\frac{m\pi}{a}\right)^2 \left(\frac{n\pi}{b}\right)^2 + \left(\frac{n\pi}{b}\right)^4 \right] - n_{xx,el} \left(\frac{m\pi}{a}\right)^2 \right] \sin\left(\frac{m\pi x}{a}\right) \sin\left(\frac{n\pi y}{b}\right) = 0 \quad (\text{A.13})$$

in which the loading $n_{xx,el}$ is considered positive in compression.

Above expression can be simplified to:

$$n_{xx,el} = \pi^2 D \left(\frac{a}{m}\right)^2 \left[\left(\frac{m}{a}\right)^2 + \left(\frac{n}{b}\right)^2 \right]^2 \quad (\text{A.14})$$

It can be seen that above equation yields a minimum if the $n = 1$. Applying and simplifying further results in the following expression:

$$n_{xx,el} = \frac{\pi^2 D}{b^2} \left(\frac{bm}{a} + \frac{a}{bm} \right)^2 \quad (\text{A.15})$$

often written as:

$$n_{xx,el} = k_c \frac{\pi^2 D}{b^2} \quad (\text{A.16})$$

with

$$k_c = \left(\frac{bm}{a} + \frac{a}{bm} \right)^2 \quad (\text{A.17})$$

which is a function that depends on the aspect ratio ($\frac{a}{b}$) and the number of half wave lengths in the loading direction. Figure A.12 shows the value of k_c , plotted against the aspect ratio for different values of m . It is seen that the lower bound for this value becomes $k_c = 4$.

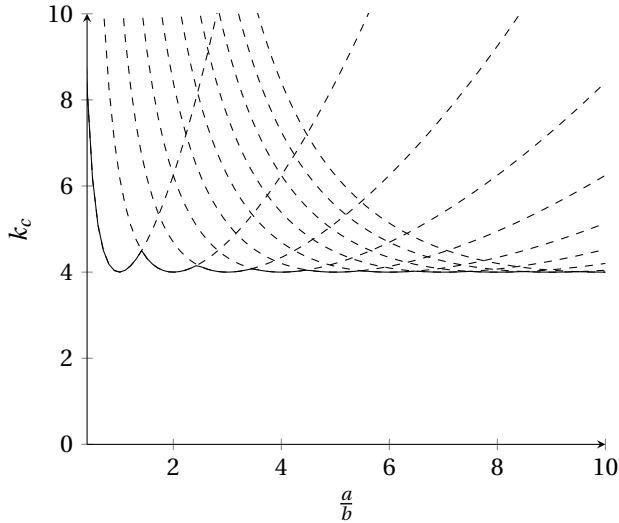


Figure A.12: Values for k_c depending on aspect ratio and number of half wave lengths

A.5.2. Plate buckling in compression and bending

The derivation of the behaviour of a simply supported plate under in-plane bending and compression is somewhat more cumbersome than in the case of pure compression. The loading will be varying linearly according to the following distribution:

$$N_x = N_0 \left(1 - \alpha \frac{y}{b} \right) \quad (\text{A.18})$$

in which the N_0 is the compressive line force at $y = 0$ and α is the rate of change in line force, with $\alpha = 0$ for pure compression and $\alpha = 2$ for pure bending. All of the symbols are according to figure A.11.

The shape of the deflection that is to be assumed has to include higher order deflections to describe the situation well enough. Therefore, the assumed deflection is in the form of:

$$w_b(x, y) = \sum_{m=1}^{\infty} \sum_{n=1}^{\infty} a_{mn} \sin\left(\frac{m\pi x}{a}\right) \sin\left(\frac{n\pi y}{b}\right) \quad (\text{A.19})$$

in which a_{mn} is the relative amplitude of the mode shape.

The buckling resistance can then be determined by applying the principle of virtual work. According to Timoshenko and Gere [3], the energy dissipated in bending of a thin plate is as follows:

$$\text{Timoshenko [3] eq. 8-35} \quad \Delta U = \frac{\pi^4 ab}{8} D \sum_{m=1}^{\infty} \sum_{n=1}^{\infty} a_{mn}^2 \left(\frac{m^2}{a^2} + \frac{n^2}{b^2} \right)^2 \quad (\text{A.20})$$

in which equation A.19 is used as the input for the deflection.

The work that is exerted by the loading is described by equation 8-32 of Timoshenko [3]. Filling in the loading expression yields:

$$\text{Timoshenko [3] eq. 8-32} \quad \Delta T = -\frac{1}{2} \iint \left[N_0 \left(1 - \alpha \frac{y}{b} \right) \left(\frac{\partial w}{\partial x} \right)^2 \right] dx dy \quad (\text{A.21})$$

When inputting the expressions for deflection, the work done can be determined by equation A.22. Hereby, it is noted that the multiplication of the sine terms is as follows:

$$\begin{aligned} \int_0^b y \sin\left(\frac{i\pi y}{b}\right) \sin\left(\frac{j\pi y}{b}\right) dy &= \frac{b^2}{4} && \text{for } i = j \\ \int_0^b y \sin\left(\frac{i\pi y}{b}\right) \sin\left(\frac{j\pi y}{b}\right) dy &= 0 && \text{for } i \neq j, \text{ and } i \pm j \text{ an even number} \\ \int_0^b y \sin\left(\frac{i\pi y}{b}\right) \sin\left(\frac{j\pi y}{b}\right) dy &= -\frac{4b^2}{\pi^2} \frac{ij}{(i^2 - j^2)^2} && \text{for } i \neq j, \text{ and } i \pm j \text{ an odd number} \end{aligned}$$

$$\Delta T = \frac{N_0}{2} \frac{ab}{4} \sum_{m=1}^{\infty} \sum_{n=1}^{\infty} a_{mn}^2 \frac{m^2 \pi^2}{a^2} - \frac{N_0}{2} \frac{\alpha a}{2b} \sum_{m=1}^{\infty} \frac{m^2 \pi^2}{a^2} \left[\frac{b^2}{4} \sum_{n=1}^{\infty} a_{mn}^2 - \frac{8b^2}{\pi^2} \sum_{n=1}^{\infty} \sum_i \frac{a_{mn} a_{mi} n i}{(n^2 - i^2)^2} \right] \quad (\text{A.22})$$

in which only the i is chosen, such that $n \pm i$ is always odd.

Now equating the bending energy of equation A.20 and the virtual work of equation A.22 and isolating the force component N_0 yields the expression for the critical buckling load $N_{0,cr}$:

$$N_{0,cr} = \frac{\pi^4 D \sum_{m=1}^{\infty} \sum_{n=1}^{\infty} a_{mn}^2 \left(\frac{m^2}{a^2} + \frac{n^2}{b^2} \right)}{\sum_{m=1}^{\infty} \sum_{n=1}^{\infty} a_{mn}^2 \frac{m^2 \pi^2}{a^2} - \frac{\alpha}{2} \sum_{m=1}^{\infty} \frac{m^2 \pi^2}{a^2} \left[\sum_{n=1}^{\infty} a_{mn}^2 - \frac{32}{\pi^2} \sum_{n=1}^{\infty} \sum_i \frac{a_{mn} a_{mi} n i}{(n^2 - i^2)^2} \right]} \quad (\text{A.23})$$

in which the i is chosen, such that $n \pm i$ is always odd.

Since we are interested in the minimum value of the loading as a function of the deflection per buckling shape, the derivative of the above function with respect to a_{mn} is taken and worked out to equate to zero. This results in the following system of linear equations:

$$D a_{mn} \pi^4 \left(\frac{m^2}{a^2} + \frac{n^2}{b^2} \right)^2 = N_{0,cr} \left[a_{mn} \frac{m^2 \pi^2}{a^2} - \frac{\alpha}{2} \frac{m^2 \pi^2}{a^2} \left[a_{mn} - \frac{16}{\pi^2} \sum_i \frac{a_{mi} n i}{(n^2 - i^2)^2} \right] \right] \quad (\text{A.24})$$

The plate is subdivided in parts with m half-waves in the x -direction, which simplifies the expression for deflection:

$$w = \sin\left(\frac{m\pi x}{a}\right) \sum_{n=1}^{\infty} a_{mn} \sin\left(\frac{n\pi y}{b}\right)$$

in which the ratio $\frac{a}{m}$ is the length between two nodal points of zero deflection in the plate field.

Above expression for the deflection is applied in equation A.24, and by setting all m to one, the following expression is obtained:

$$a_{1n} \left(\left(1 + \frac{a^2 n^2}{b^2} \right)^2 - \frac{N_{0,cr} a^2}{\pi^2 D} \left(1 - \frac{\alpha}{2} \right) \right) - 8\alpha \frac{a^2}{\pi^4 D} N_{0,cr} \sum_i \frac{a_{1i} n i}{(n^2 - i^2)^2} = 0 \quad (\text{A.25})$$

in which, again, the i is chosen, such that $n \pm i$ is always odd.

By means of the above expression, the exact solution of plate buckling under bending and compression can be approximated by taking into account an increasing number of summation terms. By including only the first of these terms (i.e. all factors a_{1n} equal to zero, except for a_{11}), the approximation becomes:

$$N_{0,cr} = \frac{\pi^2 D}{a^2} \left(1 + \frac{a^2}{b^2} \right)^2 \frac{1}{1 - \frac{\alpha}{2}} = \frac{\pi^2 D}{b^2} \left(\frac{b}{a} + \frac{a}{b} \right)^2 \frac{1}{1 - \frac{\alpha}{2}} \quad (\text{A.26})$$

which tends to give inaccurate results for large values of α . However, it can be seen that for $\alpha = 0$, the expression is equivalent to equation A.16, when $m = 1$ is applied.

Timoshenko and Gere [3] shows that the results are accurate enough when three summation are considered. An error of 0.33% is observed when comparing the third and the fourth approximation for a square plate under pure bending ($\alpha = 2$). The system of equations that needs to be solved for the approximation is obtained by applying the first three terms of equation A.25, which is done as follows:

$$\begin{aligned} a_{11} \left[\left(1 + \frac{a^2}{b^2}\right)^2 - \frac{N_{0,cr} a^2}{\pi^2 D} \left(1 - \frac{\alpha}{2}\right) \right] - 8\alpha \frac{a^2}{\pi^4 D} N_{0,cr} \frac{2a_{12}}{9} &= 0 \\ a_{12} \left[\left(1 + \frac{4a^2}{b^2}\right)^2 - \frac{N_{0,cr} a^2}{\pi^2 D} \left(1 - \frac{\alpha}{2}\right) \right] - 8\alpha \frac{a^2}{\pi^4 D} N_{0,cr} \left(\frac{2a_{11}}{9} + \frac{6a_{13}}{25} \right) &= 0 \\ a_{13} \left[\left(1 + \frac{9a^2}{b^2}\right)^2 - \frac{N_{0,cr} a^2}{\pi^2 D} \left(1 - \frac{\alpha}{2}\right) \right] - 8\alpha \frac{a^2}{\pi^4 D} N_{0,cr} \frac{6a_{12}}{25} &= 0 \end{aligned} \quad (\text{A.27})$$

The above system of equations can be solved for $N_{0,cr}$ by setting the determinant to zero. This means that either none or infinitely many solutions arise for the values of a_{mn} , which indicates the instability. In order to do this, the equations are written in matrix notation:

$$\det \begin{bmatrix} \left(1 + \frac{a^2}{b^2}\right)^2 - \frac{N_{0,cr} a^2}{\pi^2 D} \left(1 - \frac{\alpha}{2}\right) & -\frac{16}{9} \alpha \frac{a^2}{\pi^4 D} N_{0,cr} & 0 \\ -\frac{16}{9} \alpha \frac{a^2}{\pi^4 D} N_{0,cr} & \left(1 + \frac{4a^2}{b^2}\right)^2 - \frac{N_{0,cr} a^2}{\pi^2 D} \left(1 - \frac{\alpha}{2}\right) & -\frac{48}{25} \alpha \frac{a^2}{\pi^4 D} N_{0,cr} \\ 0 & -\frac{48}{25} \alpha \frac{a^2}{\pi^4 D} N_{0,cr} & \left(1 + \frac{9a^2}{b^2}\right)^2 - \frac{N_{0,cr} a^2}{\pi^2 D} \left(1 - \frac{\alpha}{2}\right) \end{bmatrix} = 0 \quad (\text{A.28})$$

The system of equations is solved for $\alpha = 2$, indicating a pure bending moment. Setting the determinant to zero and isolating the loading term gives:

$$N_{0,cr} = \frac{\left(1 + \frac{a^2}{b^2}\right) \left(1 + \frac{4a^2}{b^2}\right) \left(1 + \frac{9a^2}{b^2}\right)}{\frac{a^2}{\pi^4 D} \sqrt{\left(\frac{96}{25}\right)^2 \left(1 + \frac{a^2}{b^2}\right)^2 + \left(\frac{32}{9}\right)^2 \left(1 + \frac{9a^2}{b^2}\right)^2}} \quad (\text{A.29})$$

in which it is assumed that one half wave occurs in the direction of the loading. In order to make the expression generally applicable, the factor m is to be reintroduced from equation A.24. Writing that expression in the format of equation A.16 provides:

$$n_{xx,b,el} = k_{c,b} \frac{\pi^2 D}{b^2} \quad (\text{A.30})$$

wherein

$$k_{c,b} = \frac{\pi^2}{\left(\frac{a}{b}\right)^2} \frac{\left(m^2 + \frac{a^2}{b^2}\right) \left(m^2 + \frac{4a^2}{b^2}\right) \left(m^2 + \frac{9a^2}{b^2}\right)}{\sqrt{\left(\frac{96}{25} m^2\right)^2 \left(m^2 + \frac{a^2}{b^2}\right)^2 + \left(\frac{32}{9} m^2\right)^2 \left(m^2 + \frac{9a^2}{b^2}\right)^2}} \quad (\text{A.31})$$

The above equation is plotted for integer values of m and the aspect ratio ($\frac{a}{b}$) in figure A.13. It is seen that the minimum value for $k_{c,b} = 23.9$.

A.5.3. Plate buckling in shear

For the derivation of plate buckling in shear, two extreme cases are taken as reference to derive a conservative buckling expression. First, the derivation for a (near) square plate is given. after that a infinitely long plate is considered. Because the shear stress is uniform under pure shear loading, an infinitely long plate in the one direction is equivalent to an infinitely long plate in the other direction.

(Near) square plate

The derivation of plate buckling in shear is executed in the same way as plate buckling under combined compression and bending. The loading considered on the plate is given in figure A.14. The strain energy of

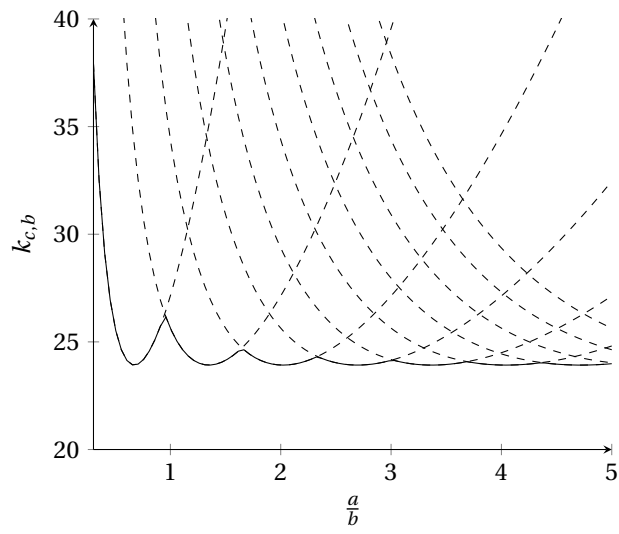


Figure A.13: Values for $k_{c,b}$ depending on aspect ratio and number of half wave lengths

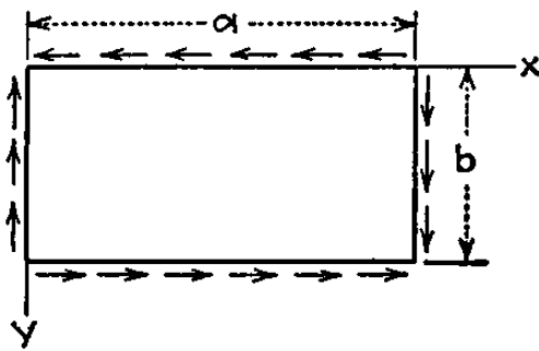


Figure A.14: Shear loading on the plate

bending in the plate is equated to the work done by the loading. Therefore, a deflection pattern is assumed as given in equation A.32.

$$w_\tau = \sum_{m=1}^{\infty} \sum_{n=1}^{\infty} a_{mn} \sin\left(\frac{m\pi x}{a}\right) \sin\left(\frac{n\pi y}{b}\right) \quad (\text{A.32})$$

in which a_{mn} is the relative amplitude of the mode shape and all other symbols are according to figure A.11.

Then for the bending energy in the buckled plate, expression A.20 is applicable:

$$\Delta U = \frac{\pi^4 ab}{8} D \sum_{m=1}^{\infty} \sum_{n=1}^{\infty} a_{mn}^2 \left(\frac{m^2}{a^2} + \frac{n^2}{b^2} \right)^2 \quad (\text{A.33})$$

For the work done by the loading, expression 8.32 of Timoshenko and Gere [3] is applied. Inputting the shear loading N_{xy} gives the following expression:

$$\Delta T = -N_{xy} \int \int \frac{\partial w}{\partial x} \frac{\partial w}{\partial y} dx dy \quad (\text{A.34})$$

In order to keep general applicability, the deflection field of equation A.32 is rewritten to be the following in the derivation:

$$\begin{aligned} \frac{\partial w}{\partial x} &= \sum_{m=1}^{\infty} \sum_{n=1}^{\infty} a_{mn} \frac{m\pi}{a} \cos\left(\frac{m\pi x}{a}\right) \sin\left(\frac{n\pi y}{b}\right) \\ \frac{\partial w}{\partial y} &= \sum_{p=1}^{\infty} \sum_{q=1}^{\infty} a_{pq} \frac{q\pi}{a} \sin\left(\frac{p\pi x}{a}\right) \cos\left(\frac{q\pi y}{b}\right) \end{aligned} \quad (\text{A.35})$$

Substitution of equation A.35 in equation A.34 gives:

$$\Delta T = -N_{xy} \sum_{m=1}^{\infty} \sum_{n=1}^{\infty} \sum_{p=1}^{\infty} \sum_{q=1}^{\infty} \int_0^a \int_0^b a_{mn} a_{pq} \frac{m\pi}{a} \frac{q\pi}{b} \cos\left(\frac{m\pi x}{a}\right) \sin\left(\frac{p\pi x}{a}\right) \sin\left(\frac{n\pi y}{b}\right) \cos\left(\frac{q\pi y}{b}\right) dx dy \quad (\text{A.36})$$

This expression can be simplified using the following:

$$\begin{aligned} \int_0^l \sin\left(\frac{i\pi x}{l}\right) \cos\left(\frac{j\pi x}{l}\right) dx &= 0 && \text{if } i \pm j \text{ is an even number} \\ \int_0^l \sin\left(\frac{i\pi x}{l}\right) \cos\left(\frac{j\pi x}{l}\right) dx &= \frac{2l}{\pi} \frac{i}{i^2 - j^2} && \text{if } i \pm j \text{ is an odd number} \end{aligned} \quad (\text{A.37})$$

Applying this simplification for the work equation yields:

$$\Delta T = -4N_{xy} \sum_{m=1}^{\infty} \sum_{n=1}^{\infty} \sum_{p=1}^{\infty} \sum_{q=1}^{\infty} a_{mn} a_{pq} \frac{mnpq}{(p^2 - m^2)(n^2 - q^2)} \quad (\text{A.38})$$

in which m , n , p , and q are chosen such that $m \pm p$ and $n \pm q$ are odd numbers.

The critical shear force is now determined by equating the bending energy of the plate and the work produced by the loading:

$$\frac{abD\pi^4}{8} \sum_{m=1}^{\infty} \sum_{n=1}^{\infty} a_{mn}^2 \left(\frac{m^2}{a^2} + \frac{n^2}{b^2} \right)^2 - 4N_{xy,cr} \sum_{m=1}^{\infty} \sum_{n=1}^{\infty} \sum_{p=1}^{\infty} \sum_{q=1}^{\infty} a_{mn} a_{pq} \frac{mnpq}{(p^2 - m^2)(n^2 - q^2)} = 0 \quad (\text{A.39})$$

The above equation can be optimized for $N_{xy,cr}$ by variation of the a_{mn} and a_{pq} terms. Timoshenko [3] states that for near square plates ($0.5 \leq \frac{a}{b} \leq 2$), only the values of a_{mn} should be considered for which $m + n = \text{even}$.

By equations A.37, it is implied that also $p + q = \text{even}$ (since $m + p = \text{odd} \wedge n + q = \text{odd} \implies m + n + p + q = \text{even}$, then if $m + n = \text{even}$, also $p + q = \text{even}$). First differentiating equation A.39 with respect to a_{mn} gives:

$$a_{mn} \left[m^2 + n^2 \frac{a^2}{b^2} \right]^2 + \frac{32N_{xy,cr} a^3}{b\pi^4 D} \sum_{p=1}^{\infty} \sum_{q=1}^{\infty} a_{pq} \frac{mnpq}{(m^2 - p^2)(n^2 - q^2)} = 0 \quad (\text{A.40})$$

The above system of linear equations can be composed in matrix form. For increasing number of terms included, the result would become more exact. In this case, 5 terms are taken into account. The coefficients of the matrix now become:

$$\begin{bmatrix} a_{11} & a_{22} & a_{13} & a_{31} & a_{33} \\ \frac{\lambda(1+\beta^2)^2}{\beta^2} & \frac{4}{9} & 0 & 0 & 0 \\ \frac{4}{9} & \frac{\lambda(4+4\beta^2)^2}{\beta^2} & -\frac{4}{5} & -\frac{4}{5} & \frac{36}{25} \\ 0 & -\frac{4}{5} & \frac{\lambda(1+9\beta^2)^2}{\beta^2} & 0 & 0 \\ 0 & -\frac{4}{5} & 0 & \frac{\lambda(9+\beta^2)^2}{\beta^2} & 0 \\ 0 & \frac{36}{25} & 0 & 0 & \frac{\lambda(9+9\beta^2)^2}{\beta^2} \end{bmatrix} = \begin{bmatrix} 0 \\ 0 \\ 0 \\ 0 \\ 0 \end{bmatrix} \quad (\text{A.41})$$

in which:

$$\beta = \frac{a}{b} \quad (\text{A.42})$$

$$\lambda = -\frac{\pi^2}{32\beta} \frac{\pi^2 D}{b^2 N_{xy,cr}}$$

Finding the determinant of the above matrix is done using the symbolic capabilities of the Mathcad (see <http://www.ptc.com/engineering-math-software/mathcad>) software. Solving the found expression for λ^2 gives the following:

$$\lambda^2 = \frac{4\beta^4 (55809\beta^8 + 361764\beta^6 + 1334854\beta^4 + 361764\beta^2 + 55809)}{(2025\beta^8 + 22500\beta^6 + 40950\beta^4 + 22500\beta^2 + 2025)^2} \quad (\text{A.43})$$

which is a function of β and can be rewritten as:

$$\text{Timoshenko [3] eq. 9-i} \quad \lambda^2 = \frac{\beta^4}{81(1+\beta^2)^4} \left[1 + \frac{81}{625} + \frac{81}{25} \left(\frac{1+\beta^2}{1+9\beta^2} \right)^2 + \frac{81}{25} \left(\frac{1+\beta^2}{9+\beta^2} \right)^2 \right] \quad (\text{A.44})$$

Filling in the value for λ from equation A.44 in equation A.42 yields:

$$N_{xy,cr} = k_s \frac{\pi^2 D}{b^2} \quad (\text{A.45})$$

in which

$$k_s = \pm \frac{9\pi^2 (1+\beta^2)^2}{32\beta^3 \sqrt{1 + \frac{81}{625} + \frac{81}{25} \left(\frac{1+\beta^2}{1+9\beta^2} \right)^2 + \frac{81}{25} \left(\frac{1+\beta^2}{9+\beta^2} \right)^2}} \quad (\text{A.46})$$

The above value for k_s is plotted in figure A.15. This value It is noted that these values hold for a near square plate and give erroneous results for plates with an aspect ratio of $\frac{a}{b} \lesssim 2$.

Infinitely long plate

For infinitely long plates, it is assumed that the deflection field consists of one half wave length in the perpendicular y-direction (see figure A.16). The deflection can be expressed as follows:

$$w_s = A \sin\left(\frac{\pi y}{b}\right) \sin\left(\frac{\pi}{s}(x - \alpha y)\right) \quad (\text{A.47})$$

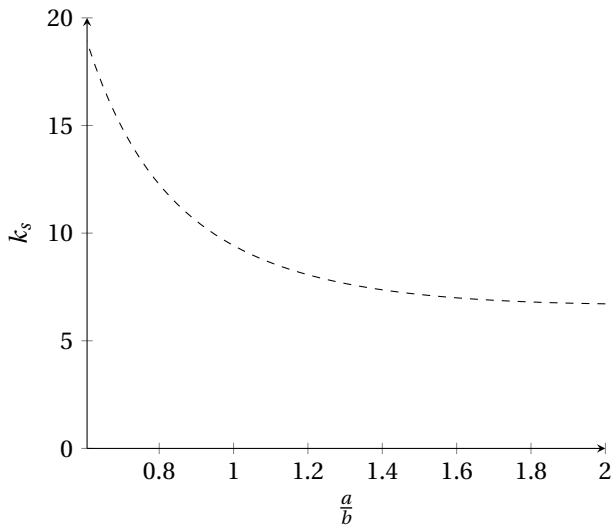


Figure A.15: Values for k_s depending on aspect ratio

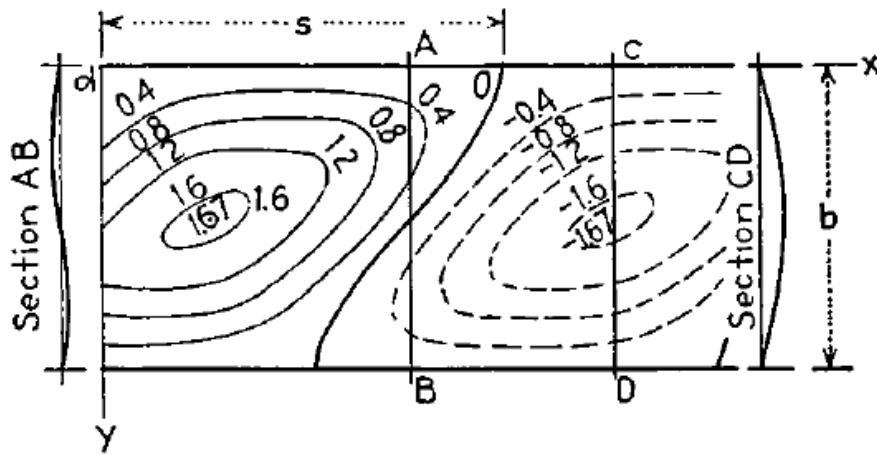


Figure A.16: Assumed deflection field for and infinitely long shear plate [3]

which complies to the boundary condition at the supported edges ($w_s = 0$ at $y = 0$ and $y = b$), and has zero deflection at the nodal lines (at every distance of s). The factor α indicates that the nodal lines are angled.

The boundary condition for moments at $y = 0$ and $y = b$ are not satisfied through the factor αy . However, according to Timoshenko [3], the error is negligible. Because the deflection field is different from that used in previous derivations, the expression for bending energy A.20 has to be considered in an earlier stage in the derivation and is given as:

$$\begin{aligned} \text{Timoshenko [3] eq. 8-29} \quad \Delta U = & \frac{D}{2} \int \int \left[\left(\frac{\partial^2 w}{\partial x^2} + \frac{\partial^2 w}{\partial y^2} \right)^2 \right. \\ & \left. - 2(1-\nu) \left(\frac{\partial^2 w}{\partial x^2} \frac{\partial^2 w}{\partial y^2} - \left(\frac{\partial^2 w}{\partial x \partial y} \right)^2 \right) \right] dx dy \end{aligned} \quad (\text{A.48})$$

Now filling in the expression for the deflection of equation A.47 into the expression for bending energy and simplifying gives:

$$\begin{aligned} \Delta U = & \frac{A^2 \pi^4 D}{2} \int_0^b \int_0^s \left[\left(\frac{1}{b^4} + \frac{2(1+\alpha^2) - 2(1-\nu)}{b^2 s^2} + \frac{(1+\alpha^2)^2 + 2(1-\nu)(1-\alpha^2)}{s^4} \right) \right] \sin^2 \left(\frac{\pi y}{b} \right) \sin^2 \left(\frac{\pi}{s} (x - \alpha y) \right) \\ & + \left[\frac{4\alpha}{sb} \left(\frac{1+\alpha^2}{s^2} + \frac{1}{b^2} \right) \right] \sin \left(\frac{\pi y}{b} \right) \sin \left(\frac{\pi}{s} (x - \alpha y) \right) \cos \left(\frac{\pi y}{b} \right) \cos \left(\frac{\pi}{s} (x - \alpha y) \right) \\ & + \left[\frac{4\alpha^2 - 2(1-\nu)}{s^2 b^2} \right] \cos^2 \left(\frac{\pi y}{b} \right) \cos^2 \left(\frac{\pi}{s} (x - \alpha y) \right) dx dy \end{aligned} \quad (\text{A.49})$$

Filling in the equation for internal work yields the following:

$$\begin{aligned} \Delta T = & -N_{xy} A^2 \int_0^b \int_0^s \frac{\pi}{s} \sin \left(\frac{\pi}{b} y \right) \cos \left(\frac{\pi}{s} (x - \alpha y) \right) \\ & \left[\frac{\pi}{b} \cos \left(\frac{\pi}{b} y \right) \sin \left(\frac{\pi}{s} (x - \alpha y) \right) \right. \\ & \left. - \frac{\pi}{s} \alpha \sin \left(\frac{\pi}{b} y \right) \cos \left(\frac{\pi}{s} (x - \alpha y) \right) \right] dx dy \end{aligned} \quad (\text{A.50})$$

Simplifying equations A.49 and A.50, respectively, give:

$$\Delta U = \frac{A^2 \pi^4 D}{8} \left[\frac{s}{b^3} + \frac{1 + 6\alpha^2 - 4(1-\nu) - 2}{sb} + \frac{((1+\alpha^2)^2 + 2(1-\nu)) b}{s^3} \right] \quad (\text{A.51})$$

$$\Delta T = \frac{N_{xy} A^2 \pi^2}{4} \frac{\alpha b}{s} \quad (\text{A.52})$$

Equating both of the above expressions and simplifying for N_{xy} gives the following:

$$N_{xy} = \frac{\pi^2 D}{2\alpha b^2} \left(\frac{s^2}{b^2} + 6\alpha^2 + 4\nu - 2 + \frac{((1+\alpha^2) + 2(1-\nu))^2 b^2}{s^2} \right) \quad (\text{A.53})$$

Disregarding the factors that take into account the Poisson's ratio, the function has a minimum for:

$$s = b * \sqrt{\alpha^2 + 1} \quad (\text{A.54})$$

$$\alpha = \frac{1}{\sqrt{2}} \quad (\text{A.55})$$

Then the maximum shear loading that can be resisted becomes:

$$N_{xy} = \frac{5.7\pi^2 D}{b^2} \quad (\text{A.56})$$

This value is an overestimation because the nodal lines are assumed to be straight. When considering a curvature in the nodal lines, the shear buckling load of an infinitely long simply supported plate can be found to be:

$$N_{xy} = \frac{5.35\pi^2 D}{b^2} \quad (\text{A.57})$$

Now combining the results from the (near) square plate and the infinitely long plate (thereby integrating quadratically), the outcome is generalised to:

$$k_s = 5.35 + 4 \left(\frac{b}{a} \right)^2 \quad (\text{A.58})$$

$$N_{xy} = k_s \frac{\pi^2 D}{b^2} \quad (\text{A.59})$$

B

Ansys APDL test script

In the comparison between Ansys APDL and Ansys Workbench of section 3.2.2, the following Ansys APDL script is used:

```
/prep7
/title, Eigenvalue Plate Buckling

!***** Parameters
NoElement = 3
ElemSize = 3000/NoElement

!***** Element type and Properties
ET,1,shell281
MP, EX,1,206000
MP, NUXY,1,0.3

!***** Geometry
KeyOpt,1,1
Sect,1,shell
SecData,15,1,,3
SecOffset,Mid
Rectng,0,3000,0,3000
CM,Plate,Area

!***** Mesh
AESize,all,ElemSize
AMesh,all

!***** Static Solution
/solu
AnType,0
PStres,on

!***** Boundary Conditions and Loading
NSel,S,loc,x,0
NSel,A,loc,x,3000
NSel,A,loc,y,0
NSel,A,loc,y,3000
D,All,UZ,0
NSel,S,loc,x,0
NSel,R,loc,y,0
D,All,UX,0
D,All,UY,0
NSel,S,loc,x,0
NSel,R,loc,y,3000
D,All,UX,0
AllSel

LSEL,S,loc,x,0
LSEL,A,loc,x,3000
SFL,All,pres,1

Solve
Finish

!***** Buckling Analysis
/solu
Antype,1
Bucopt,Lanb,4,0,0,Center
*get,NodeNum,Node,0,Count

Solve
Finish
/post1
set,list,2
*Status
```


C

SACS output

C.1. Simplified beam-column design

These are the results of the analysis performed in section 5.

C.1.1. In place condition

SACS-IV MEMBER UNITY CHECK RANGE SUMMARY

GROUP II - UNITY CHECKS GREATER THAN 0.70 AND LESS THAN 0.80

MEMBER	GROUP ID	MAXIMUM COMBINED UNITY CK	LOAD COND NO.	DIST FROM END	AXIAL STRESS N/MM2	BENDING Y N/MM2	STRESS Z N/MM2	SHEAR FY KN	FORCE FZ KN	KLY/RY	KLZ/RZ	SECOND-HIGHEST UNITY CHECK	LOAD COND	THIRD-HIGHEST UNITY CHECK	LOAD COND
0035-0037	16C	0.744	ULS	0.0	-173.60	-4.48	59.27	-32.95	2.14	35.9	35.9	0.525	SLS	0.332	COG
1254-1268	20D	0.750	ULS	5.0	-15.05	-285.98	30.50	29.68	-263.87	20.0	20.0	0.534	SLS	0.351	COG
1271-1237	20D	0.742	ULS	0.0	-15.90	281.68	-28.47	28.11	-260.69	20.0	20.0	0.530	SLS	0.351	COG
1268-1111	20E	0.784	ULS	0.0	-37.41	284.11	-18.43	29.39	-379.18	20.2	20.2	0.556	SLS	0.364	COG
1271-1060	20E	0.797	ULS	0.0	-43.21	-280.89	-21.10	33.49	379.68	20.2	20.2	0.573	SLS	0.384	COG
0048-0028	M10	0.791	ULS	5.3	-12.43	-294.14	-0.59	-0.27	-1140.71	19.1	15.5	0.566	SLS	0.396	COG
0038-0044	MES	0.769	ULS	9.0	-0.84	-281.73	-0.76	-0.18	-513.78	47.6	123.4	0.543	SLS	0.316	COG
0044-0046	MES	0.766	ULS	0.0	0.00	-281.71	0.69	-0.14	511.52	47.6	123.4	0.543	SLS	0.317	COG

SACS-IV MEMBER UNITY CHECK RANGE SUMMARY

GROUP III - UNITY CHECKS GREATER THAN 0.80

MEMBER	GROUP ID	MAXIMUM COMBINED UNITY CK	LOAD COND NO.	DIST FROM END	AXIAL STRESS N/MM2	BENDING Y N/MM2	STRESS Z N/MM2	SHEAR FY KN	FORCE FZ KN	KLY/RY	KLZ/RZ	SECOND-HIGHEST UNITY CHECK	LOAD COND	THIRD-HIGHEST UNITY CHECK	LOAD COND
0044-0029	A80	0.830	ULS	5.5	-4.15	-308.89	-0.15	-0.01	-732.63	23.6	15.0	0.589	SLS	0.366	COG
0702-0029	A80	0.841	ULS	4.5	-3.26	-314.43	-0.11	-0.06	-737.71	27.6	15.0	0.599	SLS	0.376	COG
0494-0028	M10	0.837	ULS	4.3	-13.33	-311.34	-0.18	-0.05	-1345.35	22.3	15.5	0.601	SLS	0.417	COG

*** MEMBER GROUP SUMMARY ***
 ISO 19902:2007 / EC3:2005
 (EN 1993-1-1:2005/NA NONE)

GRUP ID	CRITICAL MEMBER	LOAD COND	MAX. UNITY CHECK	DIST FROM END M	* APPLIED STRESSES *			*** ALLOWABLE STRESSES ***				CRIT COND	EFFECTIVE LENGTHS		CM * VALUES *	
					AXIAL N/MM2	BEND-Y N/MM2	BEND-Z N/MM2	AXIAL N/MM2	EULER N/MM2	BEND-Y N/MM2	BEND-Z N/MM2		KLY M	KLZ M	Y	Z
06E	0244-0264	ULS	0.15	11.2	-2.71	-58.29	-14.95	292.37	155.37	439.22	439.22	ACBI	7.9	7.9	0.85	0.85
12C	2003-3003	ULS	0.61	0.0	-112.52	-94.85	46.65	300.85	2036.59	449.31	449.31	ACBI	3.5	3.5	0.85	0.85
12D	1000-2001	ULS	0.37	0.0	-48.53	-54.41	-70.72	292.37	1261.26	435.01	435.01	ACBI	3.5	3.5	0.85	0.85
12E	0264-0265	ULS	0.46	0.0	123.41	-27.34	22.62	328.57	281.86	435.01	435.01	TN+BN	7.4	7.4	0.85	0.85
16C	0035-0037	ULS	0.74	0.0	-173.60	-4.48	59.27	282.35	1604.69	439.88	439.88	ACBI	5.0	5.0	0.85	0.85
16D	0028-0029	ULS	0.55	0.0	-138.65	-6.86	-21.37	274.35	1555.82	438.19	438.19	ACBI	5.0	5.0	0.85	0.85
16I	0050-0042	ULS	0.55	5.7	113.90	-26.31	-81.43	328.57	2486.52	429.19	429.19	TN+BN	4.0	4.0	0.85	0.85
20D	1254-1268	ULS	0.75	5.0	-15.05	-285.98	30.50	292.37	5191.79	411.93	411.93	ACBI	3.5	3.5	0.85	0.85
20E	1271-1060	ULS	0.80	0.0	-43.21	-280.89	-21.10	292.37	5064.87	434.17	434.17	ACBI	3.5	3.5	0.85	0.85
20G	0056-0327	ULS	0.42	5.5	-69.21	79.22	0.64	292.37	3950.04	443.44	443.44	ACBI	3.9	3.9	0.85	0.85
36G	0211-0215	ULS	0.51	3.5	-129.74	-26.37	-1.81	292.37	*****	420.39	420.39	ACBI	3.5	3.5	0.85	0.85
36M	100-100A	ULS	0.51	0.3	-113.57	50.85	-19.13	292.37	*****	432.22	432.22	ACBI	3.5	3.5	0.85	0.85
A55	0034-400B	ULS	0.38	8.3	-25.78	-105.16	0.55	345.00	1351.89	345.00	345.00	BN+AX	9.0	1.0	0.40	0.70
A65	0040-0308	ULS	0.41	4.0	59.26	77.47	-15.50	345.00	628.39	375.42	528.63	BN+AX	4.0	4.0	0.00	0.00
A80	0702-0029	ULS	0.84	4.5	-3.26	-314.43	-0.11	345.00	2716.38	378.15	532.60	BN+AX	9.0	1.0	0.46	0.40
DUI	0253- 100	ULS	0.29	0.1	-77.04	10.18	-3.83	292.37	*****	439.23	439.23	ACBI	3.5	3.5	0.85	0.85

I27	1002-0216	ULS	0.43	0.0	-0.37	-60.49	139.49	345.00	104.86	370.47	530.60	BN+AX	4.2	4.2	0.40	0.40
I30	0026-0237	ULS	0.24	0.0	-0.12	-90.67	-0.35	345.00	265.99	372.88	530.92	BN+AX	11.0	1.0	0.48	0.50
M10	0494-0028	ULS	0.84	4.3	-13.33	-311.34	-0.18	345.00	4160.79	390.38	543.73	BN+AX	9.0	1.0	0.49	0.60
M70	100B-0306	ULS	0.50	0.0	-69.80	-86.30	6.92	252.42	727.32	397.42	1101.10	BN+COM	3.7	3.7	0.67	0.40
MAS	0047-0048	ULS	0.67	9.0	-14.82	-235.56	-0.50	345.00	131.74	377.59	527.26	BN+AX	9.0	9.0	0.60	0.52
MES	0038-0044	ULS	0.77	9.0	-0.84	-281.73	-0.76	345.00	136.06	368.70	523.89	BN+AX	9.0	9.0	0.63	0.44
ROS	0007-0019	ULS	0.46	9.0	-15.41	-91.75	-0.98	103.58	130.75	293.89	1087.79	BN+COM	9.0	9.0	0.64	0.40

C.1.2. Lifting condition

SACS-IV MEMBER UNITY CHECK RANGE SUMMARY

GROUP II - UNITY CHECKS GREATER THAN 0.70 AND LESS THAN 0.80

MEMBER	GROUP ID	MAXIMUM COMBINED UNITY CK	LOAD COND NO.	DIST FROM END	AXIAL STRESS N/MM2	BENDING Y N/MM2	STRESS Z N/MM2	SHEAR FY KN	FORCE FZ KN	KLY/RX	KLZ/RZ	SECOND-HIGHEST UNITY CHECK	HIGHEST LOAD COND	THIRD-HIGHEST UNITY CHECK	HIGHEST LOAD COND
0204-0050	16I	0.701	LIF1	5.2	189.09	-48.38	23.95	8.54	-19.64	26.0	26.0	0.000		0.000	
1268-1111	20E	0.703	LIF1	0.0	-27.71	258.20	-55.57	91.80	-345.25	20.2	20.2	0.000		0.000	
1271-1060	20E	0.766	LIF1	0.0	-40.50	-264.95	-62.57	103.49	357.25	20.2	20.2	0.000		0.000	
0048-0028	M10	0.741	LIF1	5.3	-29.90	-254.99	-0.70	-0.28	-1028.31	19.1	15.5	0.000		0.000	
0007-0019	ROS	0.773	LIF1	9.0	-53.24	-69.56	-1.75	-0.43	-197.57	39.2	125.9	0.000		0.000	
0019-0022	ROS	0.773	LIF1	0.0	-53.22	-69.56	-1.87	0.46	197.58	39.2	125.9	0.000		0.000	

SACS-IV MEMBER UNITY CHECK RANGE SUMMARY

GROUP III - UNITY CHECKS GREATER THAN 0.80

MEMBER	GROUP ID	MAXIMUM COMBINED UNITY CK	LOAD COND NO.	DIST FROM END	AXIAL STRESS N/MM2	BENDING STRESS Y N/MM2	STRESS Z N/MM2	SHEAR FORCE		KLY/RY	KLZ/RZ	SECOND-HIGHEST		THIRD-HIGHEST	
								FY KN	FZ KN			UNITY CHECK	LOAD COND	UNITY CHECK	LOAD COND
0494-0028	M10	0.889	LIF1	4.3	-43.70	-297.10	-0.67	-0.25	-1206.65	22.3	15.5	0.000		0.000	

*** MEMBER GROUP SUMMARY ***
 ISO 19902:2007 / EC3:2005
 (EN 1993-1-1:2005/NA NONE)

GRP ID	CRITICAL MEMBER	LOAD COND	MAX. UNITY CHECK	DIST FROM END M	* APPLIED STRESSES *			*** ALLOWABLE STRESSES ***				CRIT COND	EFFECTIVE LENGTHS		CM * VALUES *	
					AXIAL N/MM2	BEND-Y N/MM2	BEND-Z N/MM2	AXIAL N/MM2	EULER N/MM2	BEND-Y N/MM2	BEND-Z N/MM2		KLY M	KLZ M	Y	Z
06E	0244-0264	LIF1	0.30	11.2	-20.46	-58.93	6.08	118.50	155.37	439.22	439.22	ACBI	7.9	7.9	0.85	0.85
12C	3002-2002	LIF1	0.53	5.0	-102.50	79.75	-34.01	300.85	2036.59	449.31	449.31	ACBI	3.5	3.5	0.85	0.85
12D	2000-1001	LIF1	0.18	5.0	-4.57	69.14	16.90	292.37	1261.26	435.01	435.01	ACBI	3.5	3.5	0.85	0.85
12E	0241-0243	LIF1	0.45	10.6	-66.44	-39.58	-2.38	192.70	281.33	435.01	435.01	ACBI	7.4	7.4	0.85	0.85
16C	0043-0021	LIF1	0.64	0.0	189.38	-20.07	-30.24	338.10	1971.33	439.88	439.88	TN+BN	4.5	4.5	0.85	0.85
16D	0021-0204	LIF1	0.53	0.0	146.05	-36.06	4.78	328.57	2305.42	438.19	438.19	TN+BN	4.1	4.1	0.85	0.85
16I	0204-0050	LIF1	0.70	5.2	189.09	-48.38	23.95	328.57	3072.69	429.19	429.19	TN+BN	3.6	3.6	0.85	0.85
20D	1254-1268	LIF1	0.69	5.0	-13.91	-257.29	56.02	292.37	5191.79	411.93	411.93	ACBI	3.5	3.5	0.85	0.85
20E	1271-1060	LIF1	0.77	0.0	-40.50	-264.95	-62.57	292.37	5064.87	434.17	434.17	ACBI	3.5	3.5	0.85	0.85
20G	0057-0334	LIF1	0.27	0.0	-42.17	-8.25	-56.50	292.37	3950.04	443.44	443.44	ACBI	3.9	3.9	0.85	0.85
36G	200A-300A	LIF1	0.31	0.0	31.99	-46.36	77.35	328.57	*****	420.39	420.39	TN+BN	3.5	3.5	0.85	0.85
36M	0204-400A	LIF1	0.37	0.3	101.61	24.29	4.12	328.57	*****	432.22	432.22	TN+BN	3.5	3.5	0.85	0.85
A55	0030-400C	LIF1	0.60	8.3	-120.15	-85.53	-3.08	345.00	1351.89	345.00	345.00	BN+AX	9.0	1.0	0.40	0.40
A65	0327-0026	LIF1	0.45	0.0	103.30	37.91	-25.27	345.00	628.39	375.42	528.63	BN+AX	4.0	4.0	0.00	0.00
A80	0702-0029	LIF1	0.69	4.5	4.96	-253.70	-0.01	345.00	2716.38	378.15	532.60	BN+AX	9.0	1.0	0.00	0.00
DUL	0287-1003	LIF1	0.06	0.0	-16.38	0.00	0.00	292.36	*****	465.70	465.70	ACBI	0.1	0.1	0.85	0.85

I27	0219-1003	LIF1	0.27	0.0	10.87	79.61	7.38	345.00	104.86	370.47	530.60	BN+AX	4.2	4.2	0.00	0.00
I30	0216-0244	LIF1	0.31	5.3	-0.07	114.57	0.23	345.00	265.99	372.88	530.92	BN+AX	11.0	1.0	0.93	0.40
M10	0494-0028	LIF1	0.89	4.3	-43.70	-297.10	-0.67	345.00	4160.79	390.38	543.73	BN+AX	9.0	1.0	0.52	0.47
M70	100A-0329	LIF1	0.13	3.7	-3.32	-39.67	-11.53	345.00	727.32	387.96	535.12	BN+AX	4.5	3.7	0.54	0.40
MAS	0047-0048	LIF1	0.60	9.0	-8.92	-215.95	0.93	345.00	131.74	377.59	527.26	BN+AX	9.0	9.0	0.60	1.00
MES	0044-0046	LIF1	0.57	0.0	-2.95	-204.66	1.11	345.00	136.06	368.70	523.89	BN+AX	9.0	9.0	0.65	0.40
ROS	0007-0019	LIF1	0.77	9.0	-53.24	-69.56	-1.75	103.58	130.75	271.75	652.43	BN+COM	9.0	9.0	0.73	0.40

C.1.3. transport condition

SACS-IV MEMBER UNITY CHECK RANGE SUMMARY

GROUP II - UNITY CHECKS GREATER THAN 0.70 AND LESS THAN 0.80

MEMBER	GROUP ID	MAXIMUM COMBINED UNITY CK	LOAD COND NO.	DIST FROM END	AXIAL STRESS N/MM2	BENDING Y N/MM2	STRESS Z N/MM2	SHEAR FY KN	FORCE FZ KN	KLY/RX	KLZ/RZ	SECOND-HIGHEST UNITY CHECK	LOAD COND	THIRD-HIGHEST UNITY CHECK	LOAD COND
3002-2002	12C	0.729	-R+H	5.0	-132.81	116.29	-55.79	-19.46	50.14	31.9	31.9	0.366	TRNS	0.178	DEAD
0002-0057	16C	0.757	-R+H	0.0	167.57	114.95	-1.38	-0.33	-47.92	29.8	29.8	0.160	TRNS	0.068	DEAD
0035-0037	16C	0.758	-R+H	0.0	-157.04	91.10	23.68	-12.27	-48.22	35.9	35.9	0.381	TRNS	0.217	DEAD
0028-0029	16D	0.756	-R+H	0.0	-148.49	99.99	-3.27	-0.85	-75.11	36.5	36.5	0.353	TRNS	0.172	DEAD
1271-1060	20E	0.778	-R+H	0.0	-37.47	-281.24	-22.51	36.45	357.44	20.2	20.2	0.364	TRNS	0.200	DEAD
0057-0334	20G	0.785	-R+H	5.5	-120.59	165.13	-4.00	1.52	261.08	22.9	22.9	0.230	TRNS	0.107	DEAD
0245-0246	36G	0.714	-R+H	3.5	-167.67	59.04	-2.08	-46.20	310.06	11.1	11.1	0.278	TRNS	0.143	DEAD
103-100C	36M	0.704	-R+H	0.3	-147.13	-83.76	-23.31	-1187.20	-4265.25	11.2	11.2	0.283	TRNS	0.145	DEAD
0026-0237	I30	0.763	-R+H	0.0	1.93	-106.80	-249.57	11.30	30.11	88.3	29.9	0.176	TRNS	0.154	DEAD
0030-0090	M10	0.707	-R+H	0.0	9.59	-226.60	53.57	-28.39	736.37	22.3	15.5	0.389	TRNS	0.159	DEAD
0309-100D	M70	0.716	-R+H	3.7	-104.77	-110.29	21.25	14.36	-203.57	12.8	53.4	0.255	TRNS	0.128	DEAD
0328-100C	M70	0.798	-R+H	3.7	-118.15	-118.33	-30.27	-20.11	-207.41	12.8	53.4	0.273	TRNS	0.132	DEAD

SACS-IV MEMBER UNITY CHECK RANGE SUMMARY

GROUP III - UNITY CHECKS GREATER THAN 0.80

MEMBER	GROUP ID	MAXIMUM COMBINED UNITY CK	LOAD COND NO.	DIST FROM END	AXIAL STRESS N/MM2	BENDING STRESS Y N/MM2	BENDING STRESS Z N/MM2	SHEAR FORCE FY KN	SHEAR FORCE FZ KN	KLY/RY	KLZ/RZ	SECOND-HIGHEST UNITY CHECK	HIGHEST LOAD COND	THIRD-HIGHEST UNITY CHECK	HIGHEST LOAD COND
0030-0019	M10	0.847	-R+H	0.0	4.19	-224.91	-140.70	231.76	1485.37	19.1	15.5	0.376	TRNS	0.189	RIG

*** MEMBER GROUP SUMMARY ***
 ISO 19902:2007 / EC3:2005
 (EN 1993-1-1:2005/NA NONE)

GRUP ID	CRITICAL MEMBER	LOAD COND	MAX. UNITY CHECK	DIST FROM END M	* APPLIED STRESSES *			*** ALLOWABLE STRESSES ***				CRIT COND	EFFECTIVE LENGTHS		CM * VALUES *	
					AXIAL N/MM2	BEND-Y N/MM2	BEND-Z N/MM2	AXIAL N/MM2	EULER N/MM2	BEND-Y N/MM2	BEND-Z N/MM2		KLY M	KLZ M	Y	Z
06E	0241-0229	-R+H	0.50	0.0	-32.73	-90.89	15.46	118.50	155.37	439.22	439.22	ACBI	7.9	7.9	0.85	0.85
12C	3002-2002	-R+H	0.73	5.0	-132.81	116.29	-55.79	300.85	2036.59	449.31	449.31	ACBI	3.5	3.5	0.85	0.85
12D	2000-1001	-R+H	0.46	5.0	-59.34	63.95	91.69	292.37	1261.26	435.01	435.01	ACBI	3.5	3.5	0.85	0.85
12E	0264-0265	-R+H	0.54	10.6	136.49	-46.62	27.59	328.57	281.86	435.01	435.01	TN+BN	7.4	7.4	0.85	0.85
16C	0035-0037	-R+H	0.76	0.0	-157.04	91.10	23.68	282.35	1604.69	439.88	439.88	ACBI	5.0	5.0	0.85	0.85
16D	0028-0029	-R+H	0.76	0.0	-148.49	99.99	-3.27	274.35	1555.82	438.19	438.19	ACBI	5.0	5.0	0.85	0.85
16I	0050-0042	-R+H	0.44	5.7	101.11	-36.20	-43.04	328.57	2486.52	429.19	429.19	TN+BN	4.0	4.0	0.85	0.85
20D	1271-1237	-R+H	0.63	0.0	-12.84	241.34	-27.31	292.37	5191.79	411.93	411.93	ACBI	3.5	3.5	0.85	0.85
20E	1271-1060	-R+H	0.78	0.0	-37.47	-281.24	-22.51	292.37	5064.87	434.17	434.17	ACBI	3.5	3.5	0.85	0.85
20G	0057-0334	-R+H	0.78	5.5	-120.59	165.13	-4.00	292.37	3950.04	443.44	443.44	ACBI	3.9	3.9	0.85	0.85
36G	0245-0246	-R+H	0.71	3.5	-167.67	59.04	-2.08	292.37	*****	420.39	420.39	ACBI	3.5	3.5	0.85	0.85
36M	103-100C	-R+H	0.70	0.3	-147.13	-83.76	-23.31	292.37	*****	432.22	432.22	ACBI	3.5	3.5	0.85	0.85
A55	0030-400C	-R+H	0.45	8.3	-39.71	-99.47	-14.99	345.00	1351.89	345.00	345.00	BN+AX	9.0	1.0	0.40	0.40
A65	0026-0334	-R+H	0.65	4.0	118.01	101.05	-21.72	345.00	628.39	375.42	528.63	BN+AX	4.0	4.0	0.00	0.00
A80	200C-0047	-R+H	0.67	0.0	-74.02	-135.05	-16.56	345.00	3711.02	345.00	345.00	BN+AX	7.7	1.0	0.46	0.40
DUI	0277- 103	-R+H	0.38	0.1	-99.82	-16.77	-4.67	292.37	*****	439.23	439.23	ACBI	3.5	3.5	0.85	0.85

I27	0040-0225	-R+H	0.65	0.0	0.63	-92.14	210.47	345.00	322.45	370.47	530.60	BN+AX	9.0	1.0	0.00	0.00
I30	0026-0237	-R+H	0.76	0.0	1.93	-106.80	-249.57	345.00	265.99	372.88	530.92	BN+AX	11.0	1.0	0.00	0.00
M10	0030-0019	-R+H	0.85	0.0	4.19	-224.91	-140.70	345.00	5684.33	390.38	543.73	BN+AX	7.7	1.0	0.00	0.00
M70	0328-100C	-R+H	0.80	3.7	-118.15	-118.33	-30.27	252.42	727.32	396.55	980.87	BN+COM	3.7	3.7	0.73	0.40
MAS	0048-0049	-R+H	0.51	0.0	-19.81	-170.00	1.40	345.00	131.74	377.59	527.26	BN+AX	9.0	9.0	0.64	0.52
MES	0044-0046	-R+H	0.47	0.0	-6.03	-167.18	1.52	345.00	136.06	368.70	523.89	BN+AX	9.0	9.0	0.67	0.40
ROS	0007-0019	-R+H	0.46	4.5	-20.15	61.15	2.89	103.58	130.75	237.99	709.89	BN+COM	9.0	9.0	0.92	0.44

C.2. Beam-column design

These are the results of the analysis performed in section 6.2.

SACS-IV MEMBER UNITY CHECK RANGE SUMMARY

GROUP I - UNITY CHECKS GREATER THAN 0.00 AND LESS THAN 0.70

MEMBER	GROUP ID	MAXIMUM COMBINED UNITY CK	LOAD COND NO.	DIST FROM END	AXIAL STRESS N/MM2	BENDING Y N/MM2	STRESS Z N/MM2	SHEAR FY KN	FORCE FZ KN	KLY/RX	KLZ/RZ	SECOND-HIGHEST UNITY CHECK	LOAD COND	THIRD-HIGHEST UNITY CHECK	LOAD COND
11-	8 16C	0.200	ULS	5.0	10.39	-73.06	0.00	0.00	-42.14	36.2	36.2	0.000		0.000	
1A-	45 16C	0.152	ULS	5.3	-20.52	-35.63	0.00	0.00	-22.26	26.8	26.8	0.000		0.000	
3A-	56 16C	0.643	ULS	5.3	172.10	-52.06	0.00	0.00	-23.23	26.8	26.8	0.000		0.000	
45-	8A 16C	0.415	ULS	5.9	-60.86	89.87	0.00	0.00	42.85	30.0	30.0	0.000		0.000	
5-	2 16D	0.391	ULS	5.0	-100.56	-11.81	0.00	0.00	-2.23	36.5	36.5	0.000		0.000	
8A-101B	20G	0.348	ULS	0.0	31.63	111.61	0.00	0.00	-162.08	22.9	22.9	0.000		0.000	
8B-111A	20G	0.620	ULS	5.5	-96.03	129.33	0.00	0.00	214.58	22.9	22.9	0.000		0.000	
101A-	7A 20G	0.092	ULS	0.0	-12.05	22.50	0.00	0.00	-20.95	21.8	21.8	0.000		0.000	
111B-	9A 20G	0.421	ULS	0.0	102.11	-48.86	0.00	0.00	14.91	21.8	21.8	0.000		0.000	
4-	1B 36G	0.226	ULS	4.1	-48.43	25.19	0.00	0.00	177.38	11.1	11.1	0.000		0.000	
6-	3B 36G	0.351	ULS	0.0	-88.26	-20.51	0.00	0.00	80.00	11.1	11.1	0.000		0.000	
7-	4 36G	0.287	ULS	5.0	-61.67	-31.88	0.00	0.00	-58.85	11.1	11.1	0.000		0.000	
10A-	7B 36G	0.445	ULS	0.0	-74.53	-79.78	0.00	0.00	388.09	11.1	11.1	0.000		0.000	
10-	10A 36M	0.406	ULS	0.0	-63.43	-81.64	0.00	0.00	388.09	11.2	11.2	0.000		0.000	
12-	12A 36M	0.585	ULS	0.6	-152.38	27.52	0.00	0.00	193.97	11.2	11.2	0.000		0.000	
1A-	1 36M	0.226	ULS	0.0	-44.99	31.34	0.00	0.00	-74.68	11.2	11.2	0.000		0.000	
1B-	1A 36M	0.205	ULS	0.6	-41.22	27.63	0.00	0.00	177.38	11.2	11.2	0.000		0.000	
3A-	3 36M	0.277	ULS	0.0	-45.16	1.13	0.00	0.00	-2189.89	11.2	11.2	0.000		0.000	
3B-	3A 36M	0.265	ULS	0.6	-75.12	3.46	0.00	0.00	80.00	11.2	11.2	0.000		0.000	
7A-	7 36M	0.280	ULS	0.3	-68.12	20.33	0.00	0.00	10.70	11.2	11.2	0.000		0.000	
7B-	7A 36M	0.265	ULS	0.6	-63.43	20.67	0.00	0.00	388.09	11.2	11.2	0.000		0.000	

SACS-IV MEMBER UNITY CHECK RANGE SUMMARY

GROUP I - UNITY CHECKS GREATER THAN 0.00 AND LESS THAN 0.70

MEMBER	GROUP ID	MAXIMUM COMBINED UNITY CK	LOAD COND NO.	DIST FROM END	AXIAL STRESS N/MM2	BENDING Y N/MM2	STRESS Z N/MM2	SHEAR FORCE FY KN	FZ KN	KLY/RY	KLZ/RZ	SECOND-HIGHEST UNITY CHECK	LOAD COND	THIRD-HIGHEST UNITY CHECK	LOAD COND
9A-	9 36M	0.568	ULS	0.0	-111.33	81.13	0.00	0.00	-2882.41	11.2	11.2	0.000		0.000	
9B-	9A 36M	0.688	ULS	0.6	-152.38	72.13	0.00	0.00	193.97	11.2	11.2	0.000		0.000	
12B-	12 36M	0.549	ULS	0.0	-159.47	0.00	0.00	0.00	0.00	11.2	11.2	0.000		0.000	
2-	1 A55	0.454	ULS	8.3	-34.25	-101.82	0.00	0.00	-248.51	27.4	14.0	0.000		0.000	
2-	3 A55	0.634	ULS	8.3	-65.62	-124.54	0.00	0.00	-262.49	27.4	14.0	0.000		0.000	
5-	45 A80	0.186	ULS	4.6	4.38	-56.34	0.00	0.00	-296.08	19.3	15.0	0.000		0.000	
5-	56 A80	0.305	ULS	1.1	-17.53	74.04	0.00	0.00	-28.83	19.3	15.0	0.000		0.000	
7-	8A A80	0.323	ULS	6.2	-32.33	64.67	0.00	0.00	-6.55	19.3	15.0	0.000		0.000	
45-	4 A80	0.254	ULS	0.0	-15.79	-60.37	0.00	0.00	249.12	19.3	15.0	0.000		0.000	
56-	6 A80	0.666	ULS	3.8	-8.17	-210.16	0.00	0.00	-676.20	19.3	15.0	0.000		0.000	
8B-	9 A80	0.612	ULS	8.2	-48.25	-135.30	0.00	0.00	-340.63	19.3	15.0	0.000		0.000	
10C-	10B DUI	0.648	ULS	0.0	-45.17	0.00	0.00	0.00	-7548.16	11.4	11.4	0.000		0.000	
12C-	12B DUI	0.372	ULS	0.0	-108.15	0.00	0.00	0.00	0.00	11.4	11.4	0.000		0.000	
101B-	11 M70	0.599	ULS	4.0	160.69	21.34	0.00	0.00	-18.78	21.5	57.1	0.000		0.000	
111B-	12 M70	0.123	ULS	0.0	3.94	-37.18	0.00	0.00	96.04	21.5	53.4	0.000		0.000	

SACS-IV MEMBER UNITY CHECK RANGE SUMMARY

GROUP II - UNITY CHECKS GREATER THAN 0.70 AND LESS THAN 0.80

MEMBER	GROUP ID	MAXIMUM COMBINED UNITY CK	LOAD COND NO.	DIST FROM END	AXIAL STRESS N/MM2	BENDING Y N/MM2	STRESS Z N/MM2	SHEAR FY KN	FORCE FZ KN	KLY/RX	KLZ/RZ	SECOND-HIGHEST UNITY CHECK	LOAD COND	THIRD-HIGHEST UNITY CHECK	LOAD COND
8-	5 16D	0.771	ULS	0.0	-142.19	118.17	0.00	0.00	-83.42	36.5	36.5	0.000		0.000	
9-	6 36G	0.730	ULS	5.0	-111.90	-146.13	0.00	0.00	-803.47	11.1	11.1	0.000		0.000	
12A-	9B 36G	0.794	ULS	3.5	-179.05	76.31	0.00	0.00	193.97	11.1	11.1	0.000		0.000	
11-111A	M70	0.736	ULS	4.0	158.33	70.18	0.00	0.00	-15.07	21.5	57.1	0.000		0.000	

SACS-IV MEMBER UNITY CHECK RANGE SUMMARY

GROUP III - UNITY CHECKS GREATER THAN 0.80

MEMBER	GROUP ID	MAXIMUM COMBINED UNITY CK	LOAD COND NO.	DIST FROM END	AXIAL STRESS N/MM2	BENDING STRESS Y N/MM2	BENDING STRESS Z N/MM2	SHEAR FORCE FY KN	SHEAR FORCE FZ KN	KLY/RY	KLZ/RZ	SECOND-HIGHEST UNITY CHECK	LOAD COND	THIRD-HIGHEST UNITY CHECK	LOAD COND
56-	8B 16C	0.917	ULS	0.0	194.58	141.35	0.00	0.00	-83.84	30.0	30.0	0.000		0.000	
10B-	10 36M	0.955	ULS	0.0	-66.61	-42.34	0.00	0.00	-7548.16	11.2	11.2	0.000		0.000	
0000-101A	M70	0.988	ULS	0.0	199.28	109.31	0.00	0.00	-249.92	21.5	49.1	0.000		0.000	



Ansys output

The results from the different Ansys models is given in this section.

D.1. Beam-column design

D.1.1. Deformations

A: Large deflection on stiff config 2 until collapse

Deformation y SLS
Type: Directional Deformation(Y Axis)
Unit: mm
Global Coordinate System
Time: 0,83333
23-11-2016 10:52

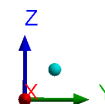
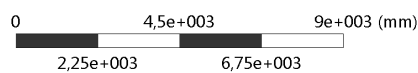
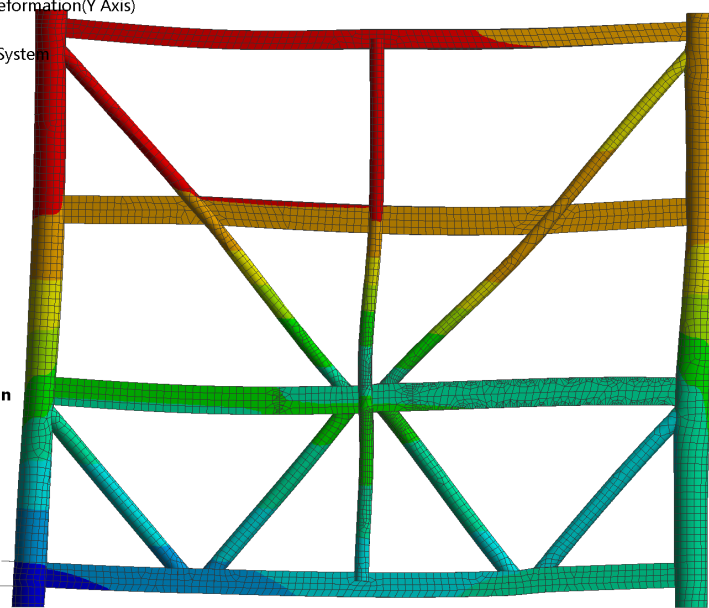
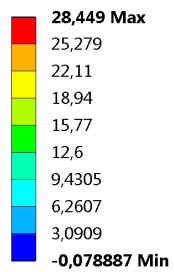


Figure D.1: Deformation of the frame in y-direction under SLS loading

A: Large deflection on stiff config 2 until collapse

Deformation y ULS

Type: Directional Deformation(Y Axis)

Unit: mm

Global Coordinate System

Time: 1

23-11-2016 10:53

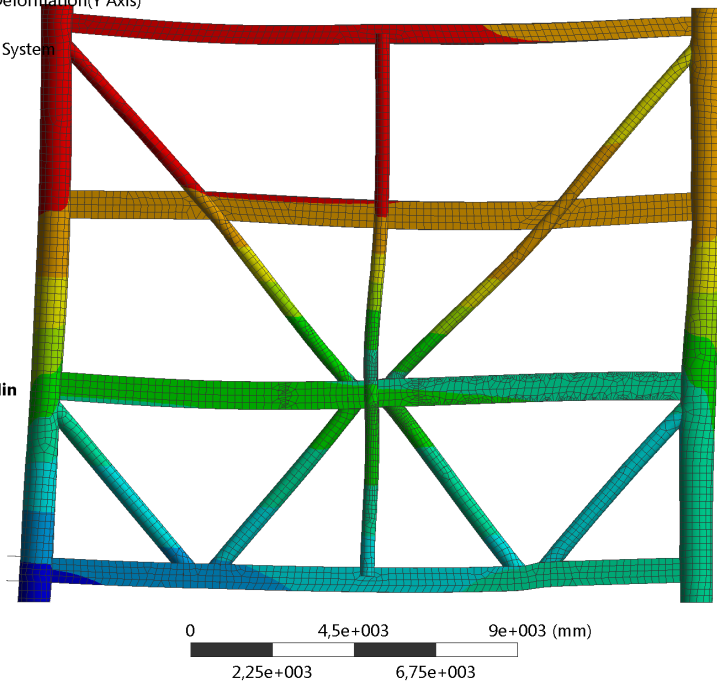
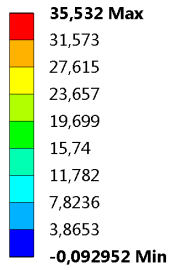


Figure D.2: Deformation of the frame in y-direction under ULS loading

A: Large deflection on stiff config 2 until collapse

Deformation y failure

Type: Directional Deformation(Y Axis)

Unit: mm

Global Coordinate System

Time: 1,3418

23-11-2016 10:53

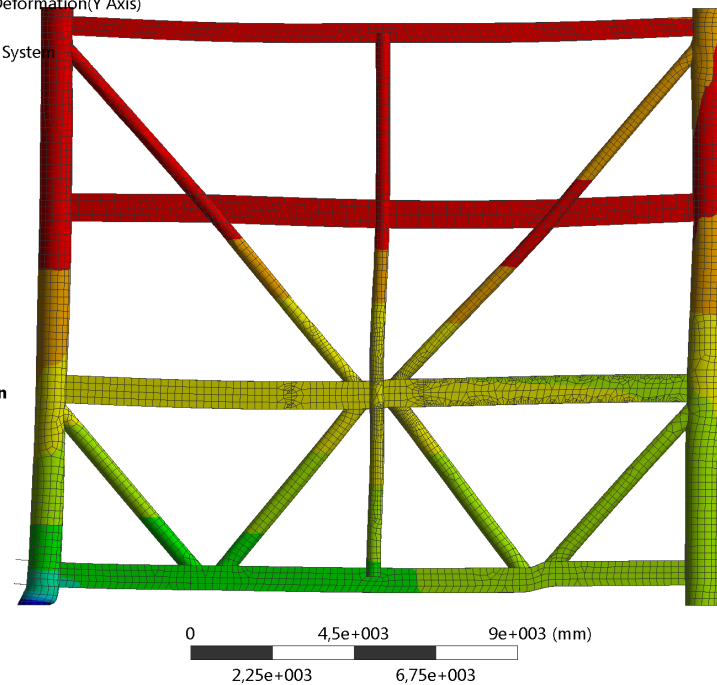
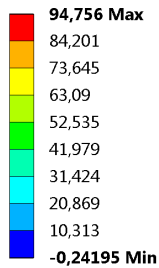


Figure D.3: Deformation of the frame in y-direction under failure loading

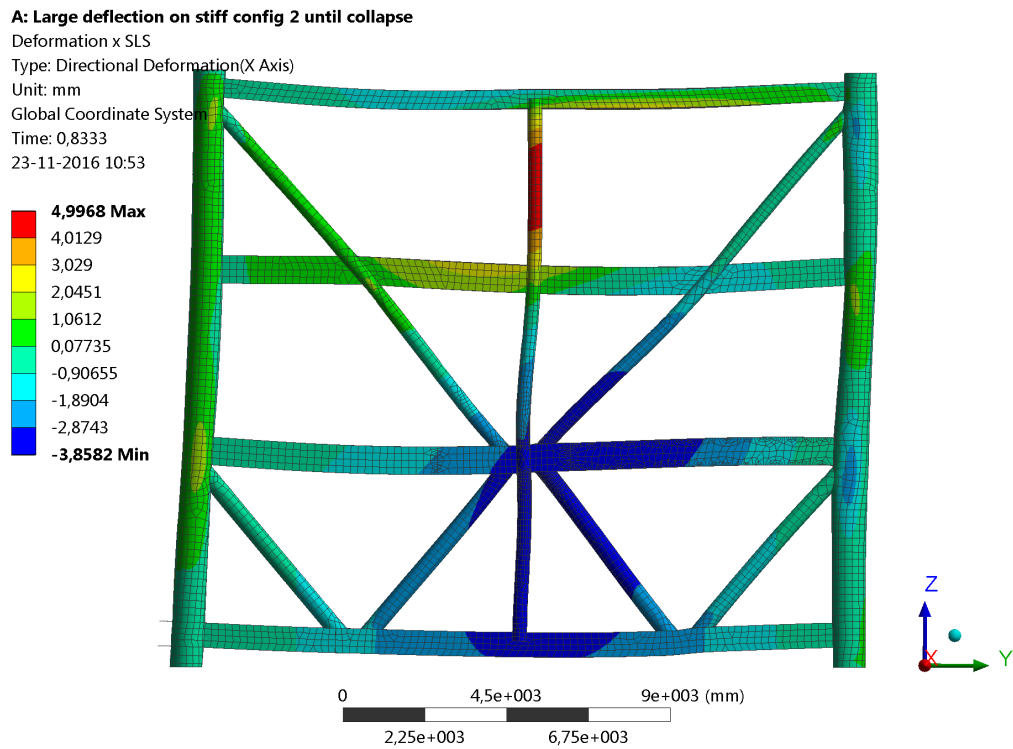


Figure D.4: Deformation of the frame in x-direction under SLS loading

D.1.2. Stresses

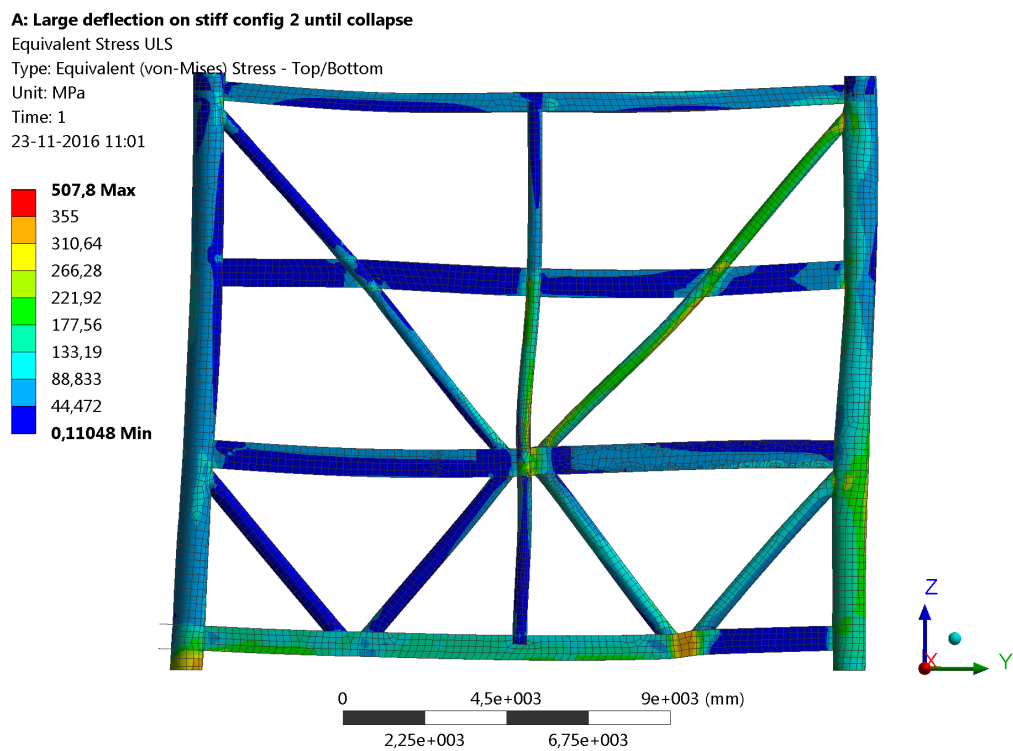


Figure D.5: Von Mises-stresses in the frame under ULS loading

A: Large deflection on stiff config 2 until collapse

Equivalent Stress failure

Type: Equivalent (von-Mises) Stress - Top/Bottom

Unit: MPa

Time: 1,3418

23-11-2016 11:01

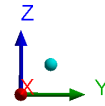
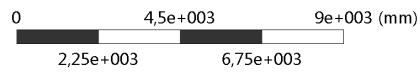
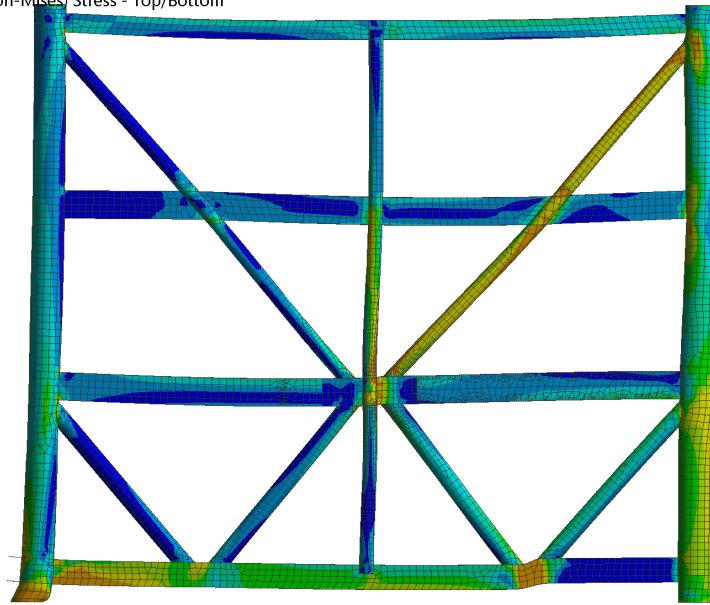
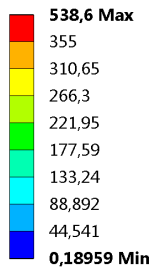


Figure D.6: Von Mises-stresses in the frame under failure loading

D.2. Stressed skin design

D.2.1. Deformations

B: Non-linear material properties until failure

Deformation x SLS

Type: Directional Deformation(X Axis)

Unit: mm

Global Coordinate System

Time: 0,83344

24-11-2016 9:35

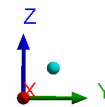
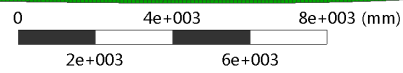
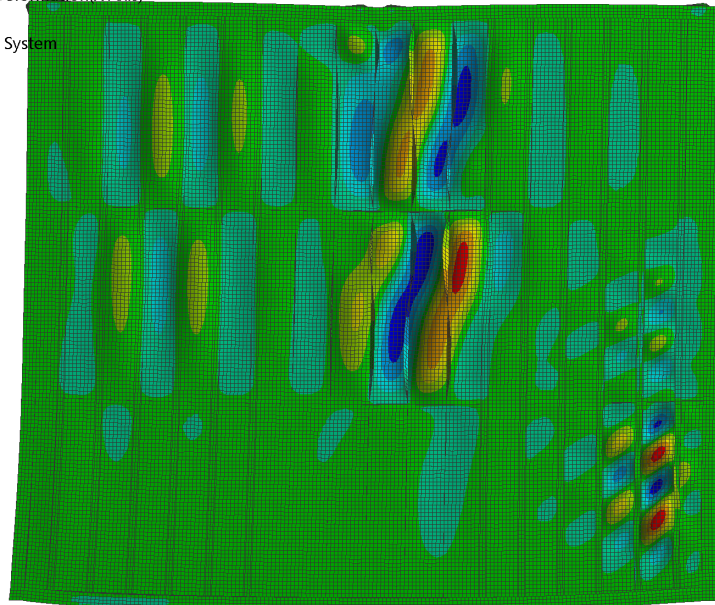
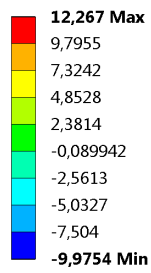


Figure D.7: Deformations in the stressed skin design in x-direction under SLS loading

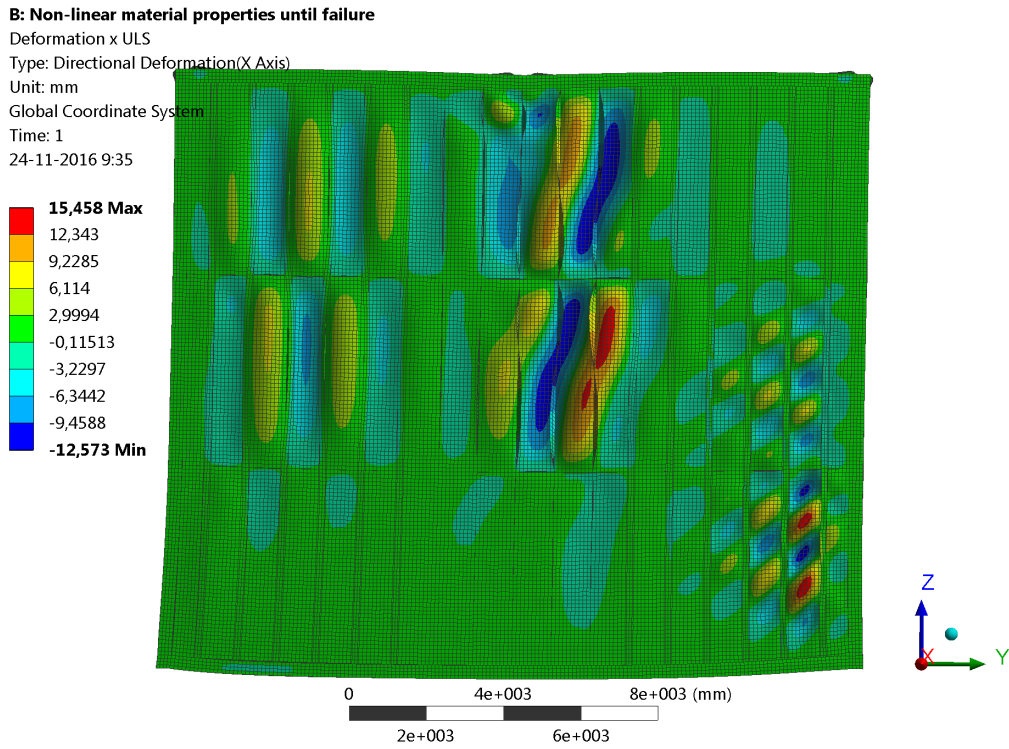


Figure D.8: Deformations in the stressed skin design in x-direction under ULS loading

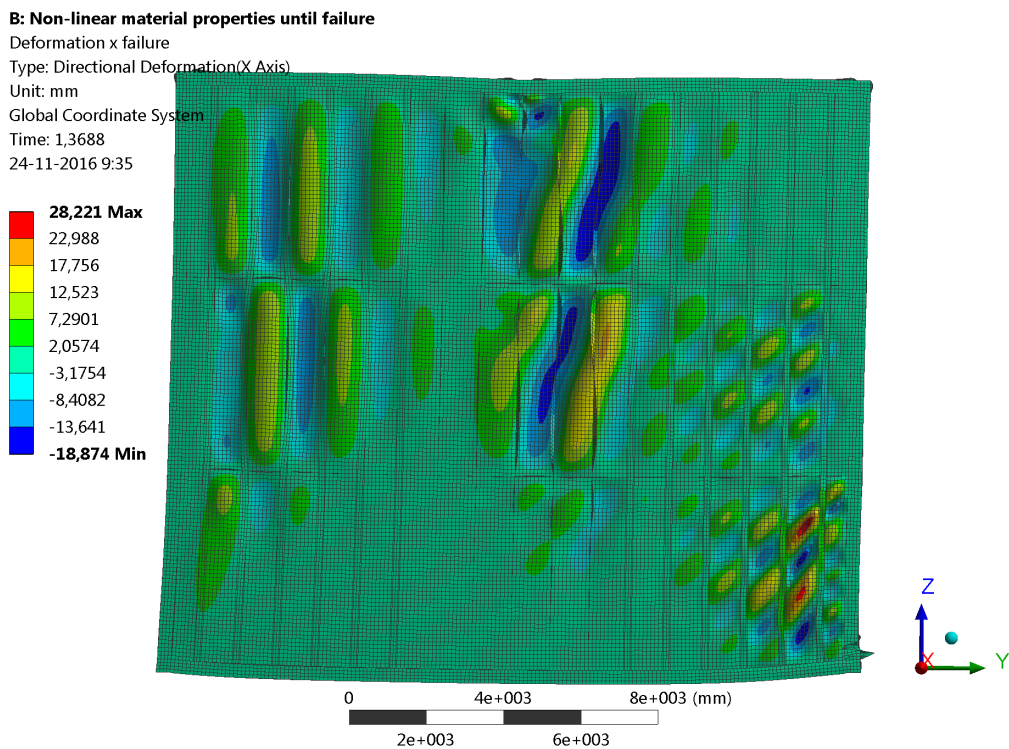


Figure D.9: Deformations in the stressed skin design in x-direction under failure loading

D.2.2. Stresses

B: Non-linear material properties until failure

Equivalent Stress ULS

Type: Equivalent (von-Mises) Stress - Top/Bottom

Unit: MPa

Time: 1

24-11-2016 9:36

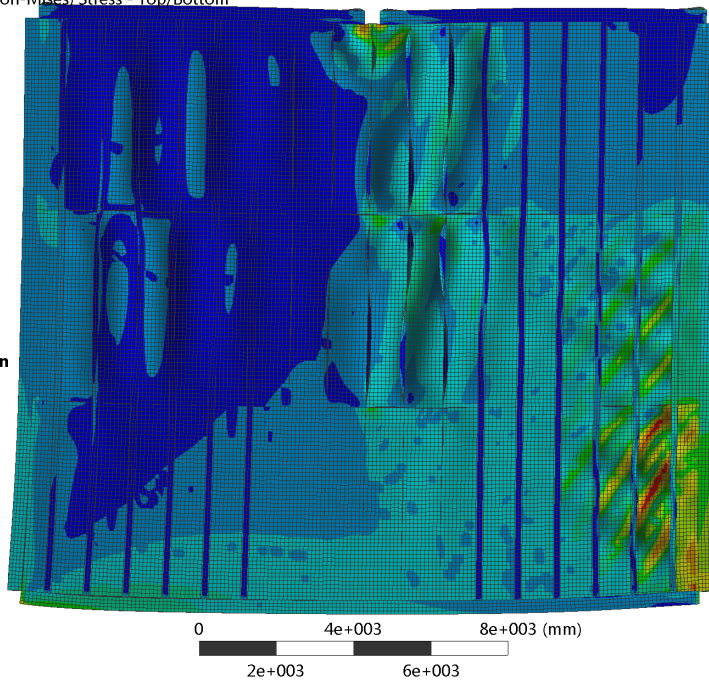
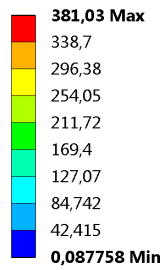


Figure D.10: Von Mises-stresses in the stressed skin design under ULS loading

B: Non-linear material properties until failure

Equivalent Stress failure

Type: Equivalent (von-Mises) Stress - Top/Bottom

Unit: MPa

Time: 1,3703

24-11-2016 9:36

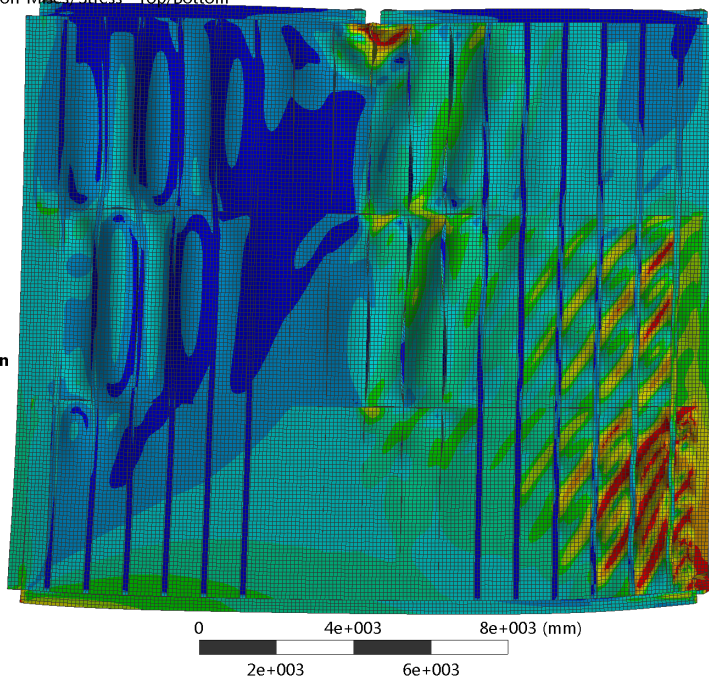
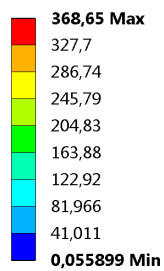
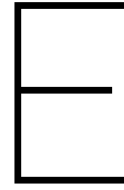


Figure D.11: Von Mises-stresses in the stressed skin design under failure loading



Hand calculations

In this appendix, the results of the SACS software, and in particular the code-checking, is verified.

E.1. Hand calculations to verify the SACS model

The results from the model considered in section 6.2 are verified in this section. Therefore, some of the governing members are looked at. These are checked according to the Eurocode and compared to the outcome from SACS. The results that are considered are given in table E.1. The corresponding verification locations are given in figure E.1. For the analyses, the cross sectional capacities are required. These are given in table E.2.

Table E.1: Member results used for the analysis

Member ID	Member cross section	Design verification	Failure mode	Axial load [kN]	Shear load [kN]	Bending moment [kNm]
56-6	HE800A	0.58	Axial force & bending	-233.5	-676.2	-1614.3
10B-10	914x30 CHS	0.96	Shear	-5549.4	-7548.2	-2630.1
9B-9A	914x30 CHS	0.69	Compression & bending	-12696	194.0	1286.0
3A-56	406x16 CHS	0.64	Tension & bending	3373.7	-23.2	-95.7

Axial force & bending

For the check on cross sectional capacity, member 56-6 is used. This member is a HE800A section, its cross sectional properties are given in table E.2. Since it is a hot rolled wide flange section, the Eurocode is applied. In table E.3, the occurring internal forces are given.

$$\text{EC3-1-1 eq.6.2} \quad \frac{N_{E,d}}{N_{R,d}} + \frac{M_{y,Ed}}{M_{y,Rd}} \leq 1 \quad (\text{E.1})$$

in which the term including bending in local z-direction is omitted, since these stresses are not present.

In order to compute the resistances, it should be determined if the plastic cross section capacities may be used for the bending moment. The cross section is primarily loaded in bending, which validates the cross section class check under pure bending moment:

$$\text{EC3-1-1 table 5.2} \quad \frac{c}{t} = \frac{674}{15} = 44.9 \leq 58.3 = 72\epsilon \quad (\text{E.2})$$

using $\epsilon = \sqrt{\frac{235}{f_y}} = 0.81$. This means the web is of cross section class 1, so the plastic cross sectional properties can be used.

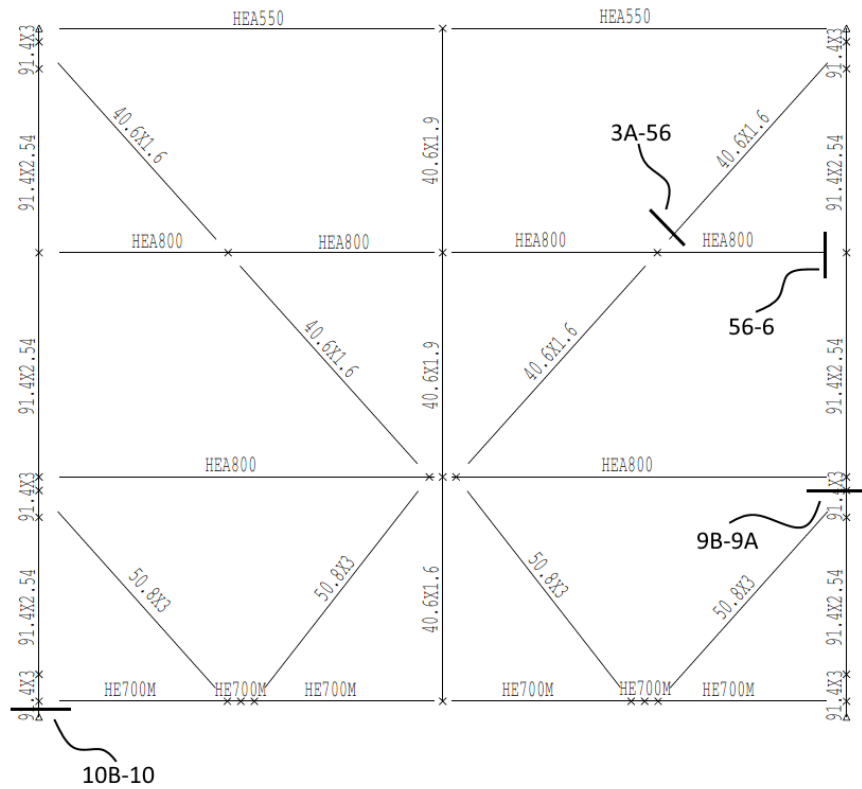


Figure E.1: Considered cross sections in the hand verification

Table E.2: Member properties of the members considered

Section type		HE800A	914x30 CHS	406x16 CHS	
Outer diameter	d_o		914	406	mm
Wall thickness	t_w		30	16	mm
Flange width	b_f	300			mm
Flange thickness	t_f	28			mm
Depth	d	790			mm
Web thickness	t_w	15			mm
Young's modulus	E		210		GPa
Shear modulus	G		80		GPa
Poisson ratio	ν		0.3		
Yield strength	f_y		345		MPa
Axial area	A	28580	83315	19604	mm ²
Mom. of inertia	I_y	$3.03 * 10^9$	$8.15 * 10^9$	$3.73 * 10^8$	mm ⁴
Mom. of inertia	I_z	$1.28 * 10^8$	$8.15 * 10^9$	$3.73 * 10^8$	mm ⁴
Shear area	$A_{v,y}$	$1.11 * 10^4$	$4.17 * 10^4$	$9.80 * 10^3$	mm ²
Tors. constant	I_t	$6.08 * 10^6$	$1.63 * 10^{10}$	$7.47 * 10^8$	mm ⁴
Warp. constant	C_w	$1.83 * 10^{13}$	N.A.	N.A.	mm ⁶
Section moduli					
Major elastic	$W_{el,y}$	$7.68 * 10^6$	$1.78 * 10^7$	$1.84 * 10^6$	mm ³
Major plastic	$W_{pl,y}$	$8.42 * 10^6$	$2.35 * 10^7$	$2.43 * 10^6$	mm ³
Cross section class flange		1			
Cross section class web		3			

Table E.3: Governing member design loads in member 56-6

Torsional moment	$M_{t,Ed}$	0.0	kNm
Bending moment	$M_{y,Ed}$	-1614.3	kNm
Bending moment	$M_{z,Ed}$	0.0	kNm
Axial force	N_{Ed}	-233.5	kN
Shear force	$V_{y,Ed}$	0.0	kN
Shear force	V_{Ed}	-676.2	kN

Now the resistances can be determined:

$$N_{R,d} = \frac{Af_y}{\gamma_{M0}} = \frac{28580 \times 345}{1.0} = 9.86 \times 10^3 kN$$

$$M_{y,Rd} = \frac{W_{pl,y} f_y}{\gamma_{M0}} = \frac{8.42 \times 10^6 \times 345}{1.0} = 2.90 \times 10^3 kNm$$
(E.3)

Filling in to equation E.1 gives:

$$\frac{233.5}{9.86 \times 10^3} + \frac{1614.3}{2.90 \times 10^3} = 0.58$$
(E.4)

which coincides with the design verification obtained via SACS in table E.1.

Shear

The design check on shear is carried out on member 10B-10, which is a 914x30 Circular hollow section (CHS). Since this is a CHS, the verification is performed using the ISO19902 [15]. The occurring internal forces are given in

Table E.4: Governing member design loads in member 10B-10

Torsional moment	$M_{t,Ed}$	0.0	kNm
Bending moment	$M_{y,Ed}$	-754.8	kNm
Bending moment	$M_{z,Ed}$	0.0	kNm
Axial force	N_{Ed}	-5549.4	kN
Shear force	$V_{y,Ed}$	0.0	kN
Shear force	V_{Ed}	-7548.2	kN

Under shear, the utilisation of a member becomes as follows:

$$\text{ISO19902 eq. 13.2-17} \quad U_m = \frac{2V\gamma_{R,v}}{Af_v}$$
(E.5)

in which V is the occurring shear force, A is the cross sectional area, $f_v = \frac{f_y}{\sqrt{3}}$ is the representative shear strength, and $\gamma_{R,v} = 1.05$ is the partial resistance factor for shear.

The utilisation ratio now becomes:

$$U_m = \frac{2 \times 7548.2 \times 10^3 \times 1.05 \times \sqrt{3}}{83315 \times 345} = 0.96$$
(E.6)

which coincides with the design verification from the SACS output in table E.1.

Compression & bending

Since tubular members are also subjected to an axial force and bending, the procedure using the ISO is elaborated. In this case, member 9B-9A is considered, which is a 914x30 CHS. The occurring internal forces are given in table E.5.

Table E.5: Governing member design loads in member 9B-9A

Torsional moment	$M_{t,Ed}$	0.0	kNm
Bending moment	$M_{y,Ed}$	1286.0	kNm
Bending moment	$M_{z,Ed}$	0.0	kNm
Axial force	N_{Ed}	-12696	kN
Shear force	$V_{y,Ed}$	0.0	kN
Shear force	V_{Ed}	194.0	kN

The utilisation of the member under bending and axial force becomes the larger value of:

$$\text{ISO19902 eq. 13.3-7} \quad U_m = \frac{\gamma_{R,c}\sigma_c}{f_c} + \frac{\gamma_{R,b}}{f_b} \sqrt{\left(\frac{C_{m,y}\sigma_{b,y}}{1 - \frac{\sigma_c}{f_{e,y}}}\right)^2 + \left(\frac{C_{m,z}\sigma_{b,z}}{1 - \frac{\sigma_c}{f_{e,z}}}\right)^2} \quad (\text{E.7})$$

$$\text{ISO19902 eq. 13.3-8} \quad U_m = \frac{\gamma_{R,c}\sigma_c}{f_{yc}} + \frac{\gamma_{R,b}\sqrt{\sigma_{b,y}^2 + \sigma_{b,z}^2}}{f_b} \quad (\text{E.8})$$

in which $\gamma_{R,c} = 1.18$ and $\gamma_{R,b} = 1.05$ are the partial resistance factors for compression and bending, respectively, $C_{m,y} = 0.85$ and $C_{m,z} = 0.85$, according to ISO19902 section 13.5. σ_c , $\sigma_{b,y}$, and $\sigma_{b,z}$ are the occurring internal stresses in compression, bending in the y-direction and bending in the z-direction, respectively. f_y is the yield strength, and:

$$f_{e,i} = \frac{\pi^2 E}{\left(\frac{K_i L_i}{r}\right)^2} \quad (\text{E.9})$$

$$f_{yc} = f_y \quad \text{for } \frac{f_y}{f_{xe}} \leq 0.170 \quad (\text{E.10})$$

$$f_{yc} = \left(1.047 - 0.274 \frac{f_y}{f_{xe}}\right) f_y \quad \text{for } 0.170 < \frac{f_y}{f_{xe}} \quad (\text{E.11})$$

$$f_{xe} = 2C_x Et / D \quad (\text{E.12})$$

where the effective length factors $K_y = 1.0$ and $K_z = 1.0$ are determined according to ISO19902 sec. 13.5, L_y and L_z are the unbraced lengths in the y- and z-direction, respectively, and r is the radius of gyration ($r = \frac{\sqrt{d_o^2 + d_i^2}}{4} = \frac{\sqrt{914^2 + 854^2}}{4} = 312.7 \text{ mm}$ for the CHS). C_x is chosen to be 0.3. Filling in the equations gives (in which $f_{e,z}$ is omitted since no bending out of plane is considered):

$$f_{e,y} = \frac{\pi^2 \times 210000}{\left(\frac{0.7 \times 5000}{312.7}\right)^2} = 16.5 * 10^3 \text{ MPa} \quad (\text{E.13})$$

$$f_{xe} = 2 \times 0.3 \times 210000 \times 30 / 914 = 4135 \text{ N/mm}^2 > \frac{f_y}{0.17} \rightarrow f_{yc} = f_y = 345 \text{ MPa} \quad (\text{E.14})$$

For the bending strength, equations 13.2-13 to 13.2-15 state the following:

$$f_b = \frac{Z_p}{Z_e} f_y \quad \text{for } \frac{f_y d_o}{Et} \leq 0.0517 \quad (\text{E.15})$$

$$f_b = \left(1.13 - 2.58 \left(\frac{f_y d_o}{Et}\right)\right) \frac{Z_p}{Z_e} f_y \quad \text{for } 0.0517 < \frac{f_y d_o}{Et} \leq 0.1034 \quad (\text{E.16})$$

$$f_b = \left(0.94 - 0.76 \left(\frac{f_y d_o}{Et}\right)\right) \frac{Z_p}{Z_e} f_y \quad \text{for } 0.1034 < \frac{f_y d_o}{Et} \leq 120 \frac{f_y}{E} \quad (\text{E.17})$$

The CHS allows for full plasticity to occur in the cross section ($\frac{f_y d_o}{E t} = 0.050$), giving:

$$f_b = \frac{Z_p}{Z_e} f_y = \frac{\frac{1}{6} (914^3 - (914 - 2 \times 30)^3)}{\frac{\frac{\pi}{64} (914^4 - (914 - 2 \times 30)^4)}{\frac{914}{2}}} \times 345 = 453.8 MPa \quad (E.18)$$

On the loading side, the following values are obtained:

$$\text{ISO19902 eq. 13.2-1} \quad \sigma_c = \frac{-N_{Ed}}{A} = \frac{12696 * 10^3}{\frac{\pi}{4} (914^2 - (914 - 2 \times 30)^2)} = 152.4 MPa \quad (E.19)$$

$$\text{ISO19902 eq.13.2-11} \quad \sigma_b = \frac{M_{y,Ed}}{Z_e} = \frac{1286.0 * 10^6}{\frac{\frac{\pi}{64} (914^4 - (914 - 2 \times 30)^4)}{\frac{914}{2}}} = 72.1 MPa \quad (E.20)$$

Since no out of plane bending is considered, the expressions can be simplified:

$$U_m = \frac{\gamma_{R,c} \sigma_c}{f_y} + \frac{\gamma_{R,b} \sigma_{b,y}}{f_b} \max\left(\frac{C_{m,y}}{1 - \frac{\sigma_c}{f_{e,y}}}, 1\right) = \frac{1.18 \times 152.4}{345} + \frac{1.05 \times 72.1}{453.8} \times \max\left(\frac{0.85}{1 - \frac{152.4}{16.5 * 10^3}}, 1\right) = 0.69 \quad (E.21)$$

which coincides with the design verification from the SACS output from table E.1.

Tension & bending

Several members show a tensile axial force. One of those is member 3A-56, which is a 406x16 CHS. The design verification on axial tension and bending is carried out using section 13.3.2 of ISO19902. The governing internal forces are given in table E.6.

Table E.6: Governing member design loads in member 3A-56

Torsional moment	$M_{t,Ed}$	0.0	kNm
Bending moment	$M_{y,Ed}$	-95.7	kNm
Bending moment	$M_{z,Ed}$	0.0	kNm
Axial force	N_{Ed}	3373.7	kN
Shear force	$V_{y,Ed}$	0.0	kN
	V_{Ed}	-23.2	kN

The member utilisation ratio can be determined with:

$$\text{ISO19902 eq. 13.3-2} \quad U_m = \frac{\gamma_{R,t} \sigma_t}{f_t} + \frac{\gamma_{R,b} \sqrt{\sigma_{b,y}^2 + \sigma_{b,z}^2}}{f_b} \quad (E.22)$$

using partial resistance factors $\gamma_{R,t} = 1.05$ and $\gamma_{R,b} = 1.05$, and:

$$\begin{aligned} \text{ISO19902} \quad f_b &= \left(1.13 - 2.58 \left(\frac{f_y d_o}{E t}\right)\right) \frac{Z_p}{Z_e} f_y \\ \text{eq. 13.2-14} &= \left(1.13 - 2.58 \left(\frac{345 \times 406}{210000 \times 16}\right)\right) \times \frac{\frac{1}{6} (406^3 - (406 - 2 \times 16)^3)}{\frac{\frac{\pi}{64} (406^4 - (406 - 2 \times 16)^4)}{\frac{406}{2}}} \times 345 = 467.0 MPa \end{aligned} \quad (E.23)$$

On the loading side, the following values are obtained:

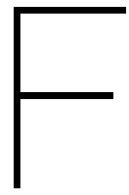
$$\text{ISO19902 eq. 13.2-1} \quad \sigma_t = \frac{N_{Ed}}{A} = \frac{3373.7 * 10^3}{\frac{\pi}{4} (406^2 - (406 - 2 \times 16)^2)} = 172.1 MPa \quad (E.24)$$

$$\text{ISO19902 eq.13.2-11} \quad \sigma_b = \frac{M_{y,Ed}}{Z_e} = \frac{-95.7 * 10^6}{\frac{\frac{\pi}{64} (406^4 - (406 - 2 \times 16)^4)}{\frac{406}{2}}} = -52.0 MPa \quad (E.25)$$

Filling in the results in equation E.22 gives the following:

$$U_m = \frac{1.05 \times 172.1}{345} + \frac{1.05 \times 52}{467.0} = 0.64 \quad (\text{E.26})$$

which coincides with the design verification from the SACS output in table E.1.



Number of weld passes

The number of weld passes required to complete a weld are determined with a sample provided by Iv-Oil & Gas. The number of weld passes required to make a butt weld and a fillet weld are given in figures F.1 and F.2.



WELDING PROCEDURE SPECIFICATION



Ref.Codes: EN/ASME/AWS/EEMUA
pWPS No: 790
No.: 104-17 Rev.no.: 0

Customer Project	TENNET / IV OIL & GAS [S9100] DOLWIN CABLE SUPPORT STRUCTURE [9100] No.: P160132-	Minimum number of welding passes per weld																												
Material (1)	S355J2G3 / 355EMZ / S355J4G2 / 355D / Y26 OR EQUIVALENT	<table border="1" style="width: 100%; border-collapse: collapse; font-size: x-small;"> <thead> <tr> <th>Wallthickn.</th> <th>Weld passes</th> <th>Wallthickn.</th> <th>Weld passes</th> </tr> </thead> <tbody> <tr> <td>2</td> <td>1</td> <td>18</td> <td>8</td> </tr> <tr> <td>3 t/m 6</td> <td>2</td> <td>21</td> <td>9-10</td> </tr> <tr> <td>7 t/m 9</td> <td>3</td> <td>28</td> <td>15-17</td> </tr> <tr> <td>11</td> <td>5</td> <td>32</td> <td>19-21</td> </tr> <tr> <td>13</td> <td>6</td> <td>36</td> <td>28-30</td> </tr> <tr> <td>15</td> <td>6</td> <td>42</td> <td>40-44</td> </tr> </tbody> </table>	Wallthickn.	Weld passes	Wallthickn.	Weld passes	2	1	18	8	3 t/m 6	2	21	9-10	7 t/m 9	3	28	15-17	11	5	32	19-21	13	6	36	28-30	15	6	42	40-44
Wallthickn.	Weld passes		Wallthickn.	Weld passes																										
2	1		18	8																										
3 t/m 6	2		21	9-10																										
7 t/m 9	3		28	15-17																										
11	5		32	19-21																										
13	6	36	28-30																											
15	6	42	40-44																											
Material (2)	S355J2G3 / 355EMZ / S355J4G2 / 355D / Y26 OR EQUIVALENT																													
Application	STRUCTURAL																													
Matr.group	AWS D1.1 - P1																													
Diameter	PLATE/PROFILE Wall thickness : 15 mm																													
Weld shape	See sketch (K-shape)																													
Weld joint prep.	Machining/Grinding																													
Opening	3,5 mm ±0,5 mm Root face : n.a.																													

TACKWELDING

Preheat tack weld: **If surround temp.<10°C.,preheat 80°-150°C.**

Place: **In the top of meltingzone**

Welding process: **SMAW(111)** Shielding gas -

Consumables: **AWS 5.5 E7018-G** Flow rate -

Manufact./type: **LINCOLN/KRYO 1** Wire thickness 3¼ mm

Parameters: **In acc.with the parameters of the "2 nd pass"**

Tack welding: **Totally removed before actual welding.**

PROCES **SMAW (111)**

Wolfram type/dia.: - Cup diameter -

Application: **Shop and field welds**

Preheating: **>80°C (-0°/+20°C)**

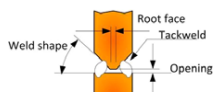
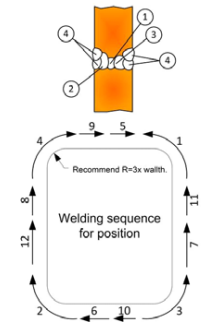
Heat treatment: **n.a.**

GENERAL : **Maxium sweepwide is 3x wire diameter. (K factor=1)**

REMARKS : **Before layer (3), layer (1) good grinding out. !!!**

PQR acc. : **EN/ASME/AWS** DE. nr. AMS540471/1

WELD PARAMETERS	1.Root	2. Pass	3.Fill layer	4.Cap layer
Welding process	SMAW(111)	SMAW(111)	SMAW.	SMAW.
ETT	3			
Welding position	ALL (excl.PG)	ALL (excl.PG)	ALL (excl. PG)	ALL (excl. PG)
Current mode	DC-	DC+	DC+	DC+
Voltage	20 - 22 V.			
Amperage	90 - 100 A.	110 - 125 A.	110 - 125 A.	110 - 125 A.
Welding rate	5,6 - 6,8 cm/min.	8 - 9,5 cm/min.	8 - 9,5 cm/min.	8,8 - 9,5 cm/min.
Heat input	15,9 - 23,6 kJ/cm	13,9 - 20,6 kJ/cm	13,9 - 20,6 kJ/cm	13,9 - 18,8 kJ/cm
Consumables	AWS 5.5 E7018-G	AWS 5.5 E7018-G	AWS 5.5 E7018-G	AWS 5.5 E7018-G
Manufacturer	LINCOLN	LINCOLN	LINCOLN	LINCOLN
Type	KRYO 1	KRYO 1	KRYO 1	KRYO 1
Wire thickness	2,5 mm	3¼ mm.	3¼ mm.	3¼ mm
Shielding gas	-	-	-	-
Flow rate	-	-	-	-
Backing gas/type	-	-	-	-
Flow rate	-	-	-	-
Cleaning	Grinding	Grinding	Grinding	Brushing
Inter pass temp.	max. 200°C.	max. 200°C.	max. 200°C.	max. 200°C.
Consum.stored	Ready Pack	Ready Pack	Ready Pack	Ready Pack

Manufacturer:  Acc.:  Date : 17-10-2016	Customer Acc.: Date :	Insp.Authority Acc.: Date :
---------------------------------------------------------------------------------------------------------------------------------------------------------------------------------------------------------------------	-----------------------------	-----------------------------------

Figure E1: Minimum weld passes required to complete a butt weld



WELDING PROCEDURE SPECIFICATION



Ref.Codes: EN/ASME/AWS/EEMUA pWPS No: 790 No.: 104-16 Rev.no.: 0

Customer: TENNET / IV OIL & GAS [S9100]
 Project: DOLWIN CABLE SUPPORT STRUCTURE [9100] No.: P160132-

Material (1): S275JR / S355J2G3 / 355EMZ / S355J4G2 / 355D OR EQUIVALENT
 Material (2): S275JR / S355J2G3 / 355EMZ / S355J4G2 / 355D OR EQUIVALENT
 Application: STRUCTURAL UNP reinforcing
 Matr.group: AWS D1.1 - P1
 Diameter: PLATE/PROFILE Wall thickness: a = 6 mm
 Weld shape: See sketch
 Weld joint prep.: Machining/Grinding
 Opening: 1,5 mm ±0,5 mm Root face: n.a.

Minimum number of welding passes per weld			
Wallthickn.	Weld passes	Wallthickn.	Weld passes
2	1	18	8
3 t/m 6	2	21	9-10
7 t/m 9	3	28	15-17
11	5	32	19-21
13	6	36	28-30
15	6	42	40-44

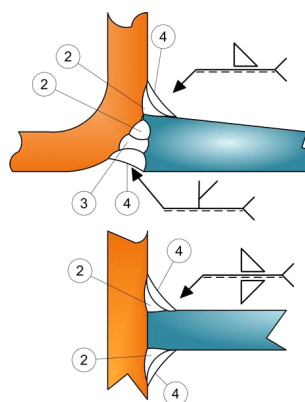
The last pass should always be welded in the middle of the weld.

TACKWELDING

Preheat tack weld: If surround temp.<10°C.,preheat 80°-150°C.
 Place: In the top of meltingzone
 Welding process: SMAW(111) Shielding gas: -
 Consumables: AWS 5.5 E7018-G Flow rate: -
 Manufact./type: LINCOLN/KRYO 1 Wire thickness: 3¼ mm
 Parameters: In acc.with the parameters of the "2 nd pass"
 Tack welding: Totally removed before actual welding.

PROCES SMAW (111)
 Wolfram type/dia.: - Cup diameter: -
 Application: Shop and field welds
 Preheating: >80°C (-0°/+20°C)
 Heat treatment: n.a.

GENERAL : Maxium sweepwide is 3x wire diameter. (K factor=1)
 REMARKS : Before and after welding MT examination
 PQR acc. : EN/ASME/AWS DE. nr. AMS540471/1



WELD PARAMETERS	1.Root	2. Pass	3.Fill layer	4.Cap layer
Welding process		SMAW(111)	SMAW.	SMAW.
ETT		3		
Welding position		ALL (excl.PG)	ALL (excl. PG)	ALL (excl. PG)
Current mode		DC+	DC+	DC+
Voltage	- V.	20 - 22 V.	20 - 22 V.	20 - 22 V.
Amperage	- A.	110 - 125 A.	110 - 125 A.	110 - 125 A.
Welding rate	- cm/min.	8 - 9,5 cm/min.	8 - 9,5 cm/min.	8,8 - 9,5 cm/min.
Heat input	- kJ/cm	13,9 - 20,6 kJ/cm	13,9 - 20,6 kJ/cm	13,9 - 18,8 kJ/cm
Consumables		AWS 5.5 E7018-G	AWS 5.5 E7018-G	AWS 5.5 E7018-G
Manufacturer		LINCOLN	LINCOLN	LINCOLN
Type		KRYO 1	KRYO 1	KRYO 1
Wire thickness		3¼ mm.	3¼ mm.	3¼ mm
Shielding gas	-	-	-	-
Flow rate	-	-	-	-
Backing gas/type	-	-	-	-
Flow rate	-	-	-	-
Cleaning		Grinding	Grinding	Brushing
Inter pass temp.		max. 200°C.	max. 200°C.	max. 200°C.
Consum.stored		Ready Pack	Ready Pack	Ready Pack

Manufacturer: Acc.: Date: 14-9-2016	Customer: Acc.: Date:	Insp.Authority: Acc.: Date:
-------------------------------------------	-----------------------------	-----------------------------------

Figure E2: Minimum weld passes required to complete a fillet weld

Bibliography

- [1] Iv-AGA. Structural design report for offshore transformer station rev c3, 2012.
- [2] J.K. Paik and A.K. Thayamballi. *Ultimate Limit State Design of Steel Plated Structures*. John Wiley & Sons, 2003.
- [3] S.P. Timoshenko and J.M. Gere. *Theory of elastic stability*. McGraw-Hill, 1961.
- [4] J. Xu. Optimal design of a module structure with sheeting, 2012.
- [5] B. Aberkrom. Defining parameters for buckling checks of plated structures in finite element software packages, 2014.
- [6] J K Paik and A K Thayamballi. Some recent developments on ultimate limit state design technology for ships and offshore. *Ocean Engineering*, 2006.
- [7] Roland Abspoel. the Maximum Bending Moment Resistance of Plate Girders. *Eurosteel 2014, Naples, Italy*, 2014.
- [8] M. Veljkovic and B. Johansson. Design of hybrid steel girders. *Journal of Constructional Steel Research*, 60(3-5):535–547, 2004.
- [9] E. Hosseinpour, S. Baharom, and Y. Yadollahi. Evaluation of steel shear walls behavior with sinusoidal and trapezoidal corrugated plates. *Advances in Civil Engineering*, 2015, 2015.
- [10] F M El –Amin, M F Abdel–Khalek, K Hassan, and E E Asham. Elastic Buckling Behavior of Steel Frames With Corrugated Steel Shear Walls. *Journal of Engineering Sciences*, 33(3):703–719, 2005.
- [11] H. H. Sun and J. Spencer. Buckling strength assessment of corrugated panels in offshore structures. *Marine Structures*, 18(7-8):548–565, 2005.
- [12] M. M. Alinia and M. Dastfan. Behaviour of thin steel plate shear walls regarding frame members. *Journal of Constructional Steel Research*, 62(7):730–738, 2006.
- [13] J. Rhodes. Some observations on the post-buckling behaviour of thin plates and thin-walled members. *Thin-Walled Structures*, 41(2-3):207–226, 2003.
- [14] S. Sabouri-Ghomi, M.H.K. Kharrazi, S.-E.-D. Mam-Azizi, and R.A. Sajadi. Buckling behavior improvement of steel plate shear wall systems. *The structural design of tall and special buildings*, 17:823–837, 2008.
- [15] CEN. En-iso19902:2013 petroleum and natural gas industries - fixed steel offshore structures, 2007.
- [16] CEN. En-iso19900:2013 petroleum and natural gas industries - general requirements for offshore structures, 2013.
- [17] Nen-en. NEN-EN 1993-1-1 + C2. Technical Report december 2011, 2015.
- [18] CEN. Eurocode 3: design of steel structures - part 1-5: Plated structural elements, 2006.
- [19] CEN. Nen-en 1993-2 - eurocode 3: Design of stel structures - part 2: Steel bridges, 2011.
- [20] CEN. Nen-en10025-2 hot rolled products of structural steel - part 2:technical delivery conditions for non-alloy structural steels, 2004.
- [21] GL Noble Denton. 0030/nd - guidelines for marine transportation, 2015.
- [22] Shell Group. Dep specification - fixed steel offshore structures, 2007.

-
- [23] R.D. Ziemian. *Guide to Stability Design Criteria for Metal Structures*. Wiley, 2010.
- [24] J.K. Paik, A. K. Thayamballi, and B.J. Kim. Large deflection orthotropic plate approach to develop ultimate strength formulations for stiffened panels under combined biaxial compression/tension and lateral pressure. *Thin-Walled Structures*, 39(3):215–246, 2001.
- [25] R. Abspoel and F.S.K. Bijlaard. *Stability of steel plated structures*. TU Delft, 2010.